Fatigue assessment of rail track detail on movable bridge in Estonia based on 2D / 3D Finite Element Modelling using hot-spot stresses

Master of Science Thesis

Department of Structural Engineering

Faculty of Civil Engineering and Geosciences

Delft University of Technology

Author:	D. Rikeros	
Committee:	Prof. Dr. M. Veljkovic	TU Delft
	Dr. P. de Vries	TU Delft
	Dr. M. Hendriks	TU Delft
	Ing. K. Wiersma PMSE	Witteveen+Bos

March, 2019

Preface

This thesis has been written in partial fulfillment for the requirements for the degree of Master of Science in Structural Engineering, Civil Engineering at Delft University of Technology. During my studies, my interests lie in both steel structures and dynamics, for which I decided to take the fatigue analysis as the focus of this thesis. Through this work, I was able to relate the theoretical knowledge gained from courses into practical real-life engineering situations, such as the analysis of a movable bridge with Witteveen+Bos.

During my stay in The Netherlands, far from home, I was able to count with the support of my family and friends, which strengthened my motivation to continue and finish my studies at this university. I want to thank my family for providing me this support and their interest in me to continuously achieve more in my life. Besides this support, I was also able to grow by adapting to a new environment as well as taking an independent lifestyle, an important experience to grow as a person. Thank you also to the friends I made during this new stage of my life. We shared different moments during these years, I was able to learn different aspects of life across different nationalities and cultures, which I find valuable as well. Thank you to all for being there for me.

Abstract

There are several methods to perform fatigue assessment as described by the Eurocode 3 and the International Institute of Welding (IIW). The codes establish the relation between stress ranges and their respective number of cycles until failure of the detail. This method is called S-N curves, however this is based mainly on nominal stresses. A different approach is analyzed in this project, the hot-spot stress method. The hot-spot stress is used to analyze stress distribution caused by geometrical discontinuities on a welded connection. Finite element modelling (FEM) is used in order to ascertain and calculate the hot-spot stress for different details. This method consists on performing a stress extrapolation based on read-out points to avoid any peak stress caused by the finite element analysis itself.

This project focuses on a project-specific welded connection in a rail track for a movable bridge located in Tallinn, Estonia, designed by the company Witteveen+Bos. Initially, the company performed a model of the complete rail track used in the movable bridge, where the welded connection is located. This project takes a more specific scenario and develops the analysis of the local model of the connection itself. The hot-spot stress approach is taken to analyze this structural detail by means of two different finite element software, RFEM and ABAQUS, to perform a validation between these programs. In this report, a comparison is performed between modelling using shell elements and solid elements as well as mesh refinement. The extrapolation of the hot-spot stress is performed by taking the normal stresses at the surface of the element.

Based on the results obtained from the analysis, this project provides recommendations when performing this type of analysis on welded connections. A design check is also performed to establish if the detail design is sufficient against fatigue, caused by the motion of the movable bridge.

Table of Contents

Preface i

Abstract ii

Table of Contents iii

Nomenclature v

Chapter 1 – Introduction 1

1.1 Background 1

1.2 Problem definition 2

1.3 Scope and Limitations 3

1.3.1 Scope 3

1.3.2 Limitations 3

1.4 Outline 4

Chapter 2 – Literature Review 5

2.1 Codes Review 5

2.2 Fatigue Methodologies 5

2.3 Stress Cycle Curve (S-N Curve) 5

2.3.1 Introduction 5

2.3.2 Detail Category 7

2.3.3 Safety Factors 10

2.3.4 Palmgren-Miner's Rule 11

2.4 Hot-Spot Stress 12

2.4.1 Introduction 12

2.4.2 Calculation Method 12

2.5 Finite Element Analysis 16

2.5.1 Introduction 16

2.5.2 Shell and Solid Modelling 16

2.6 Influence of Welding 19

2.6.1 Introduction 19

2.6.2 Residual Stresses 20

2.6.3 Weld Imperfections 20

2.6.4 Improvement of Fatigue Life 21

Chapter 3 – Global Modelling 23

3.1 Introduction 23

3.2 Normal Stresses from Opening/Closing Loads 26
3.3 Normal Stresses from Wind Loads 28
Chapter 4 – Local Modelling 30
4.1 Model Preparation 30
4.2 Local Shell Modelling 33
4.3 Local Solid Modelling 37
Chapter 5 – Discussion of Results 38
5.1 Mesh Refinement in Modelling 38
5.2 Shell Elements in Modelling 39
Chapter 6 – Verification 54
6.1 Introduction 54
6.2 Shell Element Model 54
6.3 Solid Element Model 57
Chapter 7 – Recommendations and Conclusions 66
7.1 Conclusions 66
7.2 Recommendations 66
APPENDIX A – Global Modelling Results 68
APPENDIX B – RFEM Local Shell Modelling 72
APPENDIX C – ABAQUS Local Shell Modelling 85
APPENDIX D – ABAQUS Local Solid Modelling 87
Bibliography 90

Nomenclature

Abbreviations

DNV	Det Norske Veritas
EC3	Eurocode 3
FAT	Fatigue strength class
IIW	International Institute of Welding

Symbols

D	Cumulative fatigue damage
m_{xy}	Internal shear force
m_y	Internal bending force
n_y	Internal axial force
n	Acting number of cycles
N	Number of cycles
N_E	$2x10^6$ cycles
N_R	Number of cycles (resistance)
R	Stress ratio
S	Stress
t	thickness
U.C.	Unity check
σ	Normal stress
τ	Shear stress
$\Delta\sigma$	Stress range
$\Delta\sigma_c$	Detail category class
σ_{hs}	Hot-spot stress
$\sigma_{0.4t}$	Normal stress at distance of 0.4 thickness
$\sigma_{0.5t}$	Normal stress at distance of 0.5 thickness
$\sigma_{1.0t}$	Normal stress at distance of 1.0 thickness
$\sigma_{1.5t}$	Normal stress at distance of 1.5 thickness
σ_m	Bending stress
σ_n	Axial stress
$\sigma_{E,2}$	Stress at $2x10^6$ cycles
θ	Angle (degrees)
γ_{Ff}	Fatigue load factor
γ_{Mf}	Fatigue safety factor

Chapter 1 – Introduction

1.1 Background

For structures with dynamic loads such as movable bridges, bolted and welded connections both experience fatigue during their lifetime. For bolted connections, preloaded bolts can be used to behave in a favorable way against fatigue. Bolted connections are not always possible and welded connections need to be applied. In general, welded connections are very susceptible for fatigue. Fatigue occurs when elements are subjected to repetitive loads during their service life and cracks may initiate and then propagate. When a crack propagates, based on where the crack is located, then the base material left may be insufficient to withstand the acting stresses or the weld may fail as well, causing failure of the structure itself. This crack generally initiates in areas with impurities in the metal or in geometrical or material discontinuities. In a structure, there will always be geometrical discontinuities, for instance in connections (bolts or welds).

Generally the crack starts at the weld toe location, where the stress concentrations are the highest. In fatigue analysis, two methods are mainly used, the first one is through use of S-N curves, which correlates number of cycles for a stress range value. In this method, the use of hot-spot stress is also possible to obtain the stress at the weld toe through means of extrapolation from a finite element model. This project will be focused on this first method. The second method is through fracture mechanics, where the focus is crack growth by evaluating stress intensities at crack tip. Using S-N curves, we talk about micro crack growth and crack initiation with stress concentration factors. Fracture mechanics is about stress intensities and macro crack growth. These processes are different and sequenced stages of the fatigue process.

Several design methods have been studied for the assessment of welded structures against fatigue, given by codes such as Eurocode 3 (EC3), International Institute of Welding (IIW) and Det Norske Veritas (DNV). In these codes, the S-N curves have been studied. Based on this, the codes have tabulated certain configurations as prequalified joints, for instance in Part 1-9 of EC3, allowing to obtain the resistance against fatigue (stress range) for two million cycles. However, obtaining the actual stress at the weld toe can be complex, based on the configuration of the joint. Therefore a lot of details are based on the nominal stress and stress concentrations due to the shape of a weld and its residual stresses. The use of finite element software is required to obtain the stresses in complex joints and perform an adequate fatigue analysis. In this project, the computer programs RFEM and ABAQUS will be used.

1.2 Problem definition

The consultancy engineering company Witteveen+Bos has designed the Balance Bridge in Tallinn, Estonia and is interested to obtain results of a local model of a specific joint of this bridge (located in the rail track) against fatigue. The company performed a global model of the rail track for its design, where shell elements and nominal stresses were used. Their focus is now to know how the result of the stresses in the welds would differ in a local model, realizing a hot-spot stress analysis in the welded joint located in the rail track of the bridge. The rail track used to open the bridge uses two steel casted elements, a steel connecting plate and longitudinal and transversal stiffeners. The welded joint is located between this steel connecting plate and the stiffeners. With this they can compare if the global approach is conservative or does not follow the real behavior of the welded joint and then, for these cases, if shell or solid elements are recommended based on accuracy of results. The cyclic counting for fatigue of this weld is taken for the opening/closing of this bridge where the stress variation will be made.

This report will focus on comparing the stress in the welded structure under different approaches to ascertain how the approach itself affects the result of the analysis. A global model, a local finite element 2D shell analysis (without weld modelling) and a local finite element 3D solid analysis (with and without weld modelling) will be made. Then differences and similarities between the approaches will be analyzed, giving as well the advantages and/or disadvantages of each case.

For the 2D global case, stresses are found based on results given by a global analysis of the bridge and in the local analysis, the hot spot stress will be used (instead of commonly used nominal or modified stresses). Both 2D and 3D finite element analysis are done with the finite element software RFEM, to ensure that the results will be purely affected by shell/solid comparison. However, a different software (ABAQUS) will be used to validate results obtained through RFEM.

With this modelling and analysis using hot spot stresses, a comparison will be made between an estimation based on simplified approach and through the hot spot stresses based on results on local finite element modelling. Also, results will be compared between shell modelling and solid modelling, analyzing carefully how similar or different they are, if results are reliable based on mesh refinement and if the previous simplified approach can be made or not. A comparison will be made as well from the welding approach, if the hot spot stress would vary significantly or behave almost similar from using a fillet weld compared to the full penetration welded as stated in the design of the structure.

1.3 Scope and Limitations

1.3.1 Scope

The research of this project is focused on a comparison of analysis in the rail track detail of the movable bridge when performing finite element modelling using shell elements (2D) or solid elements (3D). This analysis will be used to discern if there are any similarities and/or differences between these two types of approach to the problem.

A second point of interest is the difference of local analysis using the hot-spot stress method compared to the global analysis of this specific detail. This is also done in order to obtain deeper knowledge of stress distribution in this type of detail as this is not a standard detail presented in the Eurocode.

In the local models, the hot-spot stresses will be calculated through extrapolation from read out points specified in the codes. Different local models will be made using different configurations (mesh size). The focus will be on a comparison between the use of coarse mesh and fine mesh in a finite element model, how it influences the accuracy and results in their respective models, with the aim to ensure mesh objectivity.

From the results obtained in these analysis, this project will ascertain the service life time of this rail track under fatigue load case. This will be done by obtaining the total number of cycles the structure could withstand for a specific stress range level.

On a local modelling analysis, codes state that models can be made with or without weld modelling, then a comparison will be made if weld modelling highly influences the result of the analysis or can be kept out. This will be made in solid element modelling to include properly the shape of the weld.

The finite element software RFEM will be used to perform this analysis and ABAQUS will be used as an additional software to validate results obtained in RFEM. In RFEM, the process of refinement in the local models will be shown, where in ABAQUS, for validation, only the final configuration will be used to compare its results with results from RFEM.

1.3.2 Limitations

Several assumptions will be made in order to transform a global model (bridge) to a local model of interest (welded joint) which may influence the result. These assumptions need to be considered when checking final results of the models to ensure accuracy of the results given in the analysis of the software.

When realizing a hot-spot stress analysis, it has to be taken into account that this only considers when the crack initiates at the weld toe. This is taken as given for this work, as the focus is made through hot-spot stress analysis. Cracks can occur also in weld roots, this will no longer be applicable with hot-spot stress. This case is taken into account in the Eurocode but will not be the focus of this work.

The highest reaction force will be taken for the local modelling as it will cause the most critical case in the analysis. This will be done since all welded connections are detailed identically, however it has to be noted that not all of them will experience this load case, so the local model is affected by this assumption.

1.4 Outline

In this project, Chapter 2 consists of the literature review required for this project. The literature review consists on information of the fatigue load case under consideration, giving an introduction to fatigue and two fatigue methodologies such as the S-N curve and hot-spot stress. The global modelling of the structure (rail track) is shown on Chapter 3, while Chapter 4 consists on the local modelling of a joint in the rail track, which is the main focus of this work. All these models are made by means of the RFEM software.

Chapter 5 consists of an in-depth analysis and discussion of the results found on Chapter 3 and Chapter 4. During the development of this project, additional models were made using ABAQUS, a FEM software, to validate results obtained with RFEM, this validation is presented in Chapter 6. Finally, Chapter 7 presents the conclusions of this work as well as provide recommendations based on the results obtained in this project. Other recommendations will be based on experiences during this project's development and for further studies as well.

Chapter 2 – Literature Review

2.1 Codes Review

This section provides an overview of the considered literature for this study. It includes the considered design codes containing fatigue assessment recommendations. Also, a selection of research publications that have provided more insight on this topic is discussed.

There are several institutions world-wide that address fatigue issues, this research will take into account and limited to International Institute of Welding (IIW), Eurocode 3 (EC3) and Det Norske Veritas (DNV). These represent the most used codes in The Netherlands.

2.2 Fatigue Methodologies

This section is focused to introduce two different methodologies commonly used for fatigue assessment. These are the stress cycle curve (S-N curve) and the hot-spot stress method. Using these methods, the surface life time during the crack initiation is considered when micro cracks are forming (crack initiation life), crack growth is not considered. Fatigue occurs when a structures experiences repetitive load cycles during its service life, major structures prone to fatigue are bridges for example.

2.3 Stress Cycle Curve (S-N Curve)

2.3.1 Introduction

A stress cycle curve, also known as S-N curve, represents the performance of a material under a repetitive loading. This curve is plotted on a logarithmic scale, with the stress S on the vertical axis and the number of cycles N on the horizontal axis. This curve under this scale is typically presented by a straight line. These curves are derived from experiments, exposing specimens to repetitive loading cycles. The stress range is measured and the number of cycles it withstood until it reached failure. These results provide a graph like the following:

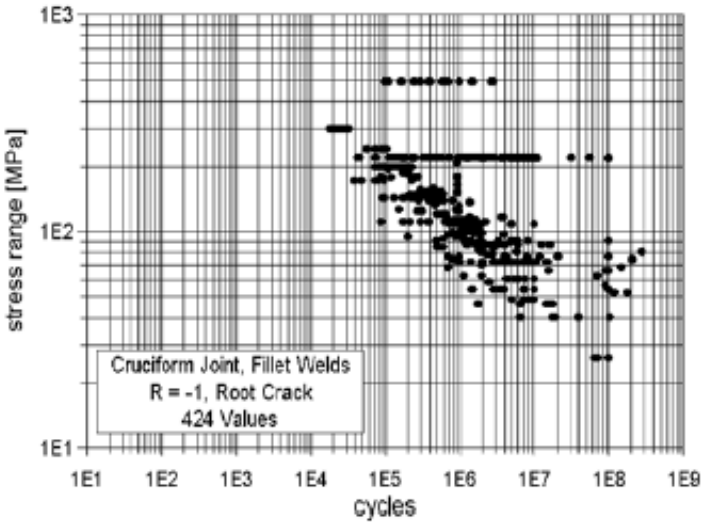

Figure 2-1 - Typical data obtained for a S-N curve [15]

The stress ratio R is the ratio between the minimum stress and maximum stress applied in the respective detail, with a given stress amplitude and average mean stress. Other experiments varying the value of R (or the applied range of stresses) will give a particular set of points for that given ratio as well. In welds, because of the welding process, high residual stresses are introduced, therefore the focus is on the stress range instead of an absolute stress level.

As seen on the previous graph, there is a large scatter in the results, causing that predicting fatigue behavior becomes more complex. For this, a curve (straight line) is fitted in the data and evaluated statistically. A characteristic curve is obtained as the S-N curve which represents a 5% failure probability of survival, based on the mean value and the standard deviation of the data previously obtained. This probability is taken due to the possible scatter of the values, if a near 100% survival probability is taken, then a design would be extremely conservative, causing a high increment in its economical aspect as well, which is not desired.

The characteristic curve for constant amplitude is shown in the following figure:

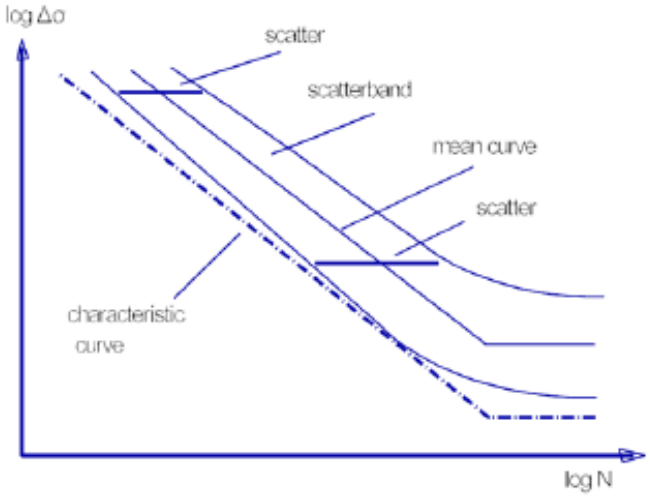

Figure 2-2 - S-N curve based on statistical evaluation for welds [15]

2.3.2 Detail Category

In the Eurocode 3 Part 1-9, category classes are used in order to give a standardization of elements and their corresponding strength to fatigue. These values are used so that for a given standard detail, its resistance will be already known through all experimental data previously found, therefore a design or check can be made through a simpler verification of standard resistance values. However, these values are for standard details, so for a more complex detail or structure, new experimental data might be needed.

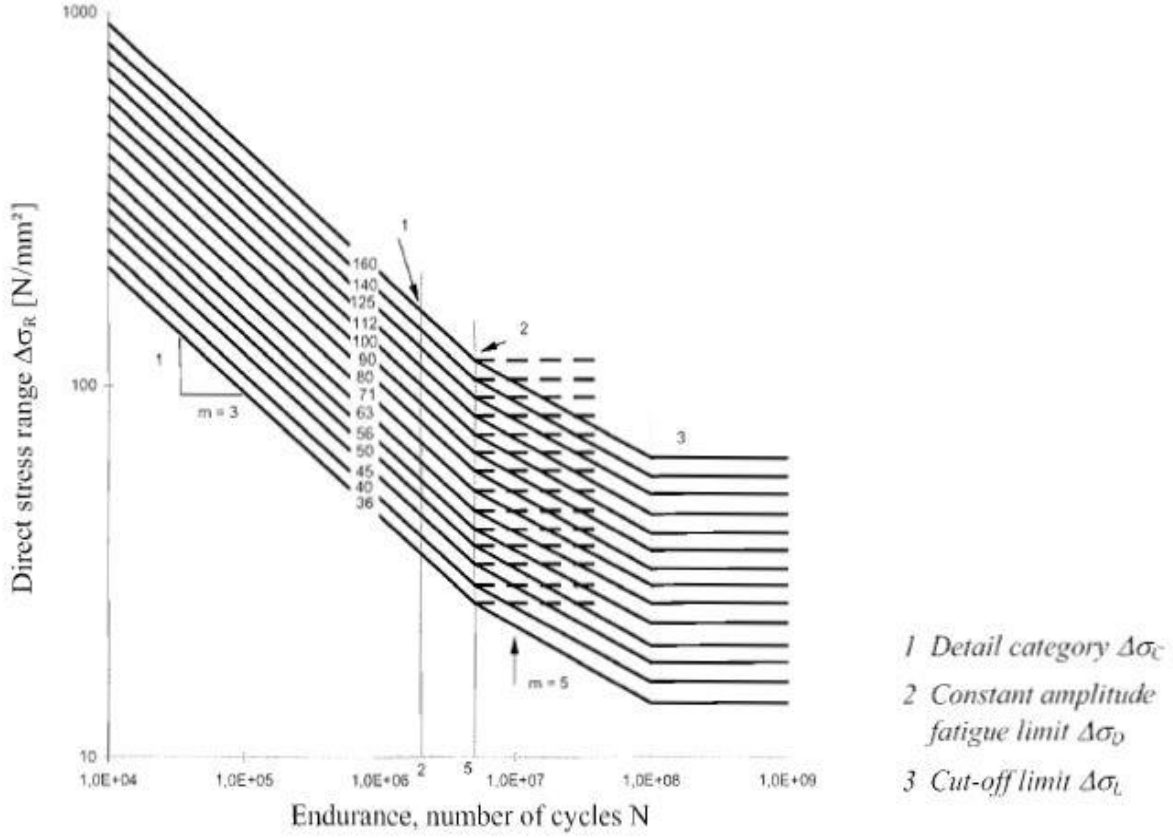

Figure 2-3 - Fatigue strength curves [10]

In this graph, we can state that the detail category class represents the stress range corresponding to the number of cycles of 2x10^6 cycles, this is usually the stress tabulated in this code for resistance check. The constant amplitude fatigue limit represents the horizontal section with constant amplitude stress. For load cases with constant amplitude changes below this limit, micro crack may form but are not progressing. With variable stress ranges, load sequence becomes important, when high stress levels occur, posterior low stress cycles may also contribute to micro cracking. The cut-off limit represents the stress range value (at 1x10^8 cycles) in which the element, loaded by a variable stress range, is considered to not have problems with fatigue, as under that stress, it can withstand an infinite number of cycles.

These detail category classes are made taking into account different effects that might influence the resistance of any joint, to consider real life situations, which are also present during experimental investigations. Some of the effects are the following:

- Structural stress concentration due to detail
- Stress concentration by weld geometry
- Weld imperfections in regard to fabrication standards or execution
- Load case (Location and direction)
- High value of residual stresses due to welding and the welding process as well
- Element conditions (Base metal and weld)

The detail category class depends on the type of joint to be analyzed, in this section we consider the case of load carrying welded joints, as it is the joint of interest.

<table>
<tr><th>Detail Category</th><th colspan="3">Construction Detail</th><th>Description</th><th>Requirements</th></tr>
<tr><td>80</td><td>l < 50mm</td><td>All t [mm]</td><td rowspan="7"> 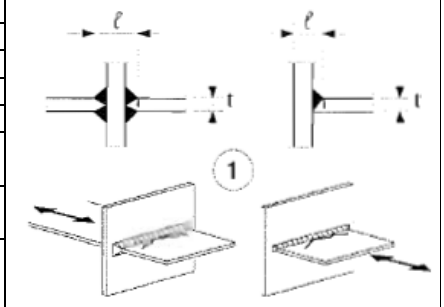 </td><td rowspan="7">Cruciform and Tee joints:

1) Toe failure in full penetration butt welds and all partial penetration joints</td><td rowspan="9">1) Inspected and found free from discontinuities and misalignments outside the tolerances of EN 1090.

2) For computing Δσ, use modified nominal stress.

3) In partial penetration joints, two fatigue assessments are required. Firstly, root cracking evaluated according to stresses defined in section 5, using category 36* for Δσw and category 80 for Δτw. Secondly, toe cracking is evaluated by determining Δσ in the load-carrying plate.

Details 1) to 3):
The misalignment of the load-carrying plates should not exceed 15% of the thickness of the intermediate plate.</td></tr>
<tr><td>71</td><td>50 < l ≤ 80</td><td>All t</td></tr>
<tr><td>63</td><td>80 < l ≤ 100</td><td>All t</td></tr>
<tr><td>56</td><td>100 < l ≤ 120</td><td>All t</td></tr>
<tr><td>56</td><td>l > 120</td><td>t < 20</td></tr>
<tr><td>50</td><td>120 < l ≤ 200
l > 200</td><td>t > 20
20 < t ≤ 30</td></tr>
<tr><td>45</td><td>200 < l ≤ 300
l > 300</td><td>t > 30
30 < t ≤ 50</td></tr>
<tr><td>40</td><td>l > 300</td><td>t > 50</td></tr>
<tr><td>As detail 1 in Table 8.5</td><td colspan="3"> 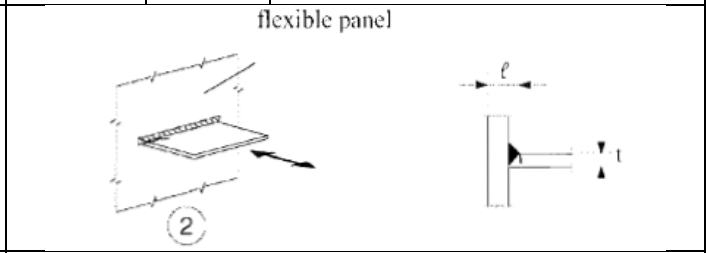 </td><td>2) Toe failure from edge of attachment to plate, with stress peaks at weld ends due to local plate deformations.</td></tr>
<tr><td>36*</td><td colspan="3"> 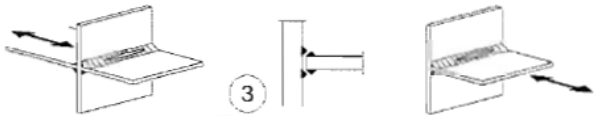 </td><td>3) Root failure in partial penetration Tee-butt joints or fillet welded joint and in Tee-butt weld, according to Figure 4.6 in EN 1993-1-8:2005</td></tr>
</table>

Table 2-1 - Detail category classes for load carrying welded joints [10]

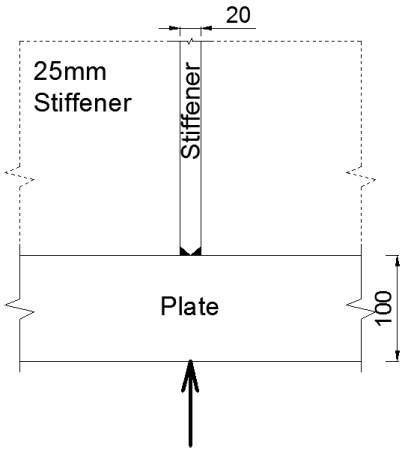

Figure 2-4 - Detail and measurements of plate and stiffener used in the bridge

From the previous table of the Eurocode 3, under load carrying welded joint, the one who resembles the most to our welded joint has a detail class of $\Delta\sigma_C = 63\ MPa$, taking l=100mm (plate), t=20mm (stiffener) and that full penetration welds are used. For this category class and under constant amplitude loading, a value of m=3 is used as in Figure 2-3. The following figure represents the section of the detail used for the detail category class.

The International Institute of Welding (IIW) also establishes standard values of fatigue strength according to classified structural details, as with the Eurocode, here it is called a fatigue class instead of detail category. This fatigue class is obtained as well through experimental data and taking in consideration a 5% probability of failure as well. The values are given in the table {3.2}-1 of the IIW, fatigue resistance for structural details on the basis of nominal stresses. The fatigue class represents the stress, in MPa, it can withstand for fatigue at 2 million cycles, similar as in the Eurocode. For the detail of interest, the following class was taken:

No.	Structural Detail	Description (St.= steel; Al.= aluminium)	FAT St.	FAT Al.	Requirements and Remarks
400	**Cruciform joints and/or T-joints**				
411	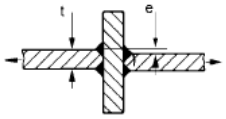	Cruciform joint or T-joint, K-butt welds, full penetration, weld toes ground, potential failure from weld toe. Single sided T-joints and cruciform joints without misalignment	80 90	28 32	Advisable to ensure that intermediate plate was checked against susceptibility to lamellar tearing. Misalignment <15% of primary plate thickness in cruciform joints.

Table 2-2 - Detail category classes for load carrying welded joints [15]

Under this configuration, it can be seen that the fatigue class to be taken for steel details is FAT80, this value is taken for cruciform joints or T-joints, given that in the analyzed detail, both configurations are present, so the most conservative is taken as safety.

According to the IIW, the fatigue class for this type of detail is of 80MPa, while in the Eurocode we obtained a detail category of 63MPa, for this analysis the resistance will be taken with the lower value, this being a resistance stress of 63MPa. It is noted that the Eurocode is more conservative than the codes established by the IIW; for this project, the Eurocode is used for the structural design.

The detail category mentioned previously are used when nominal stresses are used, both Eurocode and IIW establish a different table with different detail category values when hot-spot stress approach is used. The following tables refer to the detail categories given by the Eurocode [10] and IIW [15]:

Detail category	Constructional detail	Description	Requirements
112	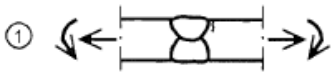	1) Full penetration butt joint.	1) - All welds ground flush to plate surface parallel to direction of the arrow. - Weld run-on and run-off pieces to be used and subsequently removed, plate edges to be ground flush in direction of stress. - Welded from both sides, checked by NDT. - For misalignment see NOTE 1.
100	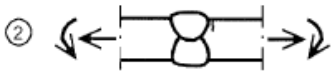	2) Full penetration butt joint.	2) - Weld not ground flush - Weld run-on and run-off pieces to be used and subsequently removed, plate edges to be ground flush in direction of stress. - Welded from both sides. - For misalignment see NOTE 1.
100	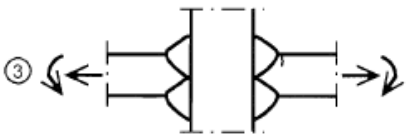	3) Cruciform joint with full penetration K-butt welds.	3) - Weld toe angle ≤60°. - For misalignment see NOTE 1.

Table 2-3 - Eurocode detail category classes using hot-spot stress method [10]

No.	Structural detail	Description	Requirements	FAT Steel	FAT Alu.
1		Butt joint	As welded, NDT	100	40
2	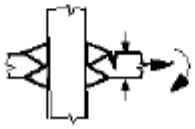	Cruciform or T-joint with full penetration K-butt welds	K-butt welds, no lamellar tearing	100	40

Table 2-4 - IIW detail category classes using hot-spot stress method [15]

For the hot-spot stress analysis, the detail category class to be used is $\Delta\sigma_c = 100\ MPa$, as observed in both tables from Eurocode and IIW.

2.3.3 Safety Factors

In fatigue design, partial safety factor are also used for fatigue strength γ_{Mf}, these values will depend on which is the assessment method and the consequence of failure we consider a given structure will have. The fatigue load factor γ_{Ff} is also used, where $\gamma_{Ff} = 1$. The safety factor for fatigue is taken by the following table, given by the Eurocode:

Assessment Method	Consequence of Failure (γ_{Mf} values)	
	Low Consequence	High Consequence
Damage Tolerant	1,00	1,15
Safe Life	1,15	1,35

Table 2-5 - Safety factors for fatigue strength [10]

Both assessment methods take into account an acceptable reliability of a structure to perform as desired during its service life. The difference in both methods relies in the inspection and maintenance control during its lifetime. Damage tolerant method includes a program to detect and correct any damages occurring during its service life, while safe life method considers that during its service life there would be no need for any inspection and/or correction of any damage related to fatigue. Due to this main difference, as it can be seen with the given values, the safe life method is much more conservative than the damage tolerant method.

The following table establish values of safety factors to be used according to the IIW:

Partial safety factor γ_M → Consequence of failure	Fail safe and damage tolerant strategy	Safe life and infinite life strategy
Loss of secondary structural parts	1.0	1.15
Loss of the entire structure	1.15	1.30
Loss of human life	1.30	1.40

Table 2-6 - Safety factors for fatigue strength [15]

While the Eurocode establish parameters as low consequence and high consequence, the IIW establish a distinction between the case of loss of the entire structure and the loss of human life (1,30 and 1,40 for the safe life strategy). This project will focus on the value given by the Eurocode, as it is the normative, while the IIW acts more as background and recommendations. Therefore, for the analyzed detail of this project, where the consequence of failure is considered high and it is considered for safe life as well (the most critical combination), a safety factor of 1,35 will be used.

2.3.4 Palmgren-Miner's Rule

Fatigue occurs when there is a repetitive cycle of a given load (stress range), however, it can also occur that there are repetitive load cases of different amplitudes, where each of those will contribute to fatigue damage in the detail over its lifetime. Palmgren-Miner's rule allows to calculate the cumulative fatigue damage D based on the acting number of cycles n in regards to the number of cycles N_R the detail can resist for the stress range with n cycles. The damage D is defined as:

$$D = \sum \frac{n}{N_R}$$

This value can have two different results, the first one is when this value is lower than 1 and the second is for a value equal or larger than 1 (note that it is not possible to have negative values). If the cumulative damage is 1 or higher, failure is expected to happen for the given joint under this stress configuration.

2.4 Hot-Spot Stress

2.4.1 Introduction

The hot-spot stress method is a method that takes into account the stresses caused by geometric discontinuities, it contains all stress concentrations except for the influence of the weld. These stresses are also known as geometric stresses (or structural stresses). However this method is limited to cases where the crack occurs at the weld toe, it does not cover cracks initiating from the weld root. Nominal stresses are the stresses where these values are not affected by any of the discontinuities located in the element.

In the codes, the hot-spot stress can be calculated using factors obtained through experimental investigation and parametric formulae. The hot spot stress can also be obtained through a finite element analysis using an extrapolation from stress values.

When performing a finite element analysis, stresses computed will be affected by both the geometric effects (as desired, since it will cause stress concentrations) and notch effects. In finite element modelling, typically at weld toe corners (notch), singularities may occur. The singularities refer to a high stress concentration but caused by computational modelling, not representing the actual stress at the weld toe. Therefore, this peak stress is discarded as the value itself and the hot spot stress is obtained by extrapolating stresses from points at a certain distance from the weld toe.

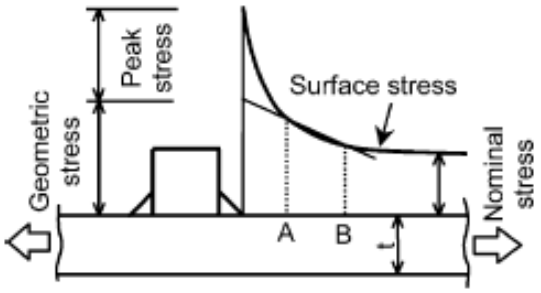

Figure 2-5 - Example of stress curve obtained through modelling [30]

2.4.2 Calculation Method

There are two methods most used for calculation of the hot-spot stress. The first one is through an extrapolation of normal stresses at the surface of the element while in the second method, the extrapolation is through the thickness of the plate.

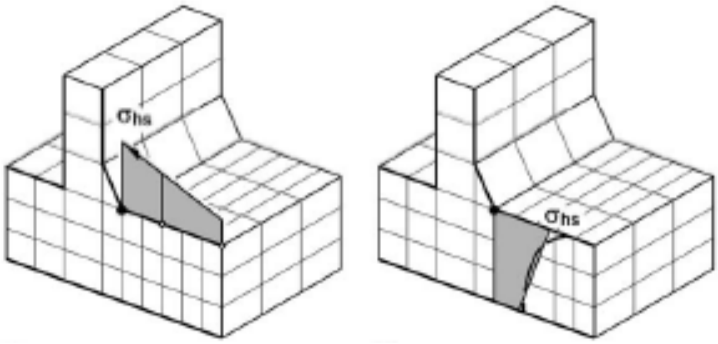

Figure 2-6 - Extrapolation at surface level (left) and through thickness (right) [12]

In this work, the extrapolation at surface level will be used by its standardized calculation through means of stipulated and regulated read out points. An extrapolation through thickness has to be made so that the tension and compression stress added or removed (from the original curve to the linearized curve) are equal in value to be considered adequate. As stated by Fricke and Kahl [11], an analysis through the thickness is considered to be more accurate than the surface extrapolation, however it is more complex and can be made only in solid elements.

In this project, the focus will be on surface level extrapolation, as shell element analysis is performed besides the solid element analysis. For a shell analysis, it is only possible to perform a surface extrapolation, as it does not consider a stress distribution across the thickness of the elements other than uniform value.

To extrapolate the value of the hot-spot stress, it is required to do so from two different points located at the surface or thickness to obtain an accurate stress that can be used. These points are defined in codes and guidelines. The IIW has given a recommendation for these points that need to be taken as follows:

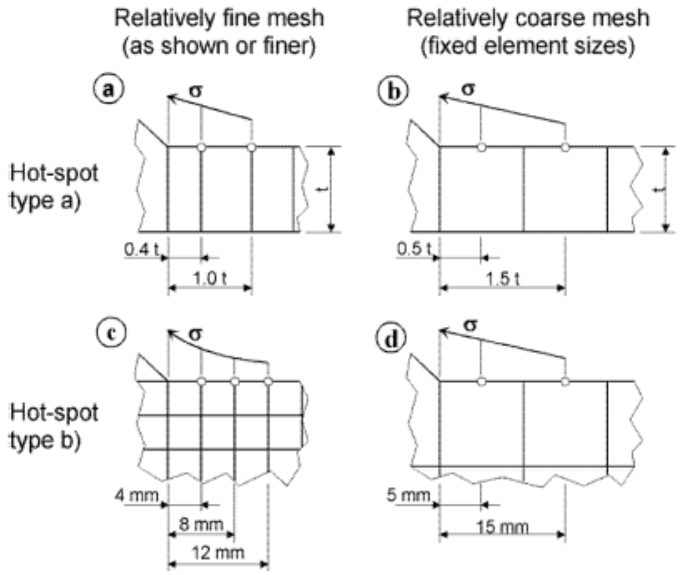

Figure 2-7 - Recommended extrapolation points [15]

Usually, a linear extrapolation through points at 0.5t and 1.5t is used when a coarse mesh is used, t is the thickness of the plate. In case of a fine mesh, points at 0.4t and 1.0t have been tested to also provide accurate results but the first case mentioned is recommended in different codes.

There are two different types of hot-spot stress, called type “a” and type “b”. Type “a” refers to when the stress distribution is dependent on the plate thickness and type “b” when the distribution does not depend on the plate thickness. In this project, type “a” hot-spot stress is used as the thickness of plates and stiffeners will influence the stress distribution over the elements.

Based on the previous figure, when using a coarse mesh the read out points are located at 0,5t and 1,5t, the hot-spot stress (extrapolated value) can be obtained through the following calculation:

$$\sigma_{hs} = 1.5 * \sigma_{0.5t} - 0.5 * \sigma_{1.5t}$$

It is to be noted that the IIW establish that for a coarse mesh, higher-order elements have to be used since reading values are at mid-side points. The software used (RFEM) does not model using higher-order elements, so the coarse mesh result is done to compare with the fine mesh result.

When using a fine mesh, the read out points are located at 0,4t and 1,0t, then the hot-spot stress is calculated by the following formula:

$$\sigma_{hs} = 1.67 * \sigma_{0.4t} - 0.67 * \sigma_{1.0t}$$

In these formulas, in the right-hand-side the sub-index of the stress components represents the location at which the stress has to be read.

A study performerd by Rong et al [25] has analyzed the effect of the weld toe radius on a rib-deck welded joint of an orthotropic steel deck for the surface stress on the rib. Through their modelling results, the following diagram was obtained:

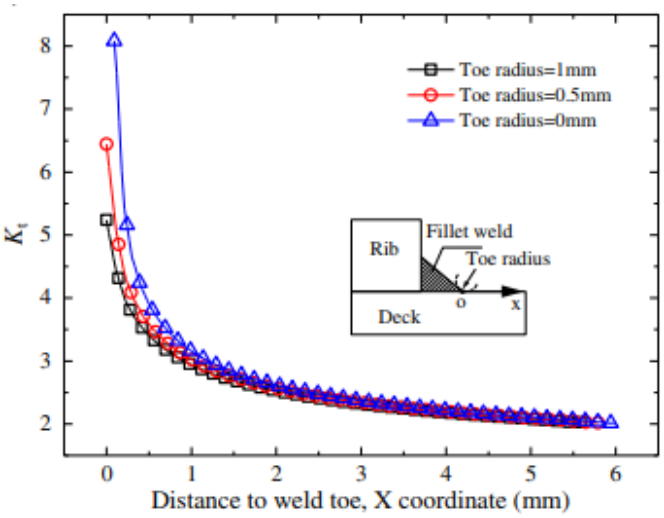

Figure 2-8 - Surface stress factor on the rib for different weld toe radius [26]

This study concluded that the most conservative case is when the analysis is performed with no weld toe radius, as the transition from the weld to the rib is less smooth in this case. The weld toe radius therefore also have an effect on the hot-spot stress accordingly, the critical case when there is no presence of a toe radius.

To corroborate the previous mention of the influence of weld toe radius, Xiao and Yamada [29] also performed a study of this influence in a cruciform welded joint, obtaining the following results:

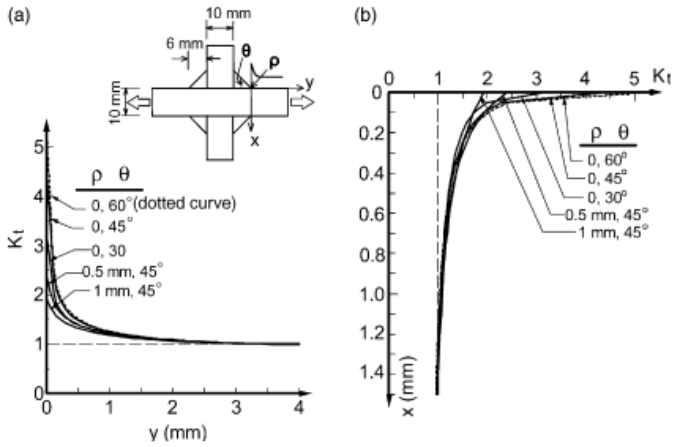

Figure 2-9 - Stresses distribution in weld toe region: (a) along surface; (b) through thickness [30]

This study focused on both extrapolation methods and confirmed as well that a weld toe radius of 0mm will yield the most unfavorable result (most conservative). Besides these two extrapolation methods, they [29] researched the 1-mm stress method approach. This method consists on obtaining the geometric stress just 1-mm below the weld toe, proving to have an advantage over the standard surface extrapolation as it has a better representation of size and thickness effect, taking a closer relation to the stress gradient around the weld toe. The results obtained through this method and the surface extrapolation are similar, as shown in the following table:

Test specimens	1 mm stress	HSS (0.4*t*, 1.0*t*)
In-plane gussets		
L–W (mm)[a]		Not applicable
50–200	1.517	(1.032)[b]
100–200	1.793	(1.845)[b]
200–200	2.164	(2.182)[b]
100–70	1.709	(1.745)[b]
100–100	1.776	(1.820)[b]
Out-of-plane gussets		
L–W–T (mm)[a]		
100–60–10	1.312	1.277
100–80–10	1.369	1.330
200–200–9	1.610	1.546
110–150–12	1.364	1.252
T- and H-attachments		
TN50	1.358	1.336
TN100	1.507	1.460
TN200	1.663	1.585
TS100	1.423	1.389
TS200	1.625	1.554
HN200	1.380	1.331
HS200	1.431	1.388

Table 2-7 - Stress factor comparison between 1-mm stress and surface extrapolation [30]

Due to the nature of this method, taking the stress 1-mm below the weld toe, this method is only applicable in finite element modelling through solid elements. Therefore, this method was decided to be excluded, since this thesis is aimed to compare fatigue analysis using shell elements and solid elements separately.

2.5 Finite Element Analysis

2.5.1 Introduction

A finite element analysis (FEA) consists in obtaining approximate solutions of certain problems in the area of engineering through computational means. This problem follows certain boundaries where different variables satisfy differential equations within certain conditions. These equations can be established using the degrees of freedom of an element (translational or rotational), by external conditions or by equilibrium of internal forces as well.

The problem is converted in a model in a software of interest, defining its geometry and the element type to be used, in this project, it will be a comparison between shell (2D) and solid (3D) elements. The properties of the elements are also defined and the external conditions (loadings) as well. Finally, a meshing of the model has to be done, this is to establish the size of the element of interest, considering that this influences the accuracy of the results as well, typically a finer mesh results in more accurate results. The reliability of the finite element methods will be directly related to a reasonable finite element mesh to yield a reasonable solution. This process has to be carefully done, otherwise if an incorrect input was realized, then the software's results will also be incorrect. The description of the model will be detailed in the modelling section.

In this project, two different finite element software will be used and a comparison between them will be made. These software are RFEM and ABAQUS. In these software, the stresses will be obtained at surface level of the elements in order to extrapolate the hot-spot stress, as mentioned in the previous section.

2.5.2 Shell and Solid Modelling

2.5.2.1 Shell Elements

A shell element consists of a 2D element representation of the element to be modelled. Shell analysis can be considered adequate when the dimension of the thickness is small compared to the other two dimensions of this element. If the thickness is not small compared to other dimensions, results may not be accurate as it may omit any influence through its thickness and therefore the use of solid elements is recommended.

The geometric shape of the elements can be triangular or rectangular. Each configuration has its benefit and disadvantage as well. Triangular elements are useful in more variety of shape of the complete element as it can fit in curved perimeters better than a rectangular shape can accomplish. The rectangular element has a higher node count than the triangular element,

considering that nodes are points where the analysis obtains values for its degrees of freedom, then a higher node count can provide a better approximation of result if done correctly. Triangular elements can be made of 3 nodes (one in each corner) or 6 nodes (3 more in mid-point in each side) which will be more accurate than its 3-noded equivalent. Same analysis can be made for a rectangular element, between a 4-noded element and an 8-noded element, similar as triangular elements. The 6-noded triangle and 8-noded rectangular are called higher-order elements, which are more complex and require higher amount of differential equations to solve in its analysis (higher amount of variables).

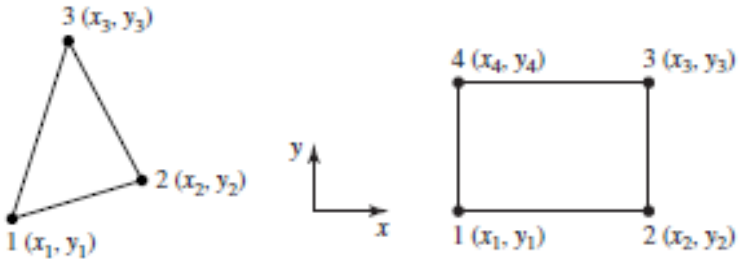

Figure 2-10 - Triangular and rectangular elements (3- and 4-noded) [17]

When realizing a model, higher-order elements include many internal nodes that sometimes are not easily connected to nodes of other elements when a mesh include different size configurations, then they are sometimes eliminated. When this elimination is done, the process is such that the mechanical effects that involved the internal nodes are taken into account by the external nodes, when a higher-order analysis is still desired and there is a possible limitation in software.

Both software used in this project involve 4-noded elements for their analysis, also since the elements in the detail are all rectangular, rectangular shape mesh is the most appropriate. When a fine mesh is used, these elements are considered to provide adequate accuracy.

2.5.2.2 Solid Elements

As a shell element is a 2D representation, solid elements are 3D representations of the elements to be modelled, it will provide more accurate results as the model is closer to the real detail. There are two main shapes, as in the 2D case, one based on extension of triangular elements and other on rectangular elements. The elements that are used in solid modelling are tetrahedrons and bricks (rectangular parallelopipeds). Tetrahedral elements correspond to 4-noded elements (or 10-noded elements as higher-order elements, similar as the shell elements), while bricks are 8-noded elements (20-noded as a higher-order element).

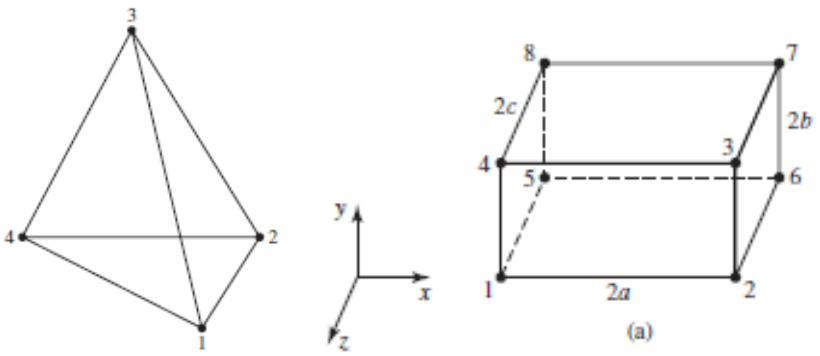

Figure 2-11 - Tetrahedral and Brick elements (4- and 8-noded) [17]

The choice of element is influenced by the geometry of the detail or structure to be modelled, as with shell elements. Due to the geometry of this project, brick elements will be used for the modelling as possible, with some variations to adapt posteriorly to the shape of the weld.

When realizing a mesh of a certain element with an irregular shape, it is recommended to use analyze properly the shape of the meshing done to the surface, both for shell and solid elements. The following figure gives an example of representing one surface by different elements; a) represents the geometry, b) triangular elements only, c) rectangular elements only and d) rectangular and quadrilateral:

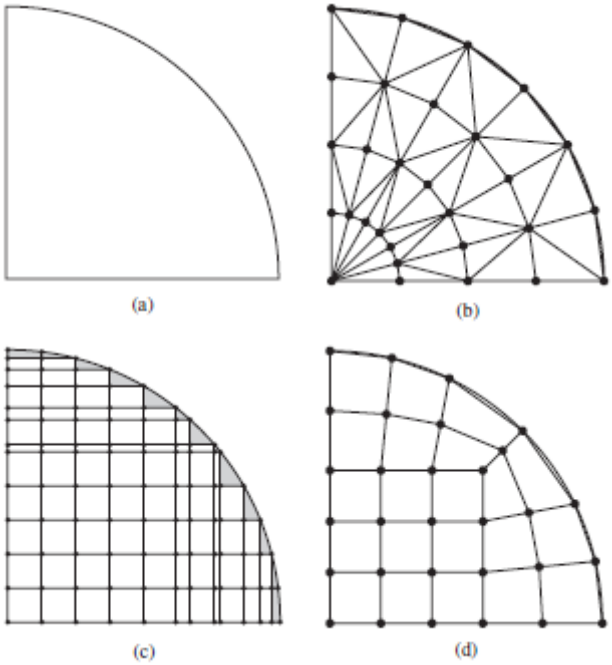

Figure 2-12 - Meshing of a surface [17]

It is observed in this figure, that while case b) allows for the best representation of the actual surface, it provides many slender elements near its inner part. For this, it is recommended the case d), where with quadrilateral elements, it is possible to represent as close as possible the curved surface. It is not advised to mix triangular elements with quadrilateral/rectangular elements (same for tetrahedral and brick elements) as these elements have different polynomial order representations in their variable field, while finite element formulation

consists of a continuous field across element boundaries. Conditions on derivatives on field variables are different in each element. A combination can be made, but due to this main difference, the accuracy of the result can be affected and decreased.

2.5.2.3 Differences

As explained previously, the shell element considers that the thickness will not influence the results, as it has a much lower dimension compared to the other dimensions of the element to be modelled. However, this may provide inadequate in some cases, solid elements are to be preferred. Solid elements take into account any variation through the thickness of the element, and as such it can provide more accurate results compared to its shell counterpart, though requiring larger software capacity. When performing a hot-spot stress analysis, two different methods were also mentioned, a surface extrapolation or through the thickness of the element. The choice of method will influence as well the decision of element to be considered for a finite element model. When modelling the weld, a solid element will provide also better and more accurate results than doing an approximation through shell elements with certain stiffness.

Another difference in use of shell and solid elements, is that when applying only shell elements result may differ from purely solid elements in the connections between the elements. A study performed by Osawa et al [21], it was proved that shell elements may provide higher curvature than solid elements in a connection or intersection between two elements. When realizing a model, transversal curvature of an element may be restrained by a certain factor by the element it is intersected by, when a solid element is taken into account. This is explained by the following figure:

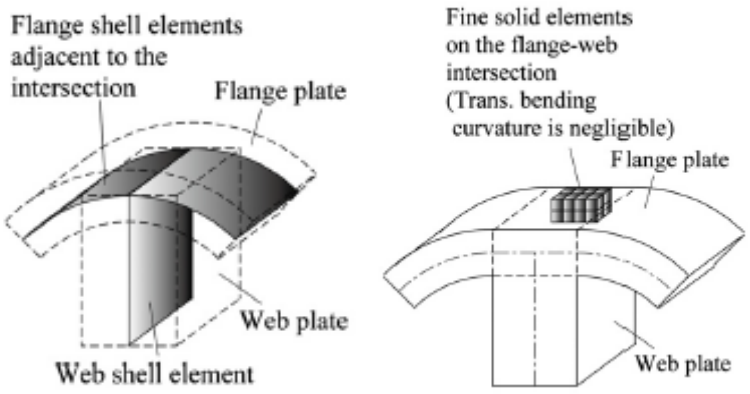

Figure 2-13 - Difference in curvature for shell and solid elements [21]

2.6 Influence of Welding

2.6.1 Introduction

As it is seen with different detail category classes, difference in stress concentration factors based on geometry and configuration, influence of any discontinuity in stress concentrations

or its distribution, welding also has an influence on the result of this stress concentration that will occur on this detail. This influence can be intrinsic in the process of welding itself, such as residual stresses that welding causes or any geometrical imperfections during welding, for which there is a quality check and tolerances. However it is also possible to influence this result also by improving the fatigue life of a weld through several methods of treatment, as long as the most likely method of failure is weld toe crack, which is the focus of this project, and not weld root crack.

2.6.2 Residual Stresses

Residual stresses occur in welded connections as a result from a heterogeneous plastic deformation that a weld will experience. These stresses can occur during the welding process, due to the thermal component in the process or introduced voluntarily for favorable situations. These are important since they may cause an adverse or beneficial effect on fatigue behavior of a welded detail. Tensile stress can have this adverse effect while compressive stress might improve fatigue resistance, when a crack is formed, tensile stress will cause growth of the crack while compressive stress may be able to prevent a growth in some cases.

These stresses may occur due to plastic deformation, because of the heating and cooling of the process itself. When welding is performed, the heating of the element is not uniform across the whole element, existing a gradient of temperature across its thickness. When steel is heated, the cooling process will also introduce residual stresses, due to inhomogeneous cooling and shrinkage of the material, the internal part of the material will cool slower than its surface and the internal crystal structure is affected by heating and cooling. The production of steel itself will also cause residual stresses when they are formed by cold working and machining, a plastic deformation is performed to obtain the desired element.

The detail categories presented by the Eurocode, and the fatigue classes by the IIW as well, already take into account the residuals stresses due to the welding process of the welded detail. Therefore it is possible to take the detail category directly, since this project is not focused on residual stresses but on the hot-spot stress of this welded detail.

2.6.3 Weld Imperfections

There are different types of imperfections that can alter the fatigue resistance of a welded detail. Some of these imperfections are volumetric and planar discontinuities, as well as imperfect shape of the weld.

Volumetric discontinuities refer to any pores inside the weld, such as gas pores formed during the welding process. These discontinuities also refer to any solid inclusions throughout the weld, such as slag, oxides or any other undesired metallic inclusions. The planar discontinuities refer to all imperfections involving cracks or similar (where there is a lack of weld), like a lack of penetration. The imperfect shape refers to any misalignment in the welded detail, linear or angular, as well as any undercut.

Among the effects that these imperfections cause, there may be an increase of general stress level due to the misalignment. Any imperfections may also cause local notch effect, which is a stress increase locally. These effects can be taken into account by formulae for stress magnification factors or by a fracture mechanics approach in crack initiation and propagation. Quality control plays an important role in execution in welding to avoid these effects as possible, also safety factors are used in order to implement these uncertainties in design and that affect the resistance of the element.

2.6.4 Improvement of Fatigue Life

There are several methods to improve fatigue life of a welded detail by realizing some modifications on the weld itself. These methods are in fact post-welding treatments, allowing to reduce stress concentrations at the location of the weld toes, reducing the risk of initiation and posterior propagation of a weld toe crack. Some of the methods that can be applied in a welded detail, which can be applied also in the detail of this project, are weld toe grinding, hammer peening and weld profiling as well.

Weld toe grinding is a method, as its name suggests, of grinding below any visible undercuts in the weld to increase as possible the fatigue life, by reducing any discontinuities that can produce higher stress concentrations. To have better performance for fatigue, it is recommended that the grinding is extended below the plate surface as to eliminate any defects present in the weld toe as well, rather than just grinding the weld. This treatment increases fatigue strength, though it is a minor increase. This method has an inconvenience though, it may extend the period in which crack initiation will start, however crack propagation would usually occur faster than if there was no grinding. A rotary burr is used for weld grinding, the shape of the weld post treatment is shown in the following figure:

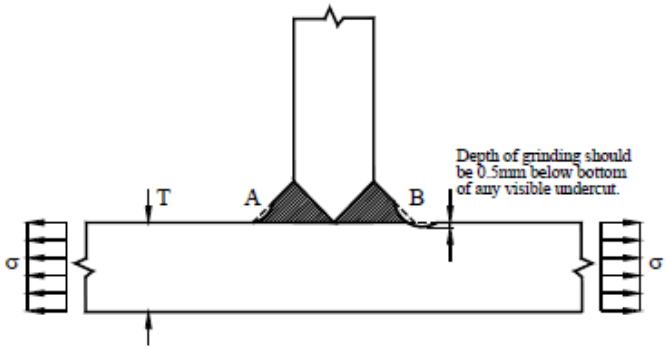

Figure 2-14 - Example of Weld Toe Grinding [6]

The method of hammer peening is done by deforming plastically the weld toe so a compressive residual stress can be introduced. This will negate tensile residual stresses caused by welding if they were present. This method is mainly used to counteract any present residual stresses caused during the process of welding.

Both weld grinding and hammer peening increase the fatigue strength of a joint, given by a factor to multiply with the fatigue class by which the joint is represented. In case of steel with

a yield value lower than 355MPa is used, the detail class can be taken with a factor of 1.3 (limited at FAT 112) and for equal or higher than 355MPa, a factor of 1.5 is used (limited at FAT 125), these factors are stated by the IIW.

Weld profiling consists in improving the shape of the surface of the weld to create a smoother transition between the two elements that are welded together. This shape can be obtained through machining or grinding of the weld, and the result is shown as the following figure illustrates:

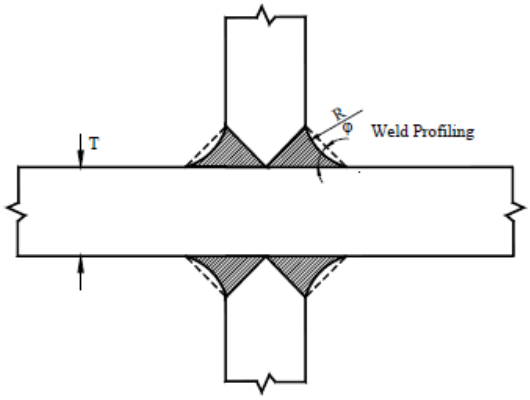

Figure 2-15 - Example of Weld Profiling [6]

By weld profiling, then the stress concentration at the weld toe is reduce due to this smoother transition, this new stress value will depend on the radius of the weld profiling as well as the angle between base metal and surface, as shown in previous figure. The fatigue life is increased by taking a lower stress concentration factor, creating also a lower stress at the weld toe. The reduced stress can be obtained through the following formula:

$$\sigma_{reduced} = \alpha * \sigma_{membrane} + \beta * \sigma_{bending}$$

Both α and β are values that will depend on the chosen profile for the weld, calculated using the following formulas:

$$\alpha = 0.47 + 0.17\,(\tan\varphi)^{0.25}(T/R)^{0.5}$$

$$\beta = 0.60 + 0.13\,(\tan\varphi)^{0.25}(T/R)^{0.5}$$

Chapter 3 – Global Modelling

3.1 Introduction

The global modelling was performed by the company Witteveen+Bos, where the rail track was modelled in RFEM using shell elements for its structure. This rail track is designed by a combination of plates and stiffeners welded together. Due to the nature of this bridge (movable), this rail track will experience cyclic loading during its service life. This will cause fatigue in the elements, therefore creating the need for verification against fatigue. Witteveen+Bos has performed a global model of the rail track, however there is no analysis using a local focus with the hot-spot stress approach method at the weld toe. This method is of importance to prove if the bridge would be safe against fatigue, as this focuses on crack initiation at the weld toe location.

The following figures shows the location of the rail track in the bridge and its detail.

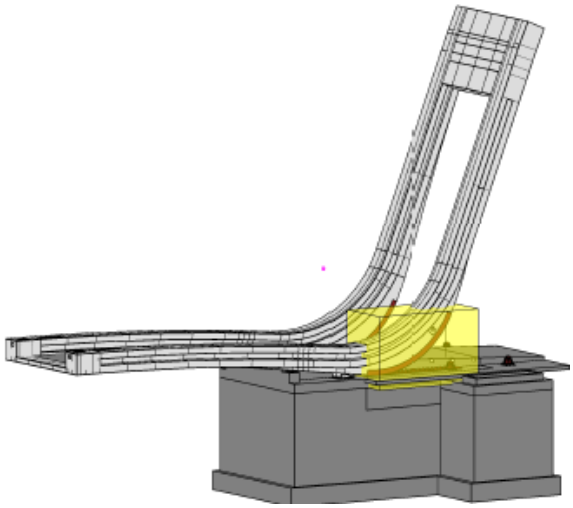

Figure 3-1 - Location of rail track in the bridge

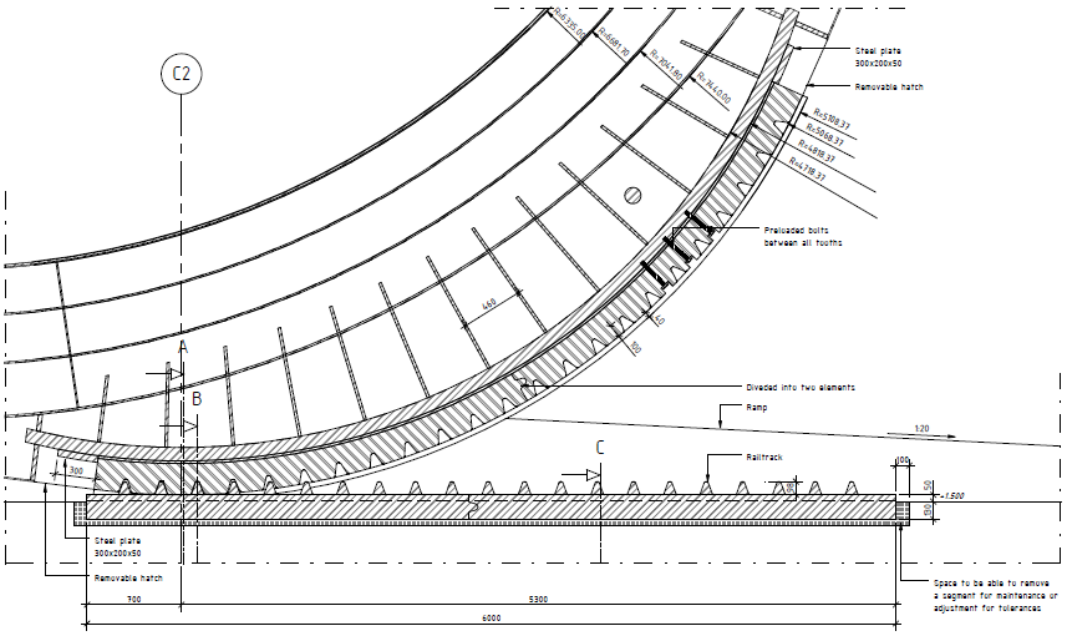

Figure 3-2 - Detail of rail track

The rail track consists of transversal stiffeners as shown in the figure and of three longitudinal stiffeners across its whole length, as it is shown on the following picture.

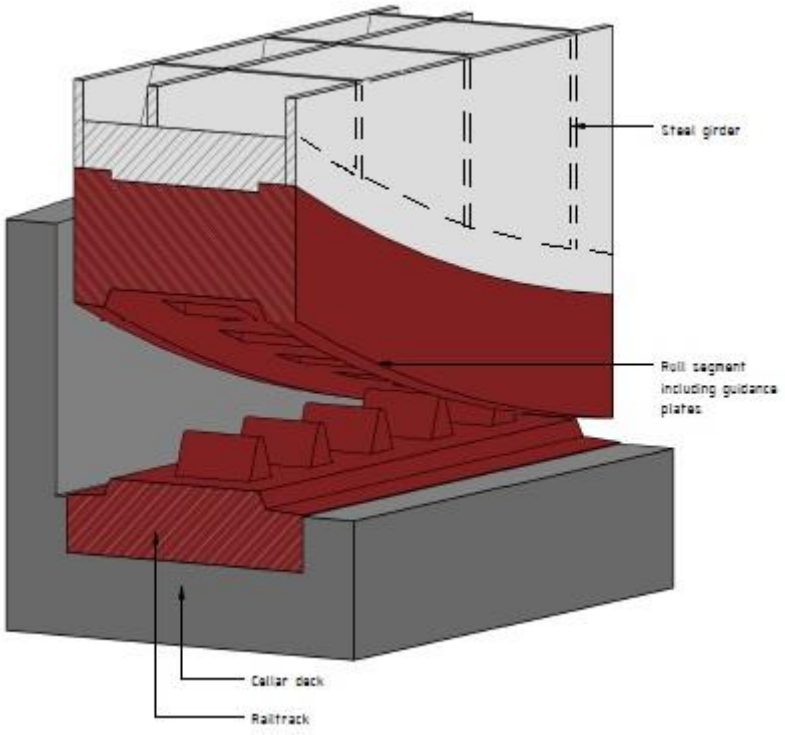

Figure 3-3 - 3D view of a section of the rail track

The model of the rail track looks as the following:

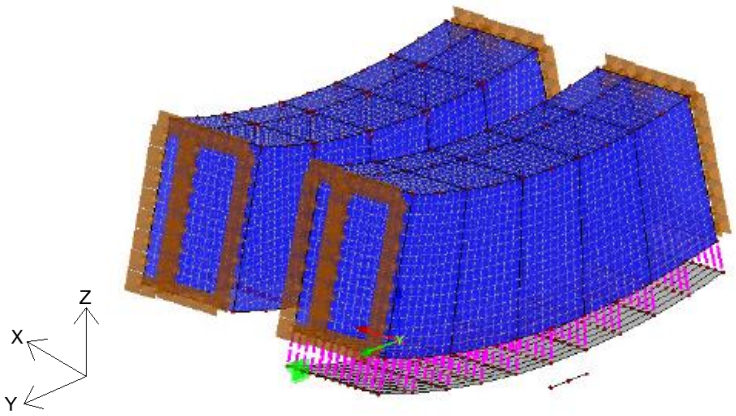

Figure 3-4 - Model of the rail track of the bridge

All elements of this structure (plates and stiffeners) are made with steel type S355. In Figure 3-4, the top plate has a thickness of 15mm, the longitudinal stiffeners are of 25mm while the transversal stiffeners are 20mm thick. The transversal stiffeners are located each 460mm, the longitudinal stiffeners are located at each side and one at 200mm from one side, a width of 600mm. There are two lower plates in this configuration, the upper one (at the top of the purple line of the drawings) is 100mm thick while the lower one has a thickness of 250mm. The radius of curvature is 5068mm. The maximum force is 1790 kN (characteristic value).

To obtain the contact stress and the contact area, the Hertz formula is used:

$$\sigma_{Hz}{}^2 = 0{,}35 * \frac{F_{Ed} * E * K}{b}$$

$$Where: \qquad E = 205000 \frac{N}{mm^2} \; ; K = \frac{1}{2R} = 9{,}866x10^{-5} mm^{-1}$$

$$F_{Ed} = 1790 \; kN = 1790000 \; N$$

$$b = 2 * 64 = 128mm \; (2 \; contact \; areas \; of \; 64mm \; width \; by \; design)$$

$$Then: \qquad \sigma_{Hz}{}^2 = 0{,}35 * \frac{1790000 * 205000 * 9{,}866x10^{-5}}{128}$$

$$\sigma_{Hz}{}^2 = 98993{,}4 \; N^2/mm^4$$

$$\sigma_{Hz} = 314{,}6 \; MPa$$

The maximum contact stress taken for local modelling is 314.6MPa (design value for fatigue used by Witteveen+Bos from Hertz formula), which will be taken for the load in the model. This stress transfers through two contact areas of 64mm width with an effective length, found as:

$$A_{eff} = b * L_{eff} = \frac{F_{Ed}}{\sigma_{Hz}}$$

$$L_{eff} = \frac{F_{Ed}}{\sigma_{Hz} * b} = \frac{1790000}{314{,}6 * 128}$$

$$L_{eff} = 44 \; mm$$

The contact stresses in the rail track (reactions) vary over the opening/closing angle of the bridge with two contact areas of 44mm x 64mm (determined by Witteveen+Bos as well). The following figure shows the location of these areas:

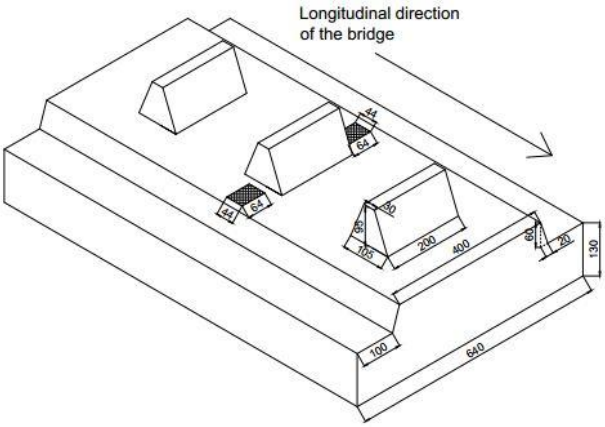

Figure 3-5 - Section of lower rail track showing two 44mmx64mm area

The purple lines (in Figure 3-4) represent a rigid element used in order to connect the shell elements that are used to model both plates, since they are in contact and there has to be a compatibility of deformations between them. At the sides, fully constrained supports are used to represent this track as enclosed by the bridge as designed. The load cases on this model represent the load imposed by the bridge under different angle openings. The forces are introduced linearly in the global model across the lower horizontal plate (linear load), while in local modelling, the force introduction is done locally and more focused (surface load). The linear load is obtained as:

$$q = \frac{F_{Ed}}{b_t} = \frac{1790kN}{0.6m} = 2983{,}3\,\frac{kN}{m}$$

This load is located across the 600mm width of the rail track and varies location (from one end of the track to the other) according to the angle of opening, from 0^o to 40^o.

3.2 Normal Stresses from Opening/Closing Loads

With this model, the stresses at the welds (full penetration welds) are found. Due to opening and closing of the bridge (different angle configurations), the results are as follows (complete results in Appendix A):

Opening angle	m_y (kNm/m)	n_y (kN/m)	t (mm)	σ_m (N/mm^2)	σ_n (N/mm^2)	σ_{n+m} (N/mm^2)	σ_{n-m} (N/mm^2)
0º	+0,20	+18	20	+3,0	+0,9	+3,9	-2,1
6º	+0,34	+32	20	+5,1	+1,6	+6,7	-3,5
11º	+0,62	-29	20	+9,3	-1,5	+7,9	-10,8
17º	+1,13	-299	20	+17,0	-15,0	+2,0	-31,9
23º	+0,15	-644	20	+2,3	-32,2	-30,0	-34,5
28º	-0,83	-253	20	-12,5	-12,7	-25,1	-0,2
34º	-0,34	-45	20	-5,1	-2,3	-7,4	+2,9
40º	-0,08	-9	20	-1,2	-0,5	-1,7	+0,8

Table 3-1 - Maximum fatigue stress (characteristic) in the welds due to opening/closing

Where $\sigma_n = \frac{n_y}{t}$ and $\sigma_m = \frac{m_y}{\frac{1}{6}t^2}$

The shear stress is neglected since it is a small value compared to the normal stress (axial and bending).

Under different opening angles of the bridge, we can observe that the stiffener experiences tension initially and compression afterwards. This is due to the location of the force related to the stiffener in the middle of the rail track, where the most critical scenario is located. When the location of the force approaches the stiffener of interest, the axial compressive force increases, reaching the highest when underneath the stiffener. The stress due to bending changes from tension to compression due to the force being located at different sides of the stiffener, bending the stiffener in the opposite direction as before.

With these results, the stress range for this joint is:

$$\Delta\sigma = +7{,}9 - (-30{,}0) = 37{,}9\ MPa$$

The estimated number of cycles during the lifetime of the bridge is n = 365000 cycles.

Converting the acting stress to an equivalent stress for $N_E = 2x10^6$ cycles (m=3), we obtain $\sigma_{E,2}$:

$$\sigma_{E,2} = \Delta\sigma * \left(\frac{n}{N_E}\right)^{1/m}$$

$$\sigma_{E,2} = 37{,}9 * \left(\frac{365000}{2x10^6}\right)^{\frac{1}{3}} = 21{,}5MPa$$

Load factor of 1 and safety factor of 1.35 (high consequence and safe life) are used. Remembering that the detail category considered taken from the Eurocode 3 is detail category class of 63MPa, then the unity check is:

$$U.C. = \frac{\gamma_{Ff} * \sigma_{E,2}}{\frac{\Delta\sigma_C}{\gamma_{Mf}}}$$

$$U.C. = \frac{1.0 * 21{,}5}{\frac{63}{1{,}35}} = 0{,}46$$

Under this analysis, the weld will not have any problem against fatigue during the estimated number of cycles based on the lifetime of the bridge.

3.3 Normal Stresses from Wind Loads

The stresses at the welds due to wind have also been obtained in the global analysis. The wind load has taken in consideration a spectrum with different wind velocities (for different stresses) and their respective estimated number of occurrences. The following table provides those results:

n	m_y min (kNm/m)	m_y max (kNm/m)	n_y min (kN/m)	n_y max (kN/m)	σ_{n+m} max (N/mm^2)	σ_{n+m} min (N/mm^2)	$\Delta\sigma$ (N/mm^2)
2	+0,49	+1,41	-1188	-433	-0,5	-52,1	51,6
20	+0,58	+1,34	-1117	-492	-4,5	-47,2	42,7
200	+0,66	+1,29	-1059	-553	-8,3	-43,1	34,8
2000	+0,74	+1,24	-1002	-601	-11,5	-39,0	27,6
2x10^5	+0,79	+1,19	-947	-637	-14,0	-35,5	21,5
2x10^6	+0,86	+1,16	-903	-684	-16,8	-32,3	15,5
2x10^7	+0,91	+1,12	-862	-707	-18,6	-29,5	10,9
2x10^8	+0,96	+1,10	-832	-741	-20,6	-27,2	6,7

Table 3-2 - Stress range in the welds due to wind loads

By using the previous formula, it is possible to calculate the number of cycles N_R for the detail category of $\Delta\sigma_C = 63\ MPa$ ($N_E = 2x10^6$). The formula is then:

$$N_R = N_E * \left(\frac{\Delta\sigma_C}{\Delta\sigma}\right)^m$$

Wind has a variable spectrum, therefore both m=3 and m=5 have to be used, for higher stresses than $\Delta\sigma_C$ and lower stresses respectively. The wind spectrum was obtained through Eurocode 1 Part 1-4 Wind Actions [9]. Using the values given of $\Delta\sigma_C$ and N_E, the following results are found for the wind case using Palmgren-Miner's rule:

n	$\Delta\sigma$ (N/mm^2)	N_R	D
2	51,6	5,43x10^6	0,00000
20	42,7	1,40x10^7	0,00000
200	34,8	3,89x10^7	0,00001
2000	27,6	1,24x10^8	0,00002
2x10^4	21,5	∞	0,00000
2x10^5	15,5	∞	0,00000
2x10^6	10,9	∞	0,00000
2x10^7	6,7	∞	0,00000
			0,00003

Table 3-3 - Fatigue cumulative damage D calculation for wind load

The cumulative damage D is 0,0005 due to wind loads. Since this value is extremely close to 0 and knowing that a value of 1 is taken as the case of failure, for this joint in this bridge, only the stress variation given by the opening/closing mechanism of the bridge is taken in

consideration. The forces caused by opening/closing are the ones to be considered on the local analysis.

Chapter 4 – Local Modelling

4.1 Model Preparation

In the global modelling, the complete rail track is taken for the model, but due to its dimensions, it is not possible to do a focused analysis on a specific joint (a local approach). The local model will be focused on the plate stiffener welded connection in the upper rail track of the bridge. The detail of the joint (horizontal plates - vertical stiffeners) in the bridge can be seen in the following figure:

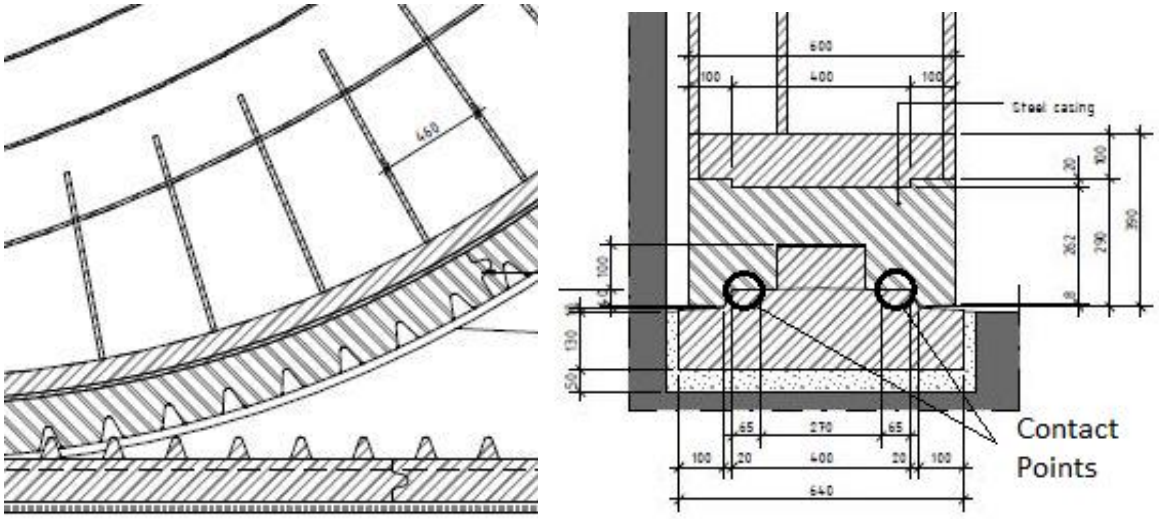

Figure 4-1 - Longitudinal and transversal cross section of the rail track

The highest stress will be caused at the location of the reaction, which will be experienced at each support point when rotating the bridge. This reaction is produced through contact stresses located just at both sides of the studs of the rail track. The following figure shows a simplified look of the upper rail track of the bridge.

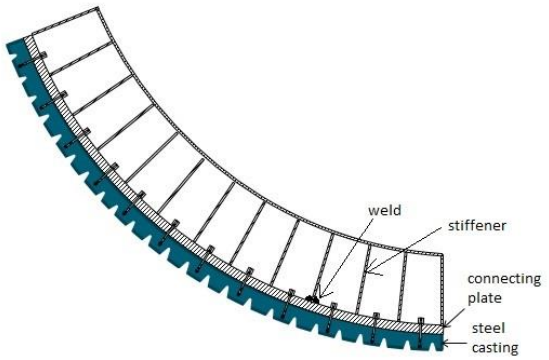

Figure 4-2 – Upper rail track where the plates and stiffeners are shown

This stress will then be distributed through the casted element towards the steel connecting plate and a uniform stress is assumed at the connecting plate. The area of influence will be

through the whole width and from mid-spans between the transversal stiffeners. The reactions, and stresses, were given from the modelling of the bridge, this load will then be taken as load for the local modelling for the joint. The maximum stress is taken in consideration by taking the highest reaction force from the reactions on all opening angles. This maximum was at the position of the hinge, located in the middle of the segment. This stress is taken as the critical case for the analysis.

The maximum contact stress taken for local modelling is 314.6MPa, as mentioned in Chapter 3, which will be taken for the load in the model. Only this will be taken as this will create the maximum stress range being the maximum stress acting on the joint. As the location where this stress occurs also varies with the motion of the bridge, the configuration of the model will be different accordingly (the location of the stress and the transversal stiffener may differ). However the first case is taken into account because this position gives the highest stress possible. The considered position is located directly under a stiffener, which will cause the highest stress concentration in that area.

All welds are designed identically, all of them as full penetration welds, so this configuration will be critical for the weld on this transversal stiffener. Other configurations may be critical on other welds, but those would be for load cases with lower loads. Therefore they will not be the critical cases for a fatigue analysis. Our analysis consists of taking the configuration under the critical case scenario, then if the weld (most critical one) is acceptable under fatigue, then the others are acceptable as well as they experience a lower stress range. This assumption is based on that its results will be a conservative approximation by having taken the critical weld under a critical load configuration.

The before mentioned contact areas provide the contact between the upper part of the rail track (where the joint is located) with the lower part of the rail track (ground level). The highest contact stress occurs at the middle of the track (opening angle of 23°), at a value of 314.6MPa, as mentioned before. The location is at the sides of the studs of the rail tracks, it can be seen in the following picture from the lower rail track:

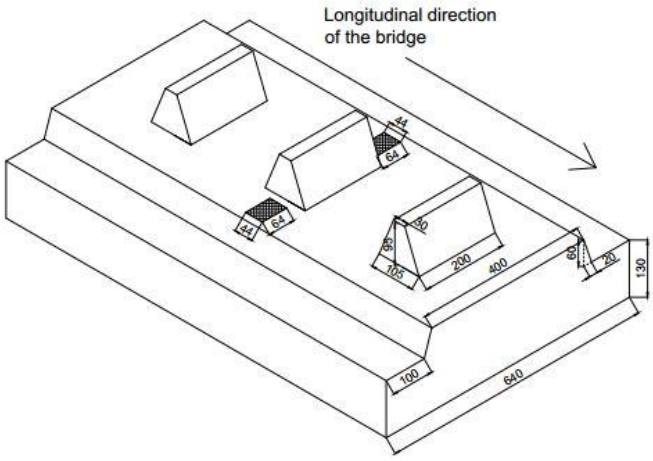

Figure 4-3 - Section of lower rail track showing two 44mmx64mm area

The supports of this model are located on the upper part of the stiffeners, since the analysis is made by taking the reaction forces as our load case. These are modelled as rigid supports, since all stiffeners are encased in the bridge (design choice), taking this as an assumption that rigid supports are a reasonable approach for a localized model. The lower plate has a thickness of 250mm while the upper plate is 100mm. The longitudinal stiffeners have a thickness of 25mm while the transversal stiffeners are 20mm thick. The following picture describes the joint using the upper plate of 100mm only. The models are taken under the assumption that there is no misalignments in the structural detail.

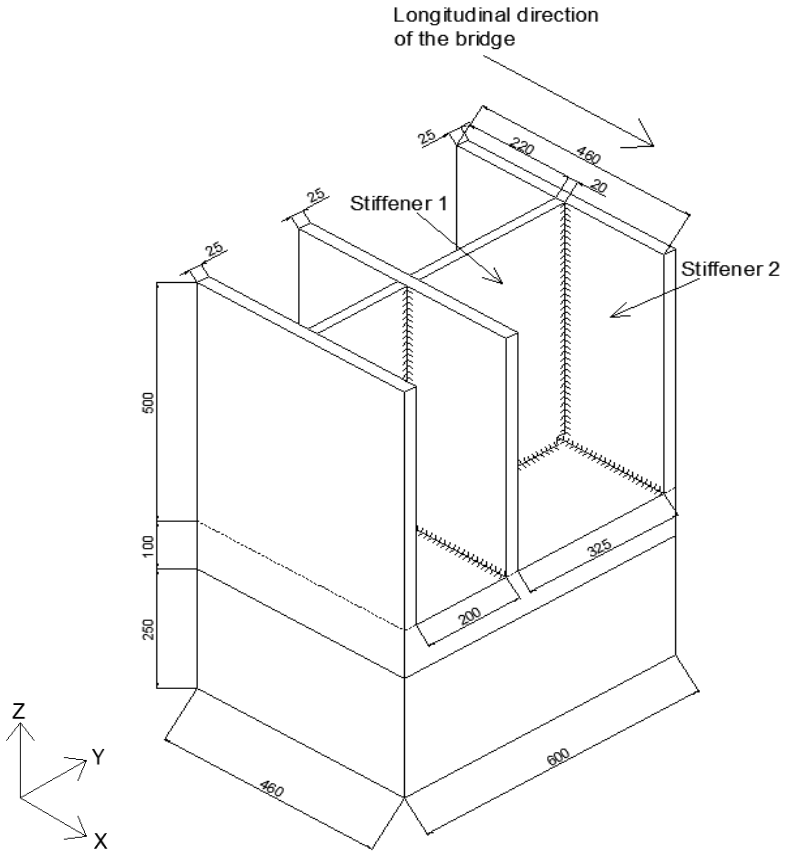

Figure 4-4 - Detail to be modelled

As seen in Figure 4-4, the transversal stiffener (20mm) will be called stiffener 1 and the longitudinal stiffener (25mm) will be referred as stiffener 2.

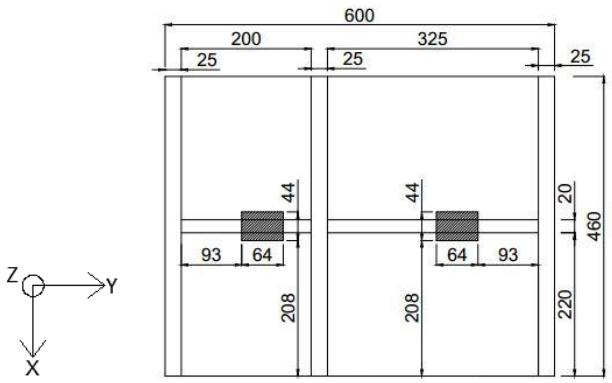

Figure 4-5 - Top view of the detail (shadow represents the locations of the forces)

The calculation of the hot-spot stress is performed on the stiffeners, through surface extrapolation of the stresses at two read-out points (A and B) established by the IIW. The following figure shows the extrapolation done on the stiffener of the detail of the rail track:

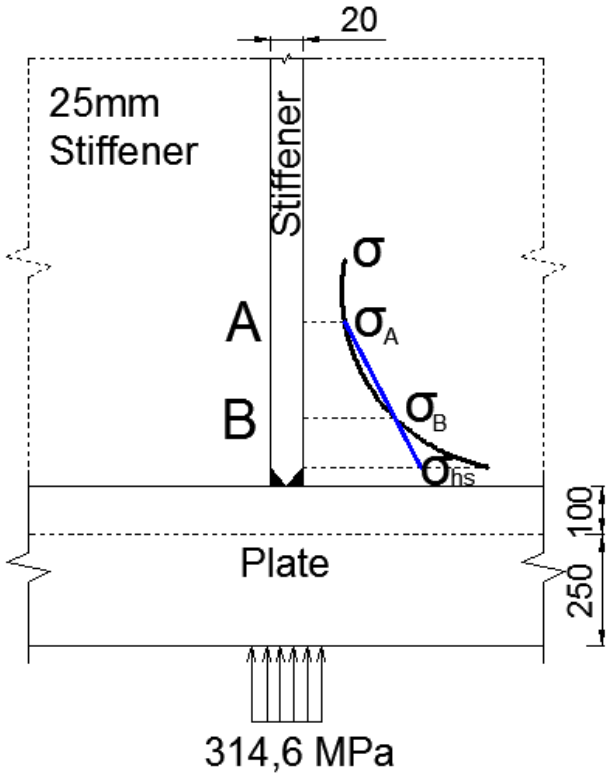

Figure 4-6 - Surface extrapolation of hot-spot stress from points A and B

The read-out points A and B are located at 1.5t and 0.5t respectively from the weld toe when performing the extrapolation on a coarse mesh and located at 1.0t and 0.4t when it is a fine mesh. Based on these two points, the extrapolation is performed up to the weld toe, where the hot-spot stress is calculated.

4.2 Local Shell Modelling

The contact stress is distributed through a thick rigid steel casted plate (250mm thick) towards the steel connecting plate (100mm thick), tightly bolted together. These plates are in contact through their length (design assumption) so they have the same deformations and stress configurations (deformation compatibility). Under this assumption, a rigid element is modelled that will connect both plates together under the shell analysis, to take into account both plates for the load distribution across the joint (when modelled). In this shell analysis, welds are not modelled, as it is not inside the scope of this project. The following picture represents the utilization of the rigid elements.

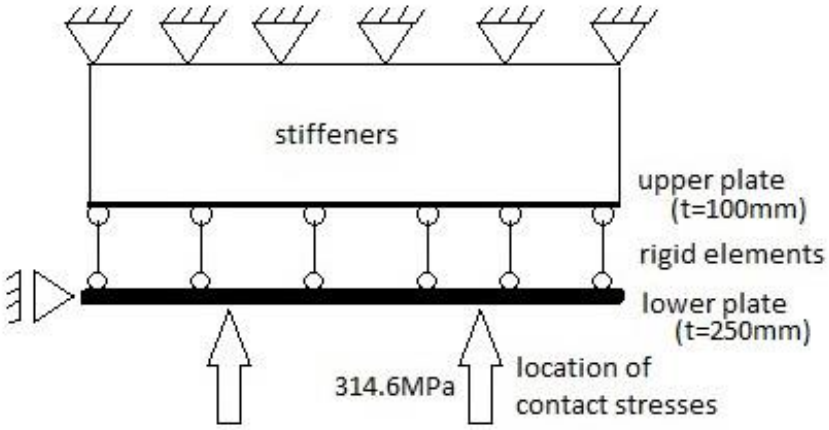

Figure 4-7 - Sketch of rigid elements that connect both plates together for the model

These elements will transmit deformations/stresses from the lower plate to the upper plate directly, hence the hinges of these elements are only constrained for rotation around the y and z axis (transverse axes) since the plates are connected together. The other degrees of freedom are set free so there will be deformation compatibility between these plates. This type of hinge is chosen to avoid influencing stresses on the plates, in order to transmit directly (unmodified) the whole load/stress composition from the lower plate to the upper plate. Since the lower plate is not supported with the support of the upper plate, instability will occur when modelling; to solve this, a translational support will be provided to allow stability in the model.

The model has to be refined to be able to have reasonable configurations of stress distributions, deformations from elements and compatibility between them as well as having an adequate mesh size in the model for adequate results. Initially, 100mm separation between the rigid elements were taken to analyze the load distribution across elements, however it caused peaks at these points, which are not reasonable considering that the elements are in contact across their surface (initial assumption from design). Then these separation were shortened to 50mm and finally to 20mm which provided a reasonable distribution across the surface without creating concentrated values or peaks due to these elements.

The mesh dimensions were done similarly, taking initially 50mm mesh size for the lower and upper plates, having both 250mm and 100mm thickness respectively. However this is not adequate for the stiffeners which are of 20 and 25mm thick. Then a mesh refinement is taken to have at least the mesh size of equal the thickness of the element, according to the definition of a coarse mesh. This was taken to obtain an initial result of the model and then a refinement was made to have a finer mesh size, which can give more accurate results than when realizing a coarse mesh. The finer mesh was taken as 0.4t (t being thickness) which is the upper limit for a definition of a fine mesh when doing hot spot stress calculations. Then an additional model was done where the mesh refinement of the stiffeners was up to 5mm. Using these final refinement, results will yield with higher accuracy and a more reasonable stress distribution.

Several models were made in order to obtain all these configurations for a posterior analysis of results, which will be performed on chapter 5 of this project. All results of these models are

present in the Annex B. The following table shows a detail of the difference between each of the models (set-ups):

No. Model	Mesh size (mm)	Distribution of rigid elements (mm)	Mesh refinement	Mesh size (mm)
1	50	115 x 100	No	/
2	20	115 x 100	No	/
3	50	50 x 50	No	/
4	20	50 x 50	No	/
5	50	20 x 20	Yes	20 – plates
6	20	20 x 20	No	/
7	20	20 x 20	Yes	10 – stiffeners
8	20	20 x 20	Yes	10 – longtidunal stiffener 8 – transversal stiffener
9	20	20 x 20	Yes	5 – all stiffeners

Table 4-1 - Detail of meshing and distribution of RFEM shell models

Based on the results of the hot-spot stresses, we can observe that the transversal stiffener shows almost no difference of hot-spot stress with the stress obtained directly from the model. This may be caused by having the concentrated load directly under the transversal stiffener. So a new configuration was taken to observe how the hot-spot stress varies on this specific stiffener. This configuration is for a slight rotation of the opening angle, where the contact is located on the area in between two transversal stiffeners instead of directly underneath them (which was the highest reaction force). By having a small variation of distances (which would be a small variation of opening angle), the same force was taken for this model. There we can see the difference of the stress distribution and how the hot-spot stress is calculated in that area.

This is called Model 10, under this new configuration, it presents with a 20mm mesh, with 5mm mesh refinement on the stiffeners with the rigid elements distributed over 20x20mm configuration. The following figure shows an example of this configuration:

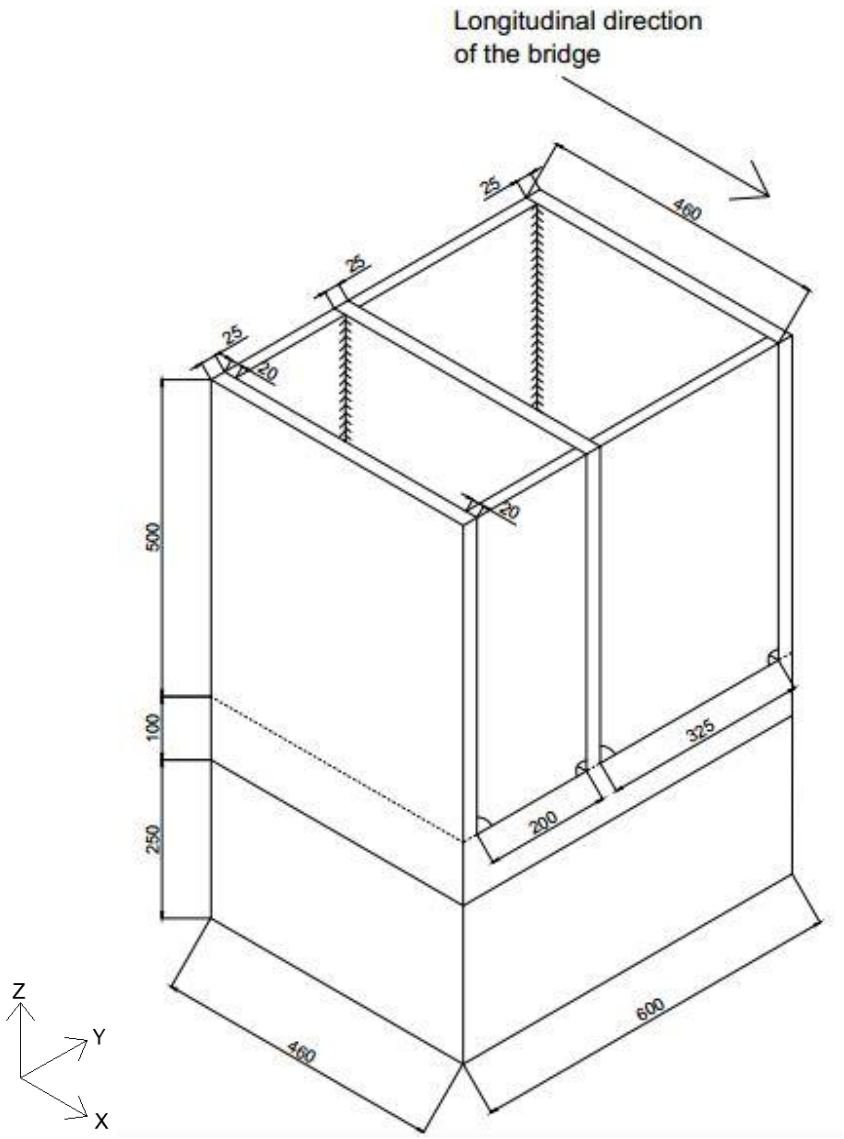

Figure 4-8 - New configuration of model, load located mid-section

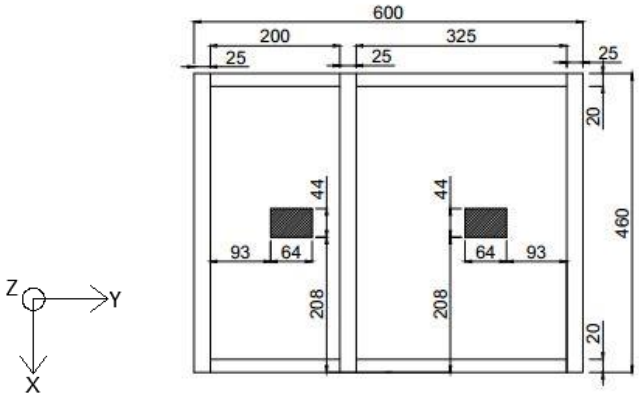

Figure 4-9 - Top view of the detail (shadow represents the locations of the forces)

4.3 Local Solid Modelling

For solid modelling, there was an inconvenience with a limitation of the version used of the software RFEM. This version had a limited capacity, therefore only a coarse mesh was taken for the stiffeners and welds, though is not as accurate as when fine meshing is used. For appropriate results, stiffeners and welds should be modelled with a fine mesh (and welds much finer than the stiffeners). The fine mesh analysis was done through the ABAQUS software, having a higher capacity than RFEM. This analysis of this fine mesh with ABAQUS is performed in Chapter 6.

Chapter 5 – Discussion of Results

After the model preparation described on the previous chapter, this chapter will focus on presenting the results of the respective modelling as well as their analysis. The objective of this analysis is to obtain the hot-spot stress on the stiffeners from the extrapolation method on the surface as explained on chapter 2.

5.1 Mesh Refinement in Modelling

For shell modelling, 10 models were explained previously, the first 5 models were implemented in order to ascertain an adequate meshing and distribution on the model to obtain possible realistic results. It was seen that in these models, there were peak stress concentrations across the horizontal plates due to the distribution of the rigid elements that connected both plates, which is not realistic when both plates are in constant contact. The mesh size was also not adequate (50mm at this point) since it caused also high variation across this distance with the rigid elements. From model 6 onwards, both meshing of the plates and distribution of these elements were at 20mm.

The following figure shows the model 6, with a mesh of 20mm across all elements:

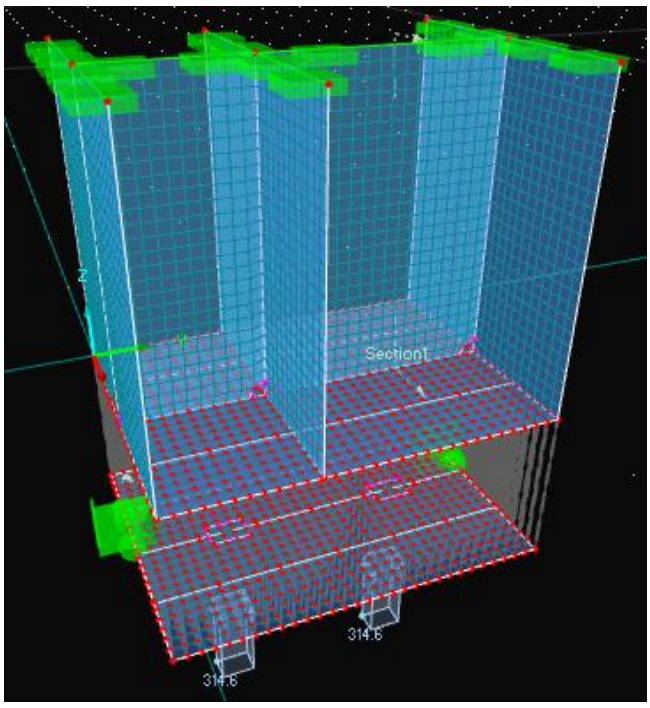

Figure 5-1 - Finite element model of the detail

This figure is also representative for models 7 to 9, where the only difference is the mesh refinement made on the stiffeners, as mentioned in Table 4-1. The mesh refinement is done in order to obtain what is considered a fine mesh, instead of the coarse mesh, which is shown in this figure. When an analysis is performed with a finer mesh, the results are more accurate as more nodes are established which are the points of calculation in a finite element analysis.

For solid modelling, only a coarse mesh was used due to the capacity of the used version of RFEM. A mesh refinement is necessary to be able to model with a reliable mesh size, which is a fine mesh. For this situation, the software ABAQUS was used to model appropriately this mesh, with a version that has the capacity needed for this type of model with a higher number of elements.

5.2 Shell Elements in Modelling

This section will be focused to show the results of the finite element modelling and the hot-spot stress and stress concentration factor will be calculated for each model situation.

In the models, the internal forces ny (axial component), my (bending component) and mxy (shear component) were obtained for the critical cases (highest stresses). By comparing the stresses on the plates and the stiffeners, the stiffeners were subjected to higher stresses than the plates, the focus will be therefore on the stiffeners. Due to the distribution of the stiffeners, there are also critical stiffeners, two stiffeners will be taken in consideration, one for 20mm stiffeners and the other for the 25mm stiffeners. The following figure shows the distribution of internal axial forces in the element:

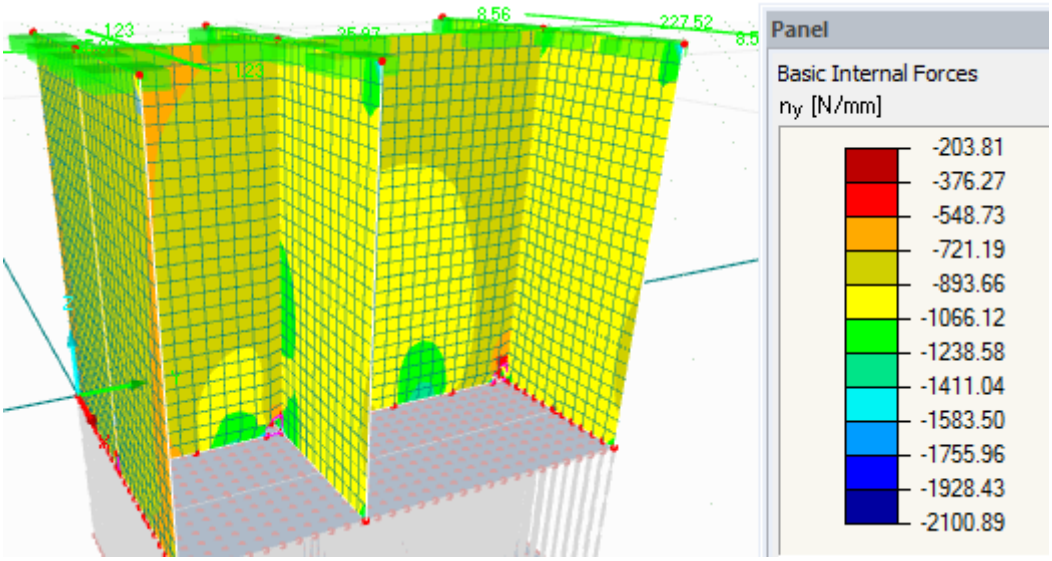

Figure 5-2 - Internal forces ny (axial) on stiffeners

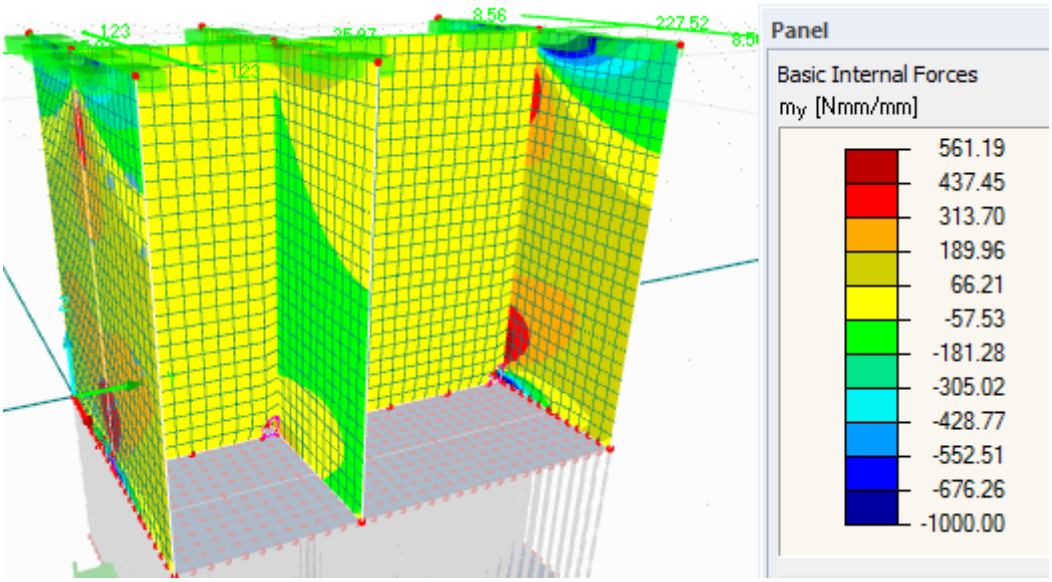

Figure 5-3 - Internal forces my (bending) on stiffeners

Due to the values of this model (and all following models as well), it can be seen that both most right stiffeners (one longitudinal and one transversal) represent the critical case, these two stiffeners will be taken into account to show all results.

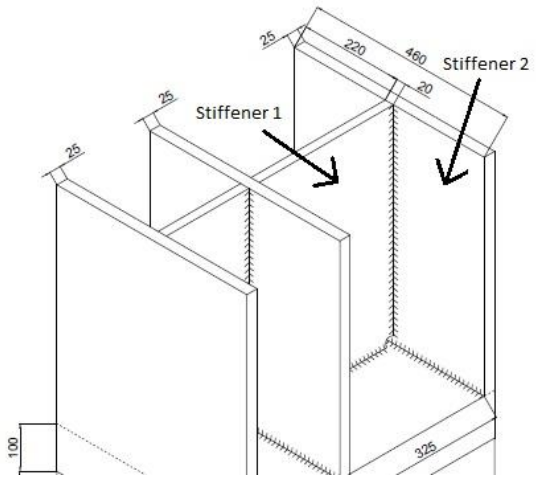

Figure 5-4 - Critical stiffener 1 (transversal) and 2 (longitudinal)

All results will be already tabulated in this chapter, while the respective model result of each stiffener will be shown in Appendix B.

The stresses will be obtained through the following formulas:

$$\text{Axial stress } \sigma_n = \frac{n_y}{t}$$

$$\text{Bending stress } \sigma_m = \frac{m_y}{\frac{1}{6}t^2}$$

$$\text{Shear stress } \tau_{xy} = \frac{m_{xy}}{\frac{1}{6}t^2}$$

The following table shows the calculated stresses for the stiffener 1 in model 6:

Distance (mm)	ny (N/mm)	my (Nmm/mm)	mxy (Nmm/mm)	σn (MPa)	σm (MPa)	σn+m (MPa)	τxy (MPa)
0	-1360,3	0,64	0,04	-68,02	0,01	-68,0	0,00
20	-1261,1	0,22	0,01	-63,06	0,00	-63,1	0,00
40	-1187,4	0,06	-0,01	-59,37	0,00	-59,4	0,00
60	-1126,3	0,03	-0,01	-56,32	0,00	-56,3	0,00
80	-1076,4	0,01	-0,01	-53,82	0,00	-53,8	0,00
100	-1037,9	0,01	0,00	-51,89	0,00	-51,9	0,00
120	-1008,2	0,00	0,00	-50,41	0,00	-50,4	0,00
150	-974,3	0,00	0,00	-48,71	0,00	-48,7	0,00
200	-932,3	0,00	0,00	-46,61	0,00	-46,6	0,00
250	-903,6	0,00	0,00	-45,18	0,00	-45,2	0,00
300	-882,8	0,00	0,00	-44,14	0,00	-44,1	0,00
400	-852,0	0,00	0,00	-42,60	0,00	-42,6	0,00

Table 5-1 - Normal and shear stresses on stiffener 1 (Model 6)

As it can be seen in this table (and following tables), the shear stress can be neglected in calculations compared to the normal stresses, also taking in consideration that the hot-spot stress is obtained through calculation of the normal stresses.

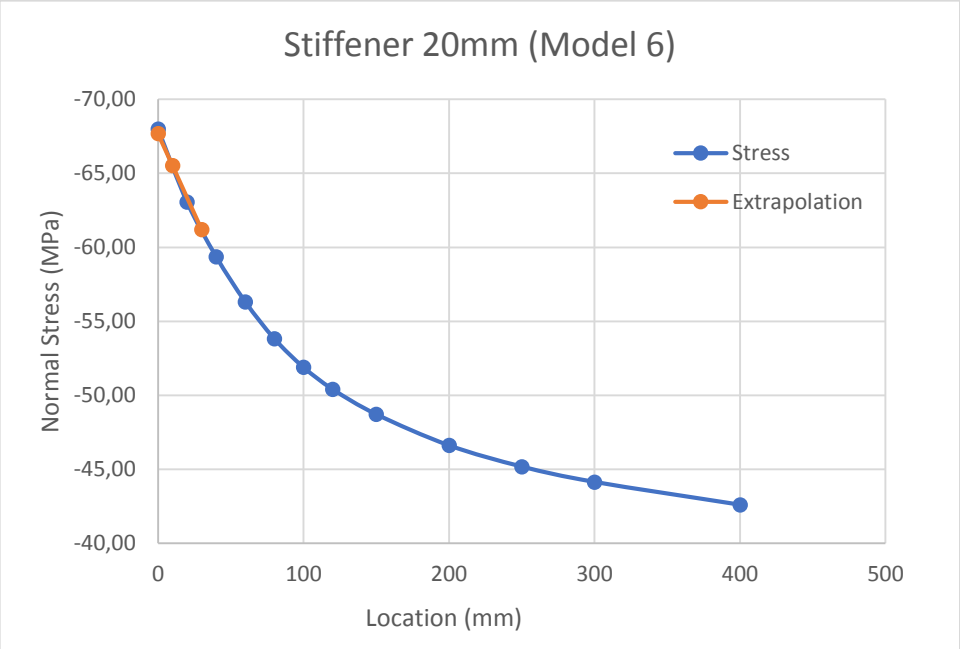

Figure 5-5 - Normal stresses on stiffener 1 and hot-spot extrapolation (Model 6)

To obtain the hot-spot stress through extrapolation, the IIW code is used (as explained in chapter 2), where the read out points are located 0,5t and 1,5t (t=thickness) away from the stiffener, then extrapolated to the same location of the stiffener-plate connection (0mm away) when there is no weld modelling. For a coarse mesh, the calculation of the hot-spot stress is the following:

$$\sigma_{hs} = 1.5 * \sigma_{0.5t} - 0.5 * \sigma_{1.5t}$$

Location	Distance (mm)	Stress (MPa)
Plate	0	-67,7
0,5 t	10	-65,5
1,5 t	30	-61,2

Table 5-2 - Extrapolation for calculation of hot-spot stress

From this table, we can obtain that the hot-spot stress is of -67,7 MPa.

The following results and calculations represent the values for the stiffener 2 on Model 6.

Distance (mm)	ny (N/mm)	my (Nmm/mm)	mxy (Nmm/mm)	σn (MPa)	σm (MPa)	σn+m (MPa)	τxy (MPa)
0	-1114,9	-951,2	142,4	-44,59	-9,13	-53,7	1,37
25	-1029,3	118,3	58,5	-41,17	1,14	-40,0	0,56
50	-963,7	417,6	43,7	-38,55	4,01	-34,5	0,42
75	-943,7	456,4	-29,8	-37,75	4,38	-33,4	-0,29
100	-946,2	423,8	-37,9	-37,85	4,07	-33,8	-0,36
125	-954,4	364,9	-36,6	-38,17	3,50	-34,7	-0,35

Table 5-3 - Normal and shear stresses on stiffener 2 (Model 6)

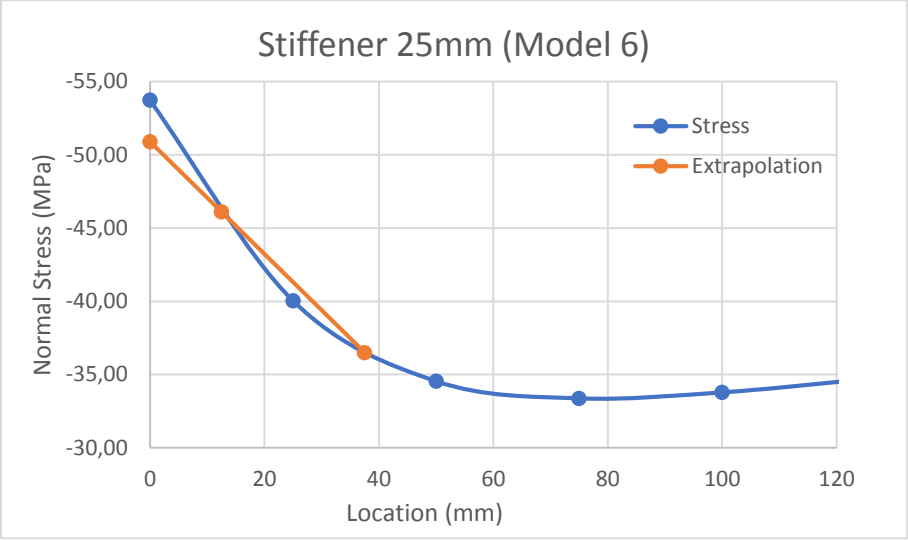

Figure 5-6 - Normal stresses on stiffener 2 and hot-spot extrapolation (Model 6)

Location	Distance (mm)	Stress (MPa)
Plate	0	-50,9
0,5 t	12,5	-46,1
1,5 t	37,5	-36,5

Table 5-4 - Extrapolation for calculation of hot-spot stress

From this table, we can obtain that the hot-spot stress is of -50,9 MPa.

The following results and calculations represent the values for the stiffener 1 on Model 7.

Distance (mm)	ny (N/mm)	my (Nmm/mm)	mxy (Nmm/mm)	σn (MPa)	σm (MPa)	σn+m (MPa)	τxy (MPa)
0	-1349,3	0,70	0,00	-67,47	0,01	-67,5	0,00
10	-1303,1	0,40	0,00	-65,16	0,01	-65,2	0,00
20	-1263,8	0,20	0,00	-63,19	0,00	-63,2	0,00
30	-1224,2	0,10	0,00	-61,21	0,00	-61,2	0,00
40	-1188,1	0,10	0,00	-59,41	0,00	-59,4	0,00
50	-1156,9	0,10	0,00	-57,85	0,00	-57,8	0,00
60	-1131,1	0,00	0,00	-56,56	0,00	-56,6	0,00
70	-1105,8	0,00	0,00	-55,29	0,00	-55,3	0,00
100	-1051,9	0,00	0,00	-52,60	0,00	-52,6	0,00
150	-992,8	0,00	0,00	-49,64	0,00	-49,6	0,00
200	-955,6	0,00	0,00	-47,78	0,00	-47, 8	0,00
250	-928,7	0,00	0,00	-46,44	0,00	-46,4	0,00
300	-907,3	0,00	0,00	-45,37	0,00	-45,4	0,00

Table 5-5 - Normal and shear stresses on stiffener 1 (Model 7)

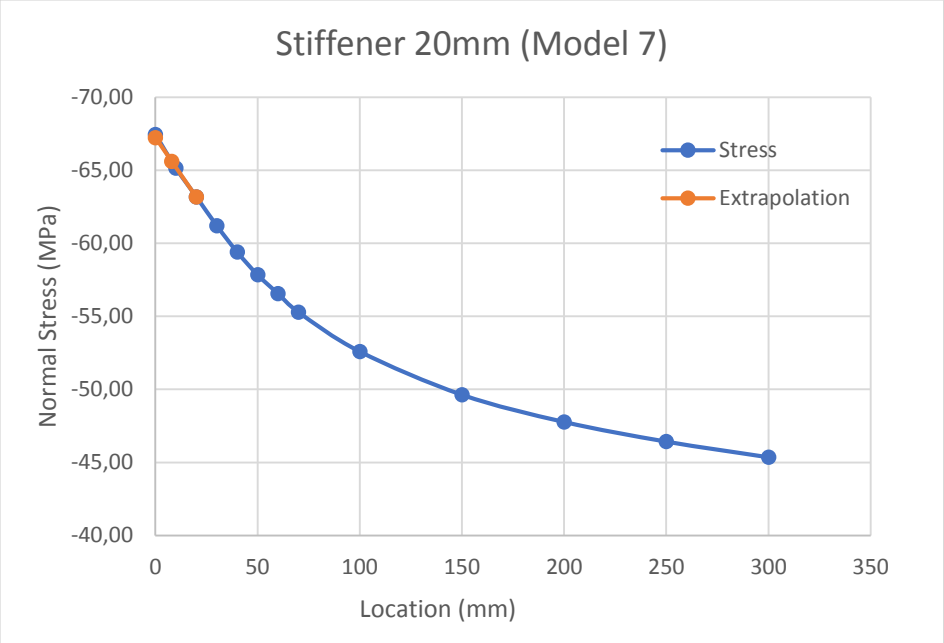

Figure 5-7 - Normal stresses on stiffener 1 and hot-spot extrapolation (Model 7)

Under this mesh refinement, this is now considered a fine mesh, so the read out points for the extrapolation are now located at 0,4t and 1,0t (t=thickness). Then the formula for the calculation of the hot-spot stress is the following:

$$\sigma_{hs} = 1.67 * \sigma_{0.4t} - 0.67 * \sigma_{1.0t}$$

Location	Distance (mm)	Stress (MPa)
Plate	0	-67,2
0,4 t	8	-65,6
1,0 t	20	-63,2

Table 5-6 - Extrapolation for calculation of hot-spot stress

From this table, we can obtain that the hot-spot stress is of -67,2 MPa.

The following results and calculations represent the values for the stiffener 2 on Model 7.

Distance (mm)	ny (N/mm)	my (Nmm/mm)	mxy (Nmm/mm)	σn (MPa)	σm (MPa)	σn+m (MPa)	τxy (MPa)
0	-1351,6	-462,9	72,7	-54,06	-4,44	-58,5	0,70
10	-1111,7	-273,4	101,6	-44,47	-2,62	-47,1	0,98
20	-985,6	-90,8	113,1	-39,42	-0,87	-40,3	1,09
30	-979,5	59,6	102,1	-39,18	0,57	-38,6	0,98
40	-978,8	172,6	78,4	-39,15	1,66	-37,5	0,75
50	-978,2	248,8	50,5	-39,13	2,39	-36,7	0,48

Table 5-7 - Normal and shear stresses on stiffener 2 (Model 7)

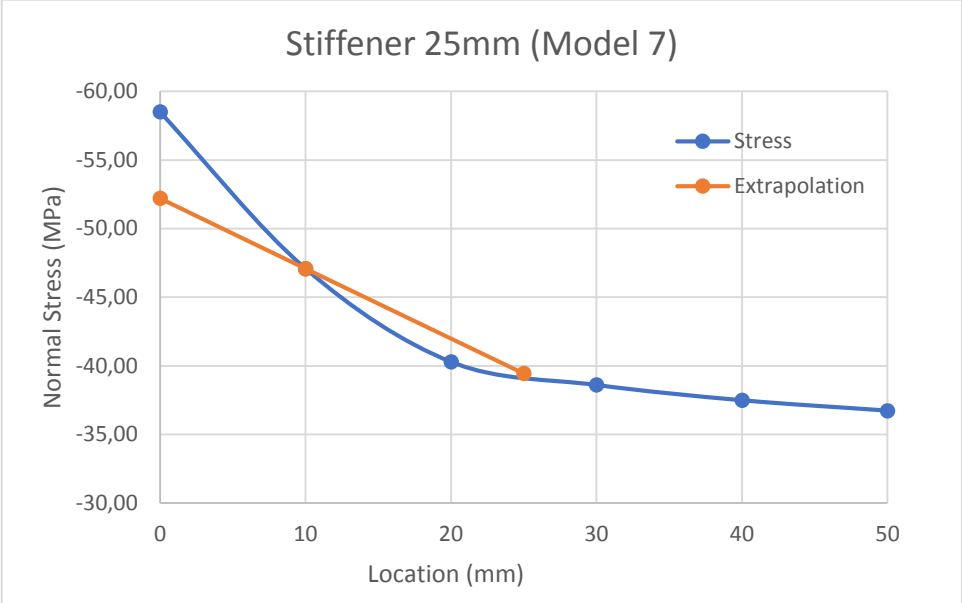

Figure 5-8 - Normal stresses on stiffener 2 and hot-spot extrapolation (Model 7)

Location	Distance (mm)	Stress (MPa)
Plate	0	-52,2
0,4 t	10	-47,1
1,0 t	25	-39,5

Table 5-8 - Extrapolation for calculation of hot-spot stress

From this table, we can obtain that the hot-spot stress is of -52,2 MPa.

The following results and calculations represent the values for the stiffener 1 on Model 8.

Distance (mm)	ny (N/mm)	my (Nmm/mm)	mxy (Nmm/mm)	σn (MPa)	σm (MPa)	σn+m (MPa)	τxy (MPa)
0	-1352,5	0,61	0,03	-67,62	0,01	-67,6	0,00
8	-1323,1	0,45	0,03	-66,16	0,01	-66,2	0,00
16	-1298,5	0,32	0,03	-64,93	0,00	-64,9	0,00
24	-1271,6	0,23	0,02	-63,58	0,00	-63,6	0,00
32	-1241,5	0,14	0,01	-62,07	0,00	-62,1	0,00
40	-1210,3	0,09	0,01	-60,52	0,00	-60,5	0,00
48	-1182,8	0,04	0,01	-59,14	0,00	-59,1	0,00
72	-1114,8	-0,01	0,01	-55,74	0,00	-55,7	0,00
104	-1054,5	-0,06	0,01	-52,73	0,00	-52,7	0,00
136	-1012,8	-0,11	0,01	-50,64	0,00	-50,6	0,00
200	-957,2	-0,16	0,01	-47,86	0,00	-47,9	0,00
280	-916,6	-0,21	0,01	-45,83	0,00	-45,8	0,00

Table 5-9 - Normal and shear stresses on stiffener 1 (Model 8)

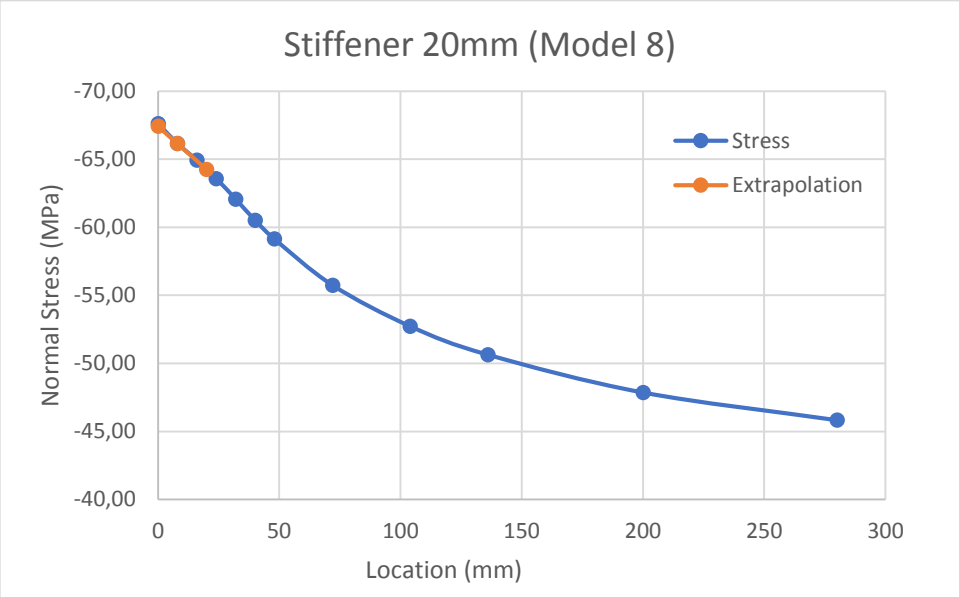

Figure 5-9 - Normal stresses on stiffener 1 and hot-spot extrapolation (Model 8)

Location	Distance (mm)	Stress (MPa)
Plate	0	-67,4
0,4 t	8	-66,2
1,0 t	20	-64,3

Table 5-10 - Extrapolation for calculation of hot-spot stress

From this table, we can obtain that the hot-spot stress is of -67,4 MPa.

The following results and calculations represent the values for the stiffener 2 on Model 8.

Distance (mm)	ny (N/mm)	my (Nmm/mm)	mxy (Nmm/mm)	σn (MPa)	σm (MPa)	σn+m (MPa)	τxy (MPa)
0	-1415,8	-723,2	110,5	-56,63	-6,94	-63,6	1,06
10	-1152,2	-404,1	127,1	-46,09	-3,88	-50,0	1,22
20	-1006,5	-106,4	126,7	-40,26	-1,02	-41,3	1,22
30	-988,8	129,4	94,1	-39,55	1,24	-38,3	0,90
40	-981,0	280,8	50,8	-39,24	2,70	-36,6	0,49
50	-974,0	362,2	13,4	-38,96	3,48	-35,5	0,13

Table 5-11 - Normal and shear stresses on stiffener 2 (Model 8)

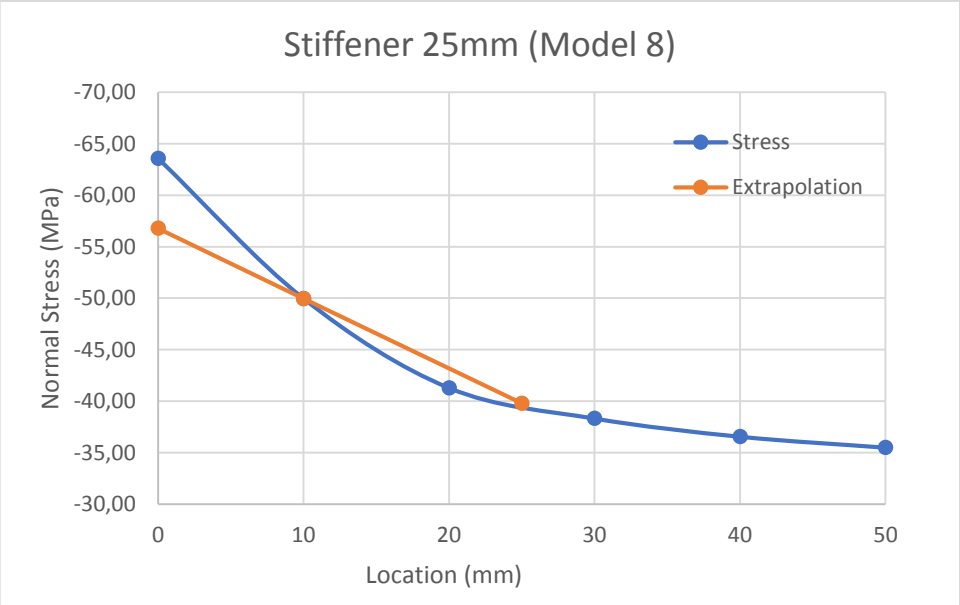

Figure 5-10 - Normal stresses on stiffener 2 and hot-spot extrapolation (Model 8)

Location	Distance (mm)	Stress (MPa)
Plate	0	-56,8
0,4 t	10	-50,0
1,0 t	25	-39,8

Table 5-12 - Extrapolation for calculation of hot-spot stress

From this table, we can obtain that the hot-spot stress is of -56,8 MPa.

The following results and calculations represent the values for the stiffener 1 on Model 9.

Distance (mm)	ny (N/mm)	my (Nmm/mm)	mxy (Nmm/mm)	σn (MPa)	σm (MPa)	σn+m (MPa)	τxy (MPa)
0	-1353,5	0,51	-0,03	-67,68	0,01	-67,7	0,00
5	-1316,3	0,40	-0,04	-65,81	0,01	-65,8	0,00
10	-1288,3	0,30	-0,04	-64,42	0,00	-64,4	0,00
15	-1265,3	0,22	-0,03	-63,26	0,00	-63,3	0,00

20	-1245,5	0,16	-0,02	-62,27	0,00	-62,3	0,00
25	-1227,1	0,12	-0,01	-61,36	0,00	-61,4	0,00
30	-1209,7	0,09	0,00	-60,49	0,00	-60,5	0,00
35	-1193,3	0,07	0,00	-59,67	0,00	-59,7	0,00
40	-1177,9	0,06	0,00	-58,89	0,00	-58,9	0,00
50	-1149,1	0,04	0,00	-57,45	0,00	-57,5	0,00
75	-1090,7	0,01	0,00	-54,54	0,00	-54,5	0,00
100	-1049,3	0,01	0,00	-52,46	0,00	-52,5	0,00
150	-992,0	0,00	0,00	-49,60	0,00	-49,6	0,00
200	-953,9	0,00	0,00	-47,70	0,00	-47,7	0,00

Table 5-13 - Normal and shear stresses on stiffener 1 (Model 9)

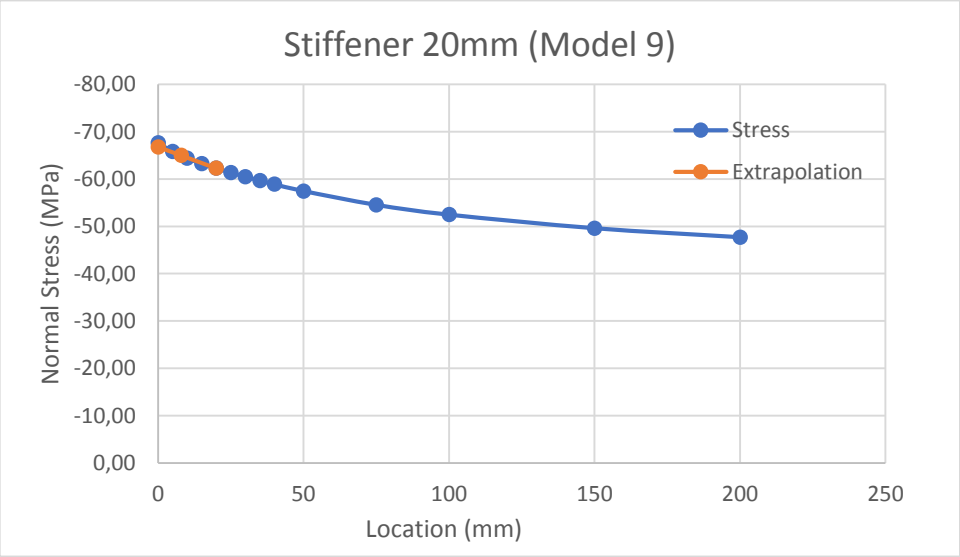

Figure 5-11 - Normal stresses on stiffener 1 and hot-spot extrapolation (Model 9)

Location	Distance (mm)	Stress (MPa)
Plate	0	-66,8
0,4 t	8	-65,0
1,0 t	20	-62,3

Table 5-14 - Extrapolation for calculation of hot-spot stress

From this table, we can obtain that the hot-spot stress is of -66,8 MPa.

The following results and calculations represent the values for the stiffener 2 on Model 9.

Distance (mm)	ny (N/mm)	my (Nmm/mm)	mxy (Nmm/mm)	σn (MPa)	σm (MPa)	σn+m (MPa)	τxy (MPa)
0	-1963,6	-711,2	170,1	-78,54	-6,83	-85,4	1,63
5	-1415,2	-539,0	111,7	-56,61	-5,17	-61,8	1,07
10	-1110,6	-367,6	110,7	-44,43	-3,53	-48,0	1,06
15	-1021,5	-205,9	123,0	-40,86	-1,98	-42,8	1,18
20	-997,7	-62,1	121,1	-39,91	-0,60	-40,5	1,16

25	-990,1	61,8	108,9	-39,60	0,59	-39,0	1,05
30	-985,9	163,5	90,0	-39,43	1,57	-37,9	0,86
35	-982,6	242,5	68,4	-39,30	2,33	-37,0	0,66
40	-979,2	301,3	47,1	-39,17	2,89	-36,3	0,45
45	-975,6	343,4	28,2	-39,02	3,30	-35,7	0,27
50	-972,0	372,4	12,2	-38,88	3,58	-35,3	0,12

Table 5-15 - Normal and shear stresses on stiffener 2 (Model 9)

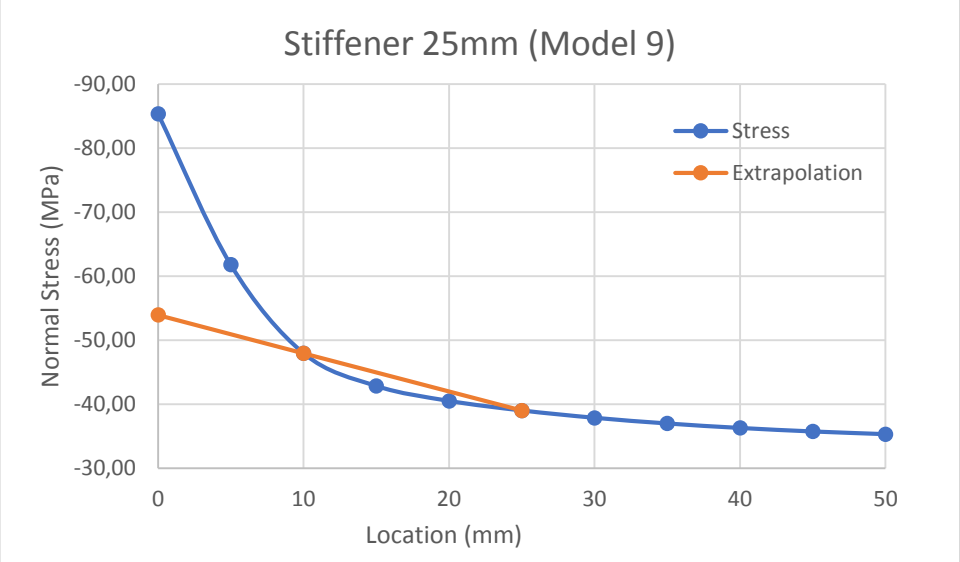

Figure 5-12 - Normal stresses on stiffener 2 and hot-spot extrapolation (Model 9)

Location	Distance (mm)	Stress (MPa)
Plate	0	-54,0
0,4 t	10	-48,0
1,0 t	25	-39,0

Table 5-16 - Extrapolation for calculation of hot-spot stress

From this table, we can obtain that the hot-spot stress is of -54,0 MPa.

The following table compiles all hot-spot stresses and stress concentration factors found in all models:

Model	Mesh	Stiffener	Hot-spot stress (MPa)
6	Coarse	1 - 20mm	-67,7
6	Coarse	2 - 25mm	-50,9
7	Fine	1 - 20mm	-67,2
7	Fine	2 - 25mm	-52,2
8	Fine	1 - 20mm	-67,4
8	Fine	2 - 25mm	-56,8
9	Fine	1 - 20mm	-66,8
9	Fine	2 - 25mm	-54,0

Table 5-17 – Hot-spot stress

From the previous table, we can see that the hot-spot stress on the 20mm stiffener oscillates from 66,8 MPa to 67,7 MPa, the 25mm stiffener has a range from 50,9 MPa to 56,8 MPa.

In the previous stress-location plots (from Figure 5-5 to Figure 5-12), it could be seen that for the model 9, where the mesh is the finest of them all (mesh refinement of 5mm), it is seen that the stress at the intersection has a much higher peak than in other models. This is due that these configurations (peak points) tend to show a higher value when a finer mesh is taken into account. The hot-spot stress allows to obtain the stress at the level of the plate without being influenced by this increased peak, as it can be seen that its value is similar to the ones obtained in other models. A finer mesh also allows for the results to be smoother and more accurate than with a coarser mesh, by the process in the finite element calculations.

It is also seen that results are similar between the models with different mesh refinement, so they can be considered accurate for the purpose of this project, where the critical case will be taken of a hot-spot stress of 67,7 MPa. The stress range for a fatigue analysis is then 67,7 MPa, as the load case was taken into account as the force that causes the highest stress range in the system. It needs to be considered that all these values are for the given specific configuration, under this load case and the boundary conditions taken into account, which are located on top of the stiffeners for this local modelling.

If we remember the detail category class table given by the Eurocode 3, for a detail similar to this case of a load located under a stiffener, the detail category class is of 100 MPa (for $2x10^6$ cycles) in a hot-spot stress analysis. The acting stress range is 67,7 MPa for 365000 cycles, which we need to convert to the equivalent stress range for $2x10^6$ cycles using the following calculation:

$$\sigma_{hs\,E,2} = \Delta\sigma_{hs} * \left(\frac{n}{N_E}\right)^{1/m}$$

$$\sigma_{hs\,E,2} = 67{,}7 * \left(\frac{365000}{2x10^6}\right)^{\frac{1}{3}} = 38{,}4MPa$$

Then the unity check, using a safety factor (1,35 - as discussed in chapter 2) and a load factor of 1), is calculated as:

$$U.C. = \frac{\gamma_{Ff} * \sigma_{E,2}}{\frac{\Delta\sigma_C}{\gamma_{Mf}}}$$

$$U.C. = \frac{1{,}0 * 38{,}4}{\frac{100}{1{,}35}} = 0{,}52$$

Under this analysis, the weld will not have any problem against fatigue during the estimated number of cycles based on the lifetime of the bridge, where the critical stress value was used from the local analysis.

With these results, it is recommended to perform a finite element model to obtain the hot-spot stress of the detail. The unity check from the global model was just 0,46, using a hot-spot

stress approach in the local model, results have a slight variation, now of 0,52. For this case, the structure is still safe against fatigue, however we can see that there is a slight increase in the unity check. If this value had been initially closer to 1, then with a more specific analysis, this value could have surpassed the limit of 1 and the structure to be considered not safe. This analysis is recommended then to ensure the safety of the design.

To obtain the service life of the rail track detail, we establish a unity check value of 1 (maximum possible value for a satisfactory design). The stress level for two million cycles is obtained as:

$$\sigma_{E,2} = \frac{U.C.* \Delta\sigma_C}{\gamma_{Ff} * \gamma_{Mf}}$$

$$\sigma_{E,2} = \frac{1{,}0 * 100}{1{,}0 * 1{,}35}$$

$$\sigma_{E,2} = 74{,}1\ MPa$$

For a constant amplitude fatigue loading, the slope m of the S-N curve is taken as m=3. Under the same hot-spot stress of 67,7 MPa obtained in the previous analysis, the number of cycles required for this stress range is then:

$$n = \left(\frac{\sigma_{E,2}}{\Delta\sigma_{hs}}\right)^m * N_E$$

$$n = \left(\frac{74{,}1}{67{,}7}\right)^3 * 2x10^6$$

$$n = 2{,}6x10^6 cycles$$

The design considers that 365000 cycles will occur on a span of 20 years. Taking this rate as a constant up to 2,6x10^6 cycles, this yields a service life time of:

$$Service\ life = \frac{2{,}6x10^6}{365000} * 20 = 142\ years$$

The value is increased by a factor of 7 (new number of cycles), the vast majority of structures (such as bridges) are usually designed with 20 or 50 years of lifetime, under the current configuration of the rail track, fatigue will not be the critical aspect during its complete lifetime.

A different configuration was taken into account as explained in chapter 4 (Model 10), where the main configuration has the load located directly underneath the transversal stiffener, this configuration has the load located in between two continuous stiffeners, as shown in figure 4-6 in the respective chapter. The model configuration is shown in the following figure:

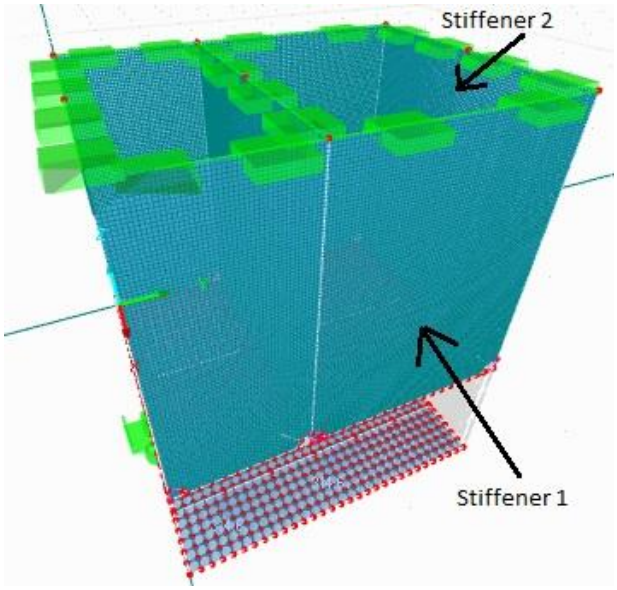

Figure 5-13 - Model with load between stiffeners (Model 10)

As in the previous configuration, the critical stiffeners are the front-right transversal stiffener (1) and the most right longitudinal stiffener (2), so these will be taken for the analysis. The results of the internal forces will be shown tabulated in this section, the model results will be shown in the Appendix B as well (with the initial configuration).

The following results and calculations represent the values for the stiffener 1 on Model 10.

Distance (mm)	ny (N/mm)	my (Nmm/mm)	mxy (Nmm/mm)	σn (MPa)	σm (MPa)	σn+m (MPa)	τxy (MPa)
0	-1216,0	-43,6	6,06	-60,80	-0,65	-61,5	0,09
5	-906,9	-42,8	3,87	-45,34	-0,64	-46,0	0,06
10	-735,9	-38,9	0,99	-36,79	-0,58	-37,4	0,01
15	-687,4	-37,6	0,37	-34,37	-0,56	-34,9	0,01
20	-676,0	-38,0	-0,22	-33,80	-0,57	-34,4	0,00
25	-673,4	-39,0	-0,72	-33,67	-0,58	-34,3	-0,01
30	-673,6	-40,4	-1,13	-33,68	-0,61	-34,3	-0,02
35	-673,8	-41,3	-1,45	-33,69	-0,62	-34,3	-0,02
40	-674,0	-44,3	-1,68	-33,70	-0,66	-34,4	-0,03

Table 5-18 - Normal and shear stresses on stiffener 1 (Model 10)

As it is seen in this table, the shear stress can be also neglected for this analysis.

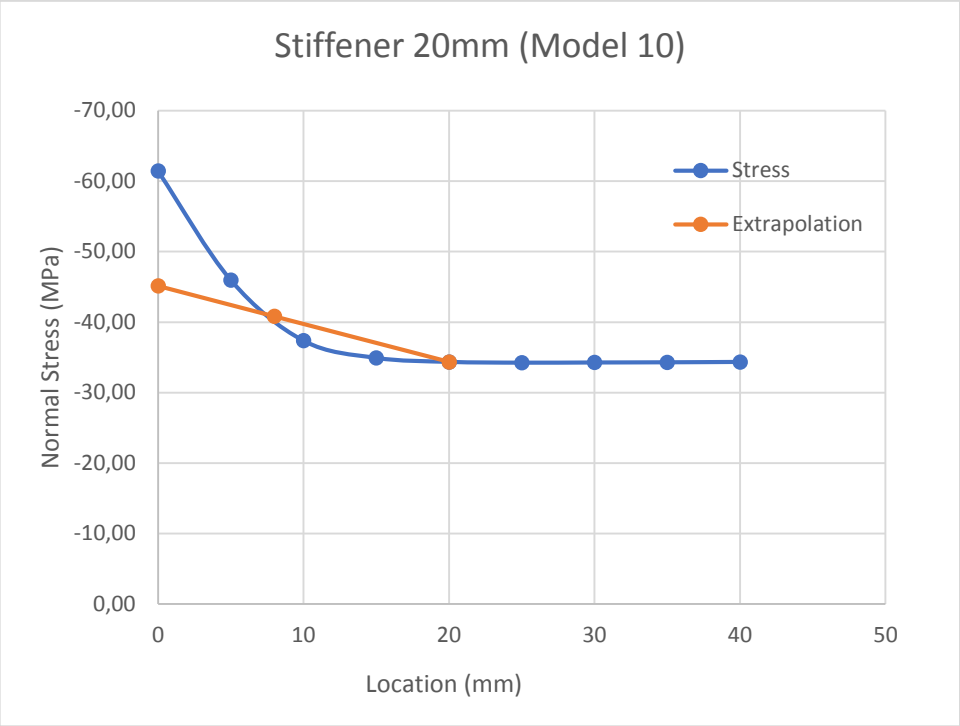

Figure 5-14 - Normal stresses on stiffener 1 and hot-spot extrapolation (Model 10)

Location	Distance (mm)	Stress (MPa)
Plate	0	-45,1
0,4 t	8	-40,8
1,0 t	20	-34,4

Table 5-19 - Extrapolation for calculation of hot-spot stress

From this table, we can obtain that the hot-spot stress is of -45,1 MPa.

The following results and calculations represent the values for the stiffener 2 on Model 10.

Distance (mm)	ny (N/mm)	my (Nmm/mm)	mxy (Nmm/mm)	σn (MPa)	σm (MPa)	σn+m (MPa)	τxy (MPa)
0	-1884,7	200,2	-5,80	-75,39	1,92	-73,5	-0,06
5	-1368,6	195,5	-8,55	-54,74	1,88	-52,9	-0,08
10	-1082,7	194,5	-7,50	-43,31	1,87	-41,4	-0,07
15	-1000,1	189,3	-6,30	-40,00	1,82	-38,2	-0,06
20	-978,9	182,0	-4,59	-39,16	1,75	-37,4	-0,04
25	-972,9	174,7	-2,69	-38,91	1,68	-37,2	-0,03
30	-970,1	168,2	-0,82	-38,80	1,61	-37,2	-0,01
35	-968,1	162,4	0,91	-38,73	1,56	-37,2	0,01
40	-966,3	157,3	2,45	-38,65	1,51	-37,1	0,02
45	-964,5	152,9	3,77	-38,58	1,47	-37,1	0,04
50	-962,7	149,0	4,89	-38,51	1,43	-37,1	0,05

Table 5-20 - Normal and shear stresses on stiffener 2 (Model 10)

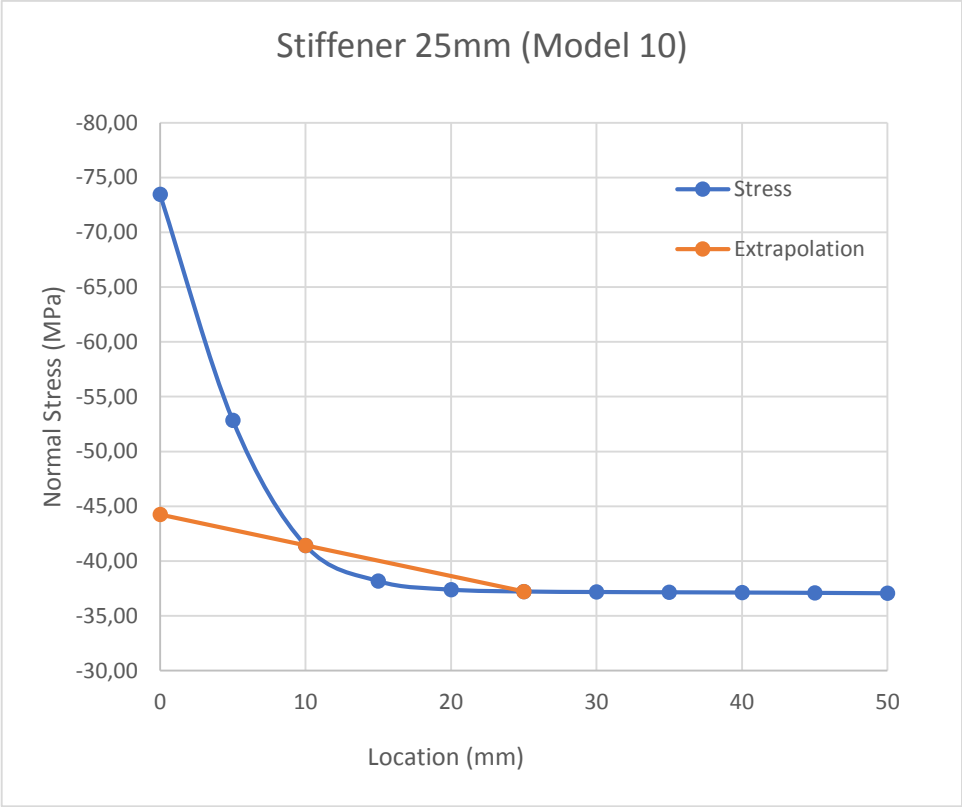

Figure 5-15 - Normal stresses on stiffener 2 and hot-spot extrapolation (Model 10)

Location	Distance (mm)	Stress (MPa)
Plate	0	-44,3
0,4 t	10	-41,4
1,0 t	25	-37,2

Table 5-21 - Extrapolation for calculation of hot-spot stress

From this table, we can obtain that the hot-spot stress is of -44,3 MPa.

Under this configuration, the results are:

Model	Mesh	Stiffener	Hot-spot stress (MPa)
10	Fine	1 - 20mm	-45,1
10	Fine	2 - 25mm	-44,3

Table 5-22 - Hot-spot stress

When the load is located between two stiffeners, the stress acting on the stiffeners is lower, as it can be seen that the hot-spot stress is now -45,1 MPa, compared to the previous -67,7 MPa. With this analysis, it can be also concluded that the critical case may occur when the load is located directly under the stiffener, this means when the stiffener is located above the point of contact between the tracks of the bridge during its opening/closing motion.

Chapter 6 – Verification

6.1 Introduction

Due to the limitation observed in solid modelling through the version of the software RFEM, an analysis is performed with the software ABAQUS, to be able to obtain results of the solid modelling when performing a fine mesh. Solid modelling is thought to be more accurate than shell modelling, since it is more representative of the actual case scenario. As established with the RFEM case, as well as by definition of the hot-spot stress, normal stresses will be shown in this analysis.

6.2 Shell Element Model

A model was performed using the software ABAQUS with shell elements using a fine mesh, to compare the results obtained by this software with the RFEM software used previously. In RFEM, rigid body elements were used to establish a connection between the two horizontal plates, but in ABAQUS, a tie constraint was performed instead, an element used by ABAQUS to connect two elements together and transfer normal and shear forces between them. The mesh used in this model is a fine mesh of 5mm, as in the fine mesh from the RFEM model. The boundary conditions are located at the top of the stiffeners and the load located on the bottom plate, same as the previous models presented in chapter 5 through RFEM. The following picture shows the shell model:

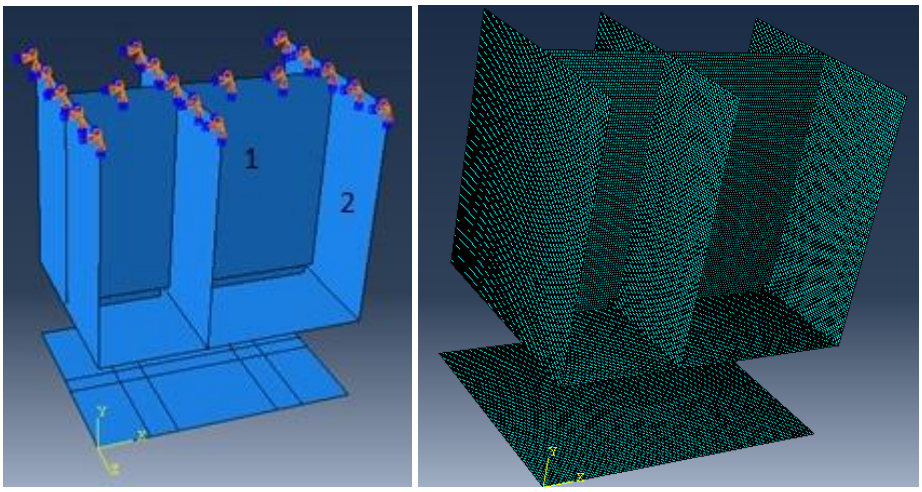

Figure 6-1 - Model with shell elements and meshed configuration

The results of the internal forces and the stresses will be shown in the following table, the diagrams obtained from ABAQUS will be shown in Appendix C.

Distance (mm)	ny (N/mm)	my (Nmm/mm)	σn (MPa)	σm (MPa)	σn+m (MPa)
0	-1365,2	0,00	-68,3	0,00	-68,3
5	-1354,1	0,00	-67,7	0,00	-67,7
10	-1331,7	0,00	-66,6	0,00	-66,6
15	-1307,9	0,00	-65,4	0,00	-65,4
20	-1283,0	0,00	-64,2	0,00	-64,2
25	-1257,9	0,00	-62,9	0,00	-62,9
30	-1233,6	0,00	-61,7	0,00	-61,7
35	-1210,5	0,00	-60,5	0,00	-60,5
40	-1189,1	0,00	-59,5	0,00	-59,5
50	-1151,2	0,00	-57,6	0,00	-57,6
75	-1081,2	0,00	-54,1	0,00	-54,1
100	-1034,8	0,00	-51,7	0,00	-51,7
150	-976,7	0,00	-48,8	0,00	-48,8
200	-940,9	0,00	-47,1	0,00	-47,1

Table 6-1 - Normal stresses on stiffener 1

Where $\sigma_n = \frac{n_y}{t}$ and $\sigma_m = \frac{m_y}{\frac{1}{6}t^2}$

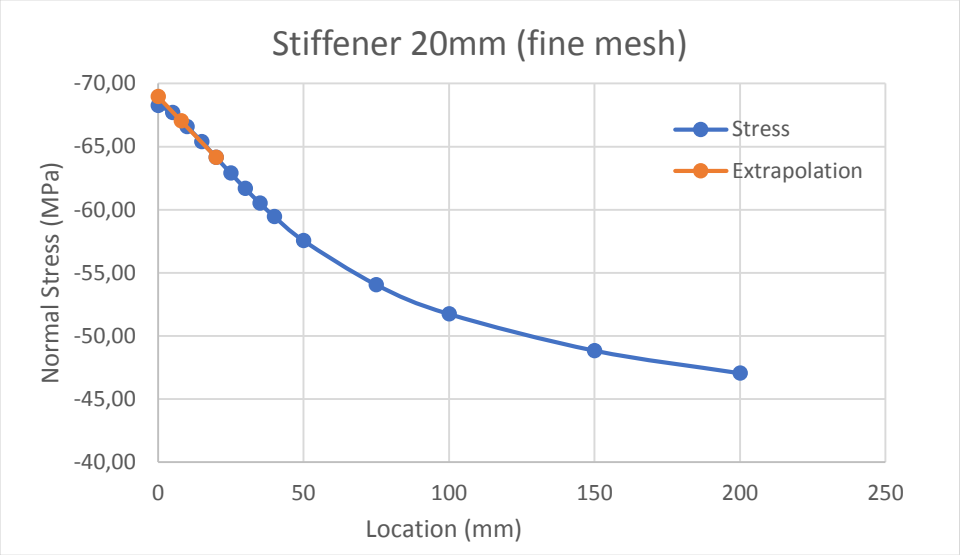

Figure 6-2 - Normal stresses on stiffener 1 and hot-spot extrapolation

Location	Distance (mm)	Stress (MPa)
Plate	0	-69,0
0,4 t	8	-67,0
1,0 t	20	-64,2

Table 6-2 - Extrapolation for calculation of hot-spot stress

From this table, we can obtain that the hot-spot stress is of -69,0 MPa.

Recalling the results obtained in Model 9 using the RFEM software, the hot-spot stress obtained from that model for the stiffener 1 (transversal stiffener) is -66,8 MPa. If we compare

these results with the results obtained through the model using ABAQUS, results are similar within a 3.2% difference, now to -69,0 MPa for the hot-spot stress.

If we analyze the stiffener 2 (longitudinal stiffener), the following results are obtained:

Distance (mm)	ny (N/mm)	my (Nmm/mm)	σn (MPa)	σm (MPa)	σn+m (MPa)
0	-934,8	-479,3	-37,39	-4,60	-42,0
5	-935,8	-455,6	-37,43	-4,37	-41,8
10	-938,0	-404,1	-37,52	-3,88	-41,4
15	-940,3	-350,6	-37,61	-3,37	-41,0
20	-942,6	-295,9	-37,70	-2,84	-40,6
25	-944,9	-241,4	-37,80	-2,32	-40,1
30	-947,2	-187,9	-37,89	-1,80	-39,7
35	-949,4	-136,4	-37,98	-1,31	-39,3
40	-951,5	-87,7	-38,06	-0,84	-38,9
45	-953,6	-42,4	-38,14	-0,41	-38,6
50	-955,5	-0,8	-38,22	-0,01	-38,2

Table 6-3 - Normal stresses on stiffener 2

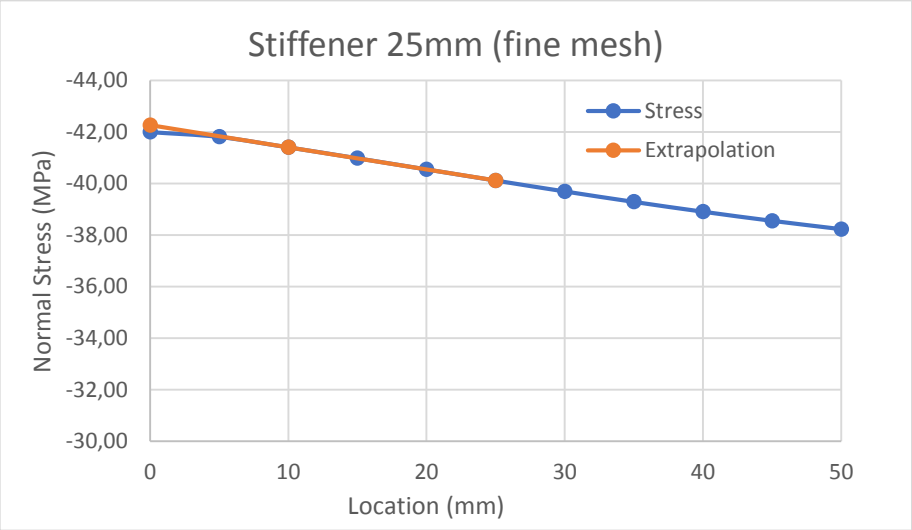

Figure 6-3 - Normal stresses on stiffener 2 and hot-spot extrapolation

Location	Distance (mm)	Stress (MPa)
Plate	0	-42,3
0,4 t	10	-41,4
1,0 t	25	-40,1

Table 6-4 - Extrapolation for calculation of hot-spot stress

From this table, we can obtain that the hot-spot stress is of -42,3 MPa.

In this stiffener, there is a variation in the results compared to the results obtained from the Model 9 from RFEM. In that analysis, the hot-spot stress obtained was -54,0 MPa. The difference in this case is due to the modelling of the horizontal plates and their interaction,

that causes a variation in distribution of the force across the plate in transversal direction, therefore to the stiffener 2 (longitudinal stiffener) as well. The software ABAQUS does not perform well this force distribution due to the way the constraint works in the model, resulting in lower forces on the intersection between the stiffener 2 and the horizontal plate. RFEM showed a more adequate distribution of forces and stresses across the elements when this type of detail and specific load configuration is modelled, for this type of shell modelling, RFEM is recommended.

6.3 Solid Element Model

Different models were performed to ascertain how different results are from a fine mesh compared to a coarse mesh. Two situations are presented using a fine mesh of 5mm, one without weld modelling and the other with weld (with a mesh of 2mm).

In this chapter, the results of the stresses will be tabulated, the diagram of the stresses will be presented in Appendix D.

The fine mesh was performed with a mesh of 5mm as shown in the following picture:

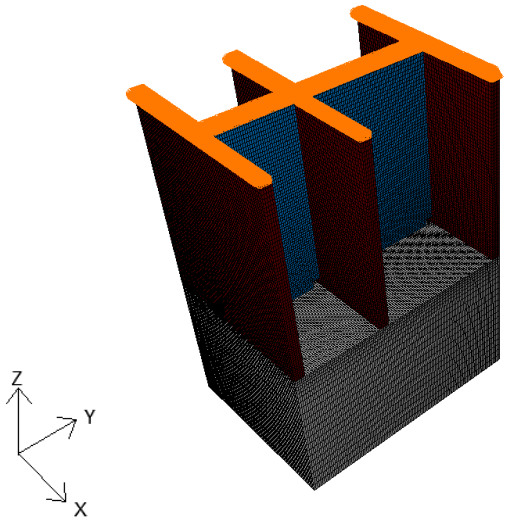

Figure 6-7 - Model with solid elements (Fine mesh)

The results for the fine mesh model are shown in the following table.

Distance (mm)	σ (MPa)
0	-61,0
5	-57,4
10	-47,6
15	-47,3
20	-47,3
25	-47,2
30	-47,2

35	-47,2
40	-47,1
45	-47,1
50	-47,1
75	-46,8
100	-46,4
125	-45,9
150	-45,3

Table 6-9 - Normal stresses on stiffener 1 (fine mesh)

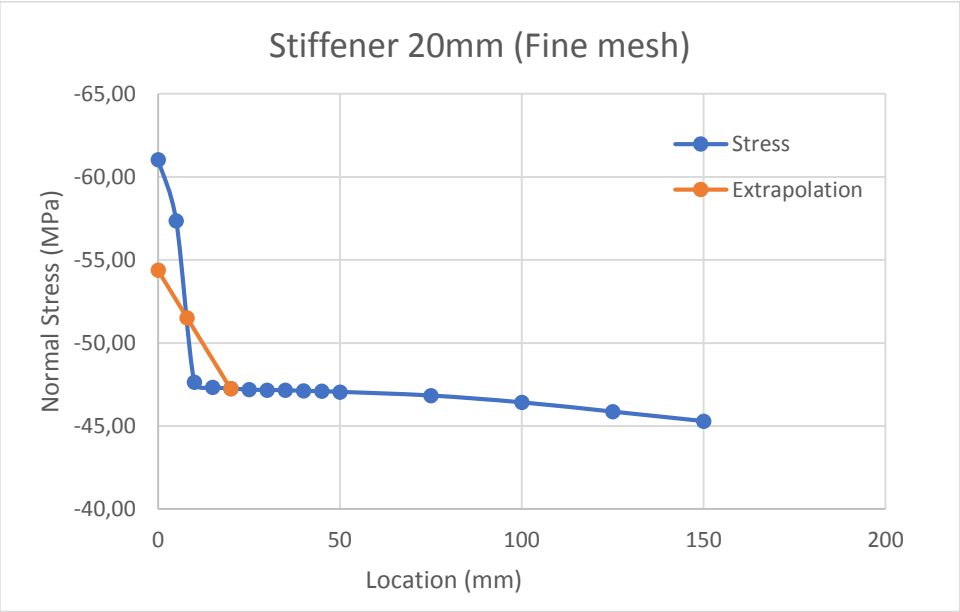

Figure 6-8 - Normal stresses on stiffener 1 and hot-spot extrapolation (Fine)

Location	Distance (mm)	Stress (MPa)
Plate	0	-54,4
0,4 t	8	-51,5
1,0 t	20	-47,3

Table 6-10 - Extrapolation for calculation of hot-spot stress

From this table, we can obtain that the hot-spot stress is of -54,4 MPa.

The results of the stiffener 2 for the fine mesh model case are the following:

Distance (mm)	σ (MPa)
0	-56,2
5	-53,3
10	-48,0
15	-46,9
20	-46,6
25	-46,5
30	-46,5

35	-46,4
40	-46,4
45	-46,3
50	-46,2
75	-45,9
100	-45,9
125	-45,1
150	-44,6

Table 6-11 - Normal stresses on stiffener 2 (fine mesh)

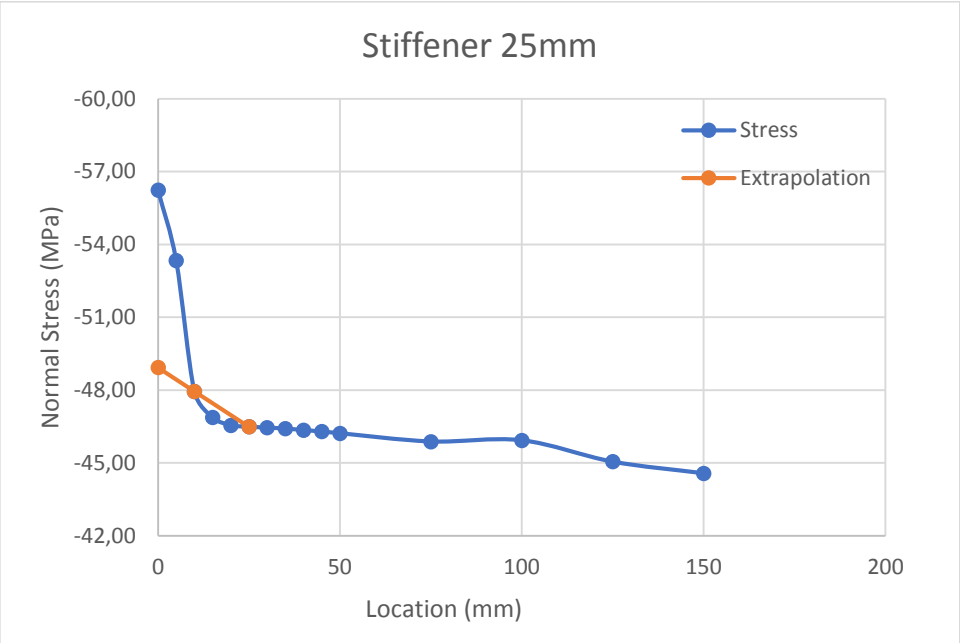

Figure 6-9 - Normal stresses on stiffener 2 and hot-spot extrapolation (Fine)

Location	Distance (mm)	Stress (MPa)
Plate	0	-48,9
0,4 t	10	-48,0
1,0 t	25	-46,5

Table 6-12 - Extrapolation for calculation of hot-spot stress

From this table, we can obtain that the hot-spot stress is of -48,9 MPa.

With these results (stiffener 1 and stiffener 2) we can observe that when the model is performed with solid elements, instead of shell elements, results vary from each other. Analysis with solid elements has better accuracy and is a better representation of the detail to be modelled, therefore these results can be considered to be more accurate than results obtained through shell modelling. These values are much lower than the values obtained in the models with shell elements, then the end result (unity check calculation) will be lower as well. When there is a significant difference in shell and solid modelling, as this case, results from the solid model case need to be considered as primary as this model represents more appropriately the real element that is considered.

The hot-spot stress is 48,9 MPa, remembering that the number of cycles is 365000, a conversion is needed, as it follows:

$$\sigma_{hs\,E,2} = \Delta\sigma_{hs} * \left(\frac{n}{N_E}\right)^{1/m}$$

$$\sigma_{hs\,E,2} = 48{,}9 * \left(\frac{365000}{2x10^6}\right)^{\frac{1}{3}} = 27{,}7MPa$$

The detail category is of 100 MPa, as established in chapter 2, load factor of 1 and safety factor of 1,35, then the unity check is:

$$U.C. = \frac{\gamma_{Ff} * \sigma_{E,2}}{\frac{\Delta\sigma_C}{\gamma_{Mf}}}$$

$$U.C. = \frac{1{,}0 * 27{,}7}{\frac{100}{1{,}35}} = 0{,}37$$

The unity check values using results from the shell elements by RFEM was 0.52, significantly higher than 0,37. For this particular design, both analysis fulfill the requirement against fatigue, however it must be noted that solid modelling is considered still a better representation (despite of the value itself).

Another model was also performed, by modelling a fillet weld between the elements, to analyze if weld modelling influence the results in a hot-spot stress analysis. On the outer surface, a butt weld is implemented to connect the elements sharing the same surface, only the fillet weld is modelled. The following figure shows a closer look of the welds in the model:

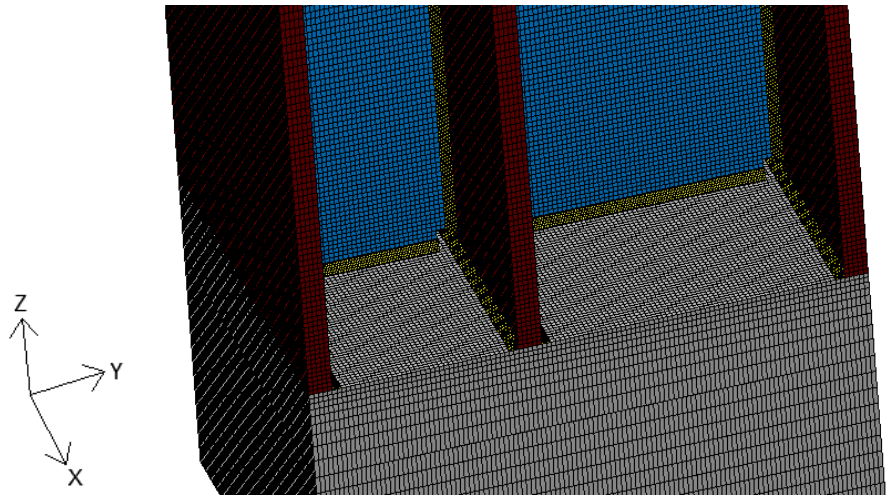

Figure 6-10 - Fillet weld modelling through solid elements (10mm weld – 45º angle)

The following table shows the normal stresses obtained for the stiffener 1:

Distance (mm)	σ (MPa)
0	-57,0
5	-52,3
10	-48,6
15	-47,6
20	-47,0
25	-46,9
30	-46,8
35	-46,8
40	-46,7
45	-46,7
50	-46,7
75	-46,5
100	-46,0
125	-45,5
150	-45,3

Table 6-13 - Normal stresses on stiffener 1 (fine mesh-weld)

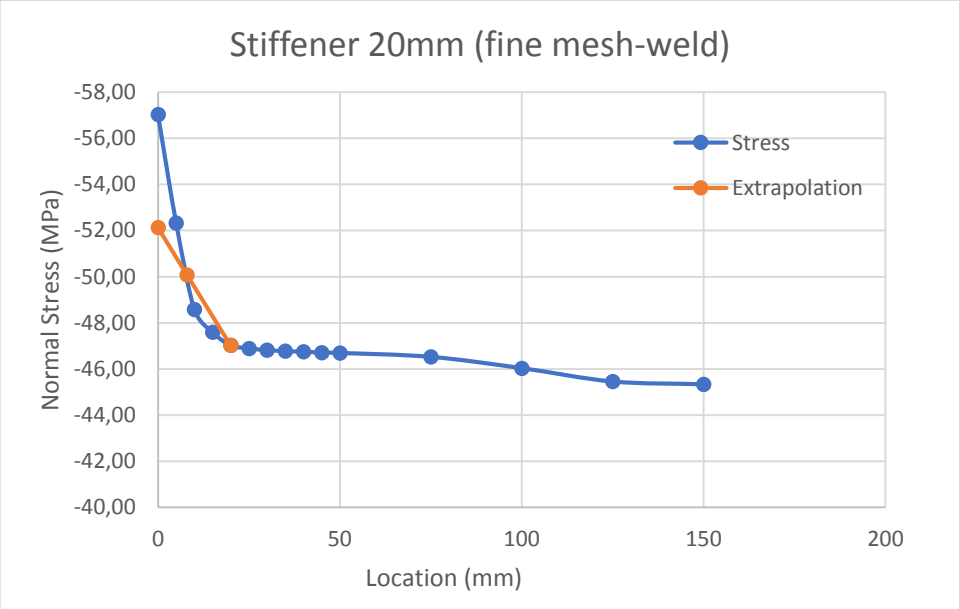

Figure 6-11 - Normal stresses on stiffener 1 and hot-spot extrapolation (Fine-weld)

Location	Distance (mm)	Stress (MPa)
Weld toe	0	-52,1
0,4 t	8	-50,1
1,0 t	20	-47,0

Table 6-14 - Extrapolation for calculation of hot-spot stress

From this table, we can obtain that the hot-spot stress is of -52,1 MPa.

The results for the stiffener 2 are the following:

Distance (mm)	σ (MPa)
0	-56,6
5	-50,7
10	-49,8
15	-49,3
20	-48,9
25	-48,6
30	-48,1
35	-47,7
40	-47,3
45	-46,8
50	-46,4
75	-44,5
100	-43,0
125	-42,1
150	-41,5

Table 6-15 - Normal stresses on stiffener 2 (fine mesh-weld)

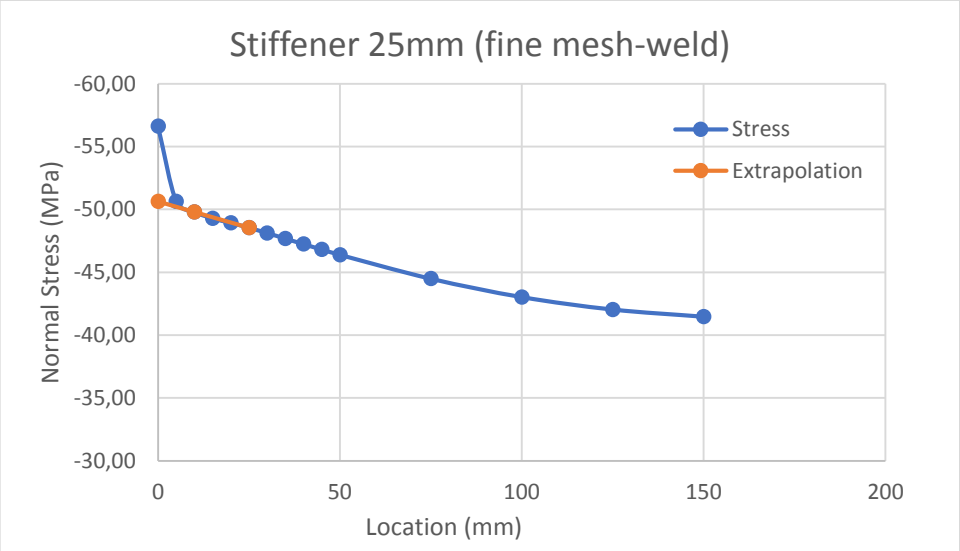

Figure 6-12 - Normal stresses on stiffener 2 and hot-spot extrapolation (Fine-weld)

Location	Distance (mm)	Stress (MPa)
Weld toe	0	-50,6
0,4 t	10	-49,8
1,0 t	25	-48,6

Table 6-16 - Extrapolation for calculation of hot-spot stress

From this table, we can obtain that the hot-spot stress is of -50,6 MPa.

Based on these results, they show similarity to the ones obtained by a model with solid elements without performing a weld modelling as well. For this type of detail, weld modelling is not a necessity, since results are similar, however it must be noted that this is not necessarily always the case. For this case, where the load is located directly under the stiffener, the presence of the weld is not highly influencing, however under different loading configurations, they might influence results, as in this case the transition from one surface to the other is less abrupt.

It must be noted that the detail category class given by the Eurocode when a fillet weld is used is of $\Delta\sigma_C$ = 36 MPa instead of 63 MPa (as stated in Table 2-1), much lower than a full penetration weld. When performing a hot-spot stress approach, the detail category used in this method is $\Delta\sigma_C$ = 90 MPa as also stated in the Eurocode 3 Part 1-9, instead of 100 MPa for the full penetration weld scenario. Another remark is that hot-spot stress method focuses only when the crack presents on weld toe; in fillet welds, weld root failure is also possible, the scope of this project does not include this failure.

An alternative was analyzed, where a restraint was introduced at the sides of the horizontal plates. The model taken in the previous analysis was taken as the conservative case, taking a stress free zone at the sides of the plates. The model is only a section of the complete rail track, therefore restraints are present from the sides caused by the rest of the rail track. These restraints will prevent displacement and rotation at these side surfaces, opposite of free stress assumption. With this configuration, stiffener 1 will be analyzed as this stiffener is the critical one and be compared to the results of the previous model.

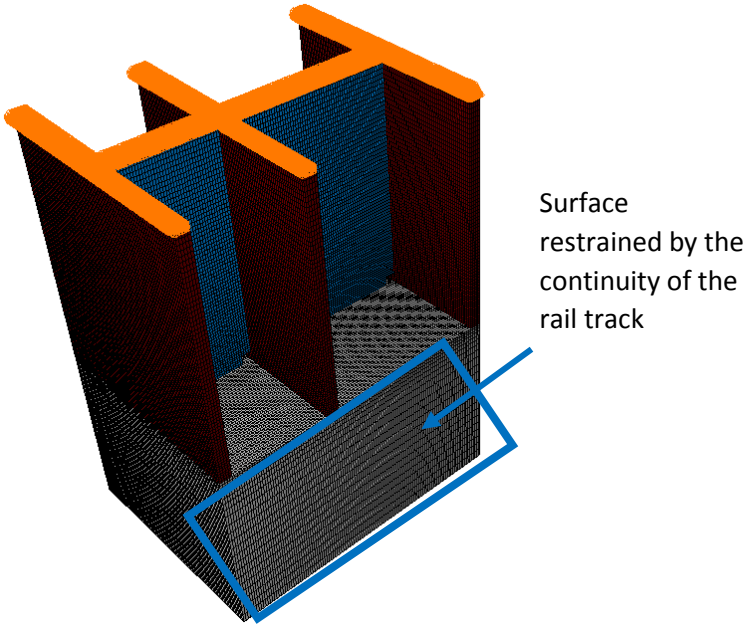

Figure 6-13 - Display of restrained surface on the local model

Under this configuration, the stresses obtained on the stiffener 1 are:

Distance (mm)	σ (MPa)
0	-51,4
5	-46,6
10	-42,4
15	-41,8
20	-41,3
25	-41,1
30	-41,0
35	-40,8
40	-40,7
45	-40,5
50	-40,3
75	-39,8
100	-39,5
125	-39,3
150	-39,1

Table 6-17 - Normal stresses on stiffener 1

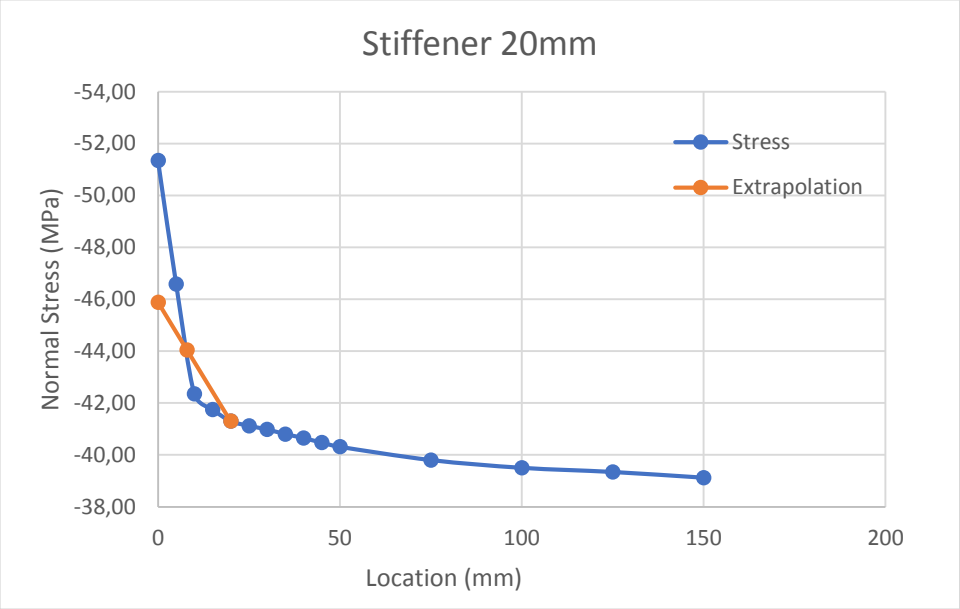

Figure 6-14 - Normal stresses on stiffener 1 and hot-spot extrapolation (Fine-weld)

Location	Distance (mm)	Stress (MPa)
Weld toe	0	-45,9
0,4 t	8	-44,0
1,0 t	20	-41,3

Table 6-18 - Extrapolation for calculation of hot-spot stress

From this table, we can obtain that the hot-spot stress is of -45,9 MPa.

Taking the results obtained previously on the initial model using solid elements, the hot-spot stress obtained was -54,4 MPa, while for this case, the hot-spot stress has reduced to a value of -45,9 MPa (84%). These results confirms the assumption that the restraints present on the rail track allows for a reduction of stresses on the stiffeners. However, a completely fixed restraint is also not precise as material may still deform at these points. For an exact knowledge of behavior, experimentation would be required, hence this project focused mainly on the most conservative case.

Chapter 7 – Recommendations and Conclusions

7.1 Conclusions

An analysis of the detail of the rail track of the Balance Bridge, in Tallinn, Estonia was performed. The unity check obtained in a global model for fatigue analysis is 0.46. The bridge has a sufficient design against fatigue load during its service life.

A hot-spot stress analysis was performed on this detail. Local models of the detail were performed, using shell elements and solid elements separately. On a shell analysis, a hot-spot stress value of 67.7 MPa was obtained, with a unity check of 0.52. From the solid element analysis, the hot-spot stress is 48.9 MPa, with a unity check of 0.37. The design is sufficient as well under an analysis using the hot-spot stress approach, for both used type of elements. It needs to be considered that a finite element analysis using solid elements has a higher reliability in results as it is a much closer representation of the detail than when shell elements are used.

It was obtained that the critical case scenario is when the loading case is located directly underneath the transversal stiffener, as it was initially thought, with a hot-spot stress of 67.7 MPa. The contact pressure used in the local model is a closer representation to reality than the assumed linear load on the global model. The assumption of a linear load should not be used in this type of analysis, as results vary for the stress distribution across the respective elements of the detail of the rail track.

An analysis was performed for different mesh refinements, where it was found that although a higher peak stress is obtained in a fine mesh, the hot-spot stress calculation will provide a solution to this situation. It was also ascertained that the size of the mesh influences the results of the model, higher accuracy with finer meshing.

7.2 Recommendations

If we note the unity check for the detail of the rail track against fatigue was 0.52 using the hot-spot stress value under shell element analysis and while being 0.37 using solid element analysis. This detail was designed with sufficient capacity against fatigue, however these values may well prove that this detail is overdesigned. It can be recommended to use finer stiffeners on the upper rail track, for instance 15 and 20mm instead of 20 and 25mm respectively. However, the slenderness of the elements need to be verified, since reducing their thickness will increase their slenderness. An increase in slenderness may require an extra support to reduce this value to acceptable limits to prevent buckling. Refining this detail may prove positively on the economy of the project, as less steel would be required.

To decrease the concentration on surface stresses and hot-spot stress, a weld toe radius of 1mm is recommended to be used. The presence of a radius in the transition between the weld and the stiffener may decrease the surface stress level as there is a smoother transition from one element to the other.

This analysis was performed on software modelling, however it is recommended to realize and obtain experimental results in order to establish a correlation between these experiments, which simulate actual real life situations, and the model, which is more of a theoretical based approach with certain assumptions on the detail. Some assumptions performed in this project were the approximation of the loads and smooth surfaces between elements. However, in reality, rough surfaces can be present, which may create extra stresses and also different distribution of loads.

A model with solid elements is recommended to be performed as this is a better representation of the detail to be modelled than when shell elements are used. As it was seen in this project, results may vary significantly. For preliminary calculations, an analysis with shell elements may be performed. An analysis based on solid elements is more computationally demanding than a shell analysis, therefore shell analysis can be recommended to be performed. However, if results are close to the capacity limit of the detail, accuracy is required, then the use of solid elements are recommended.

APPENDIX A - Global Modelling Results

In chapter 3, Table 3-1 showed the internal forces and calculated stresses in the stiffener for different opening angles. The diagrams of these forces from the model´s results are shown in this Appendix.

<table>
<tr><td colspan="2">Opening Angle 0 °</td></tr>
<tr><td>Internal force my</td><td>Internal force ny</td></tr>
<tr><td> 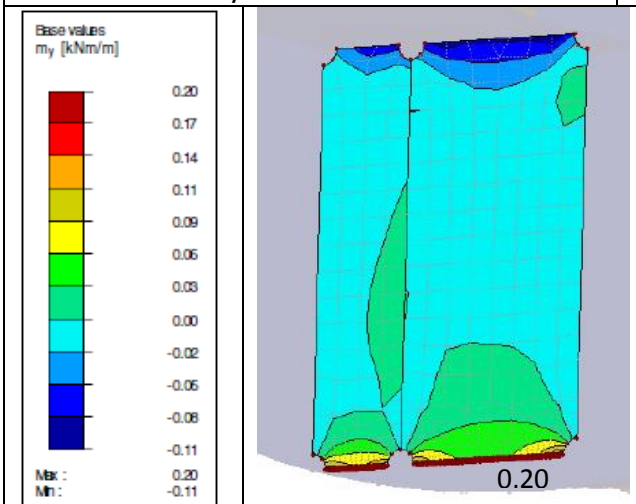
</td><td> 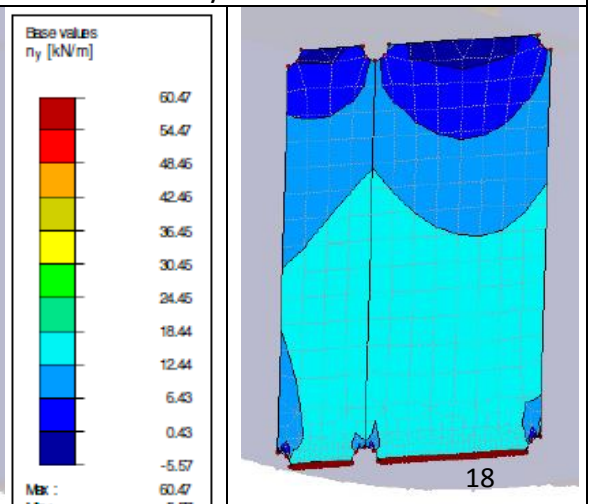
</td></tr>
<tr><td colspan="2">Opening Angle 6 °</td></tr>
<tr><td>Internal force my</td><td>Internal force ny</td></tr>
<tr><td> 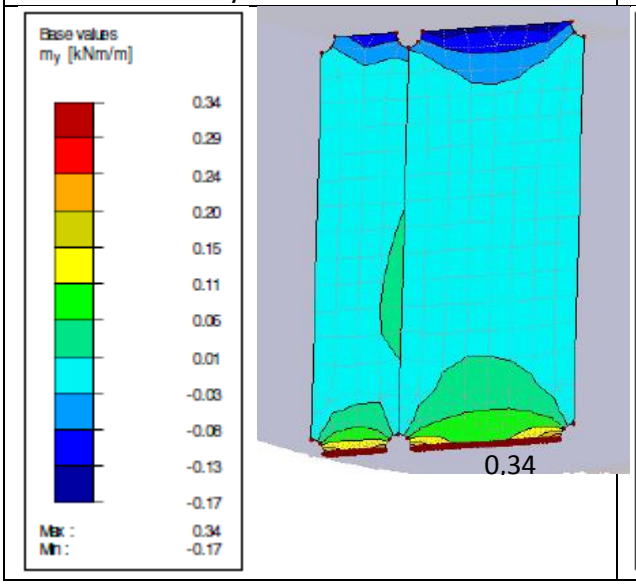
</td><td> 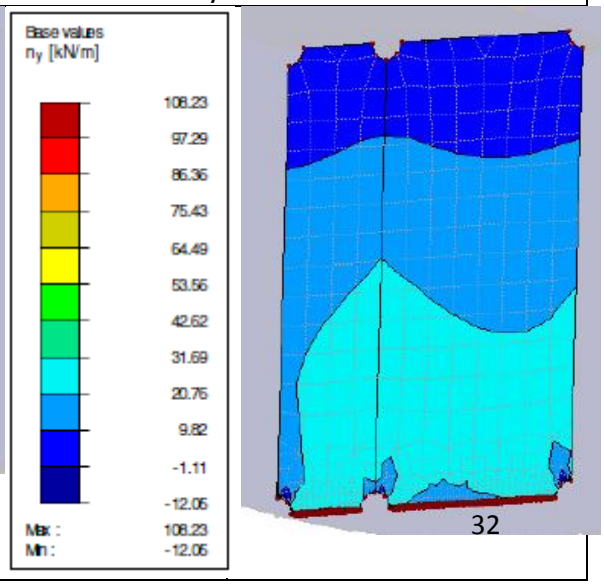
</td></tr>
</table>

Opening Angle 11 °	
Internal force my	Internal force ny
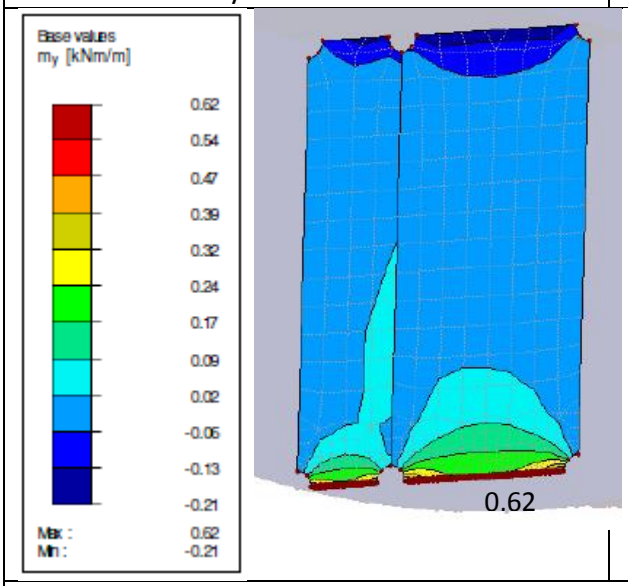	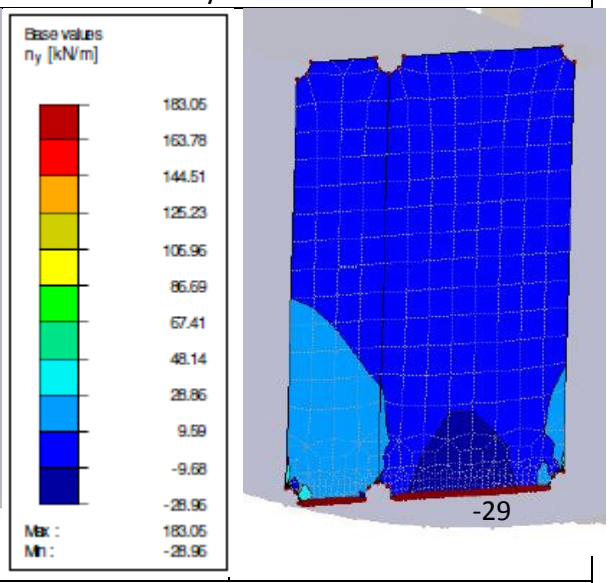
Opening Angle 17 °	
Internal force my	Internal force ny
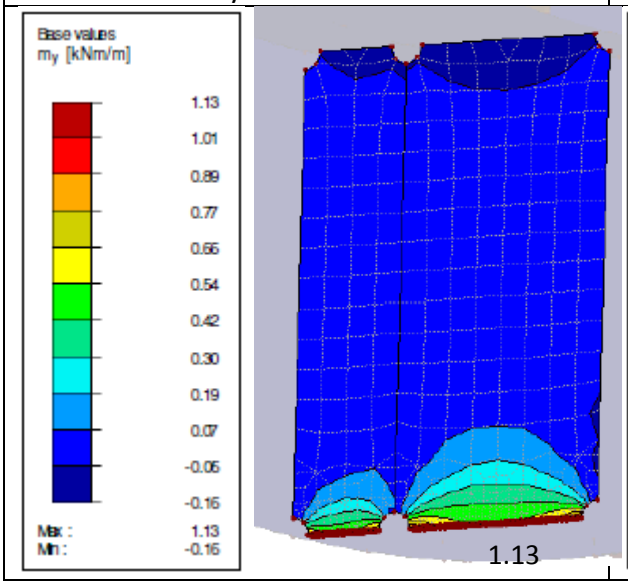	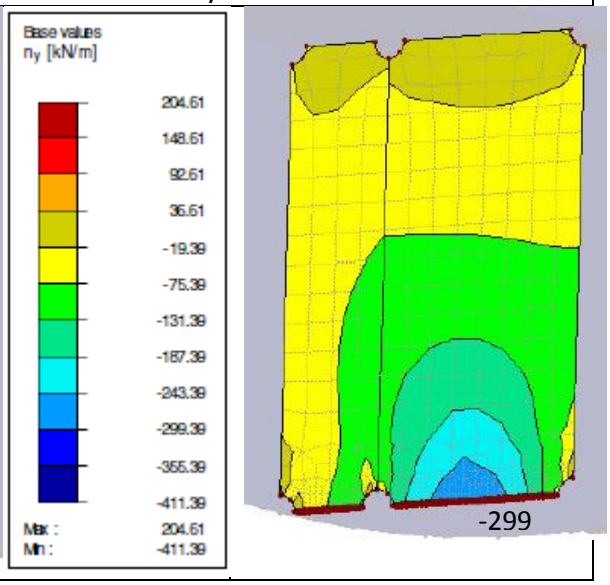

Opening Angle 23 °	
Internal force my	Internal force ny
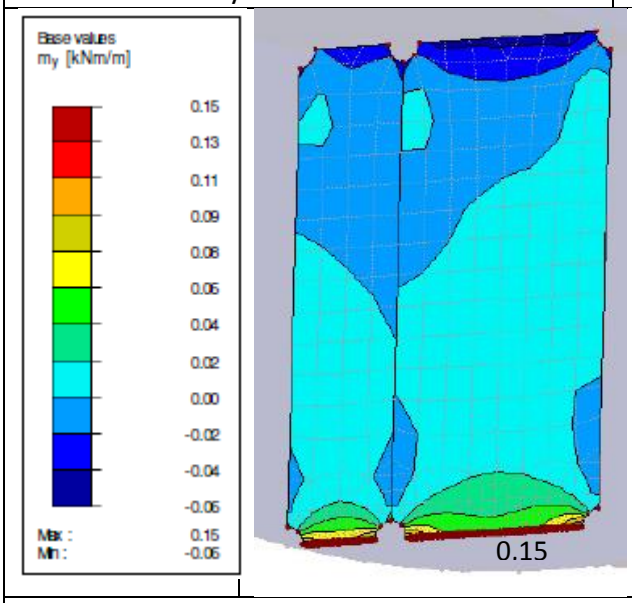	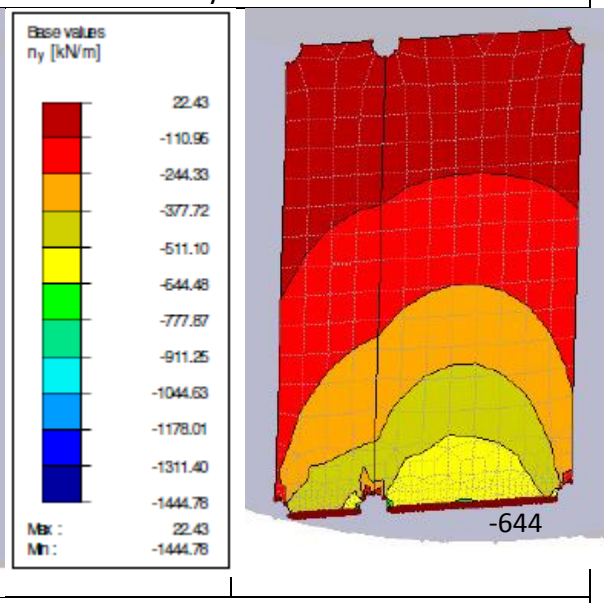
Opening Angle 28 °	
Internal force my	Internal force ny
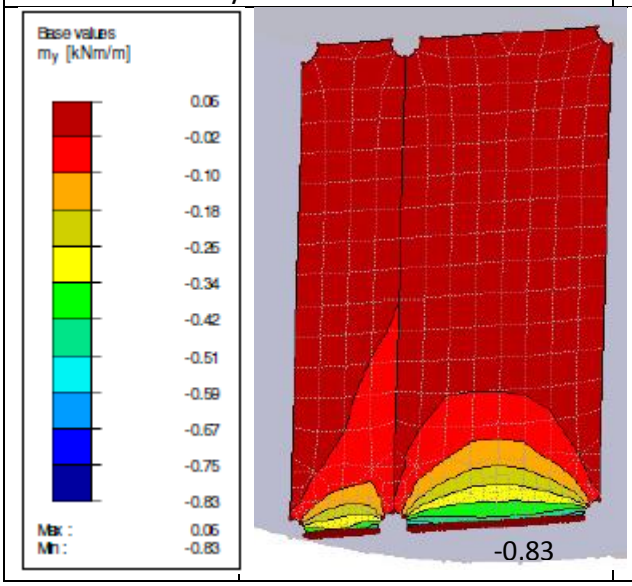	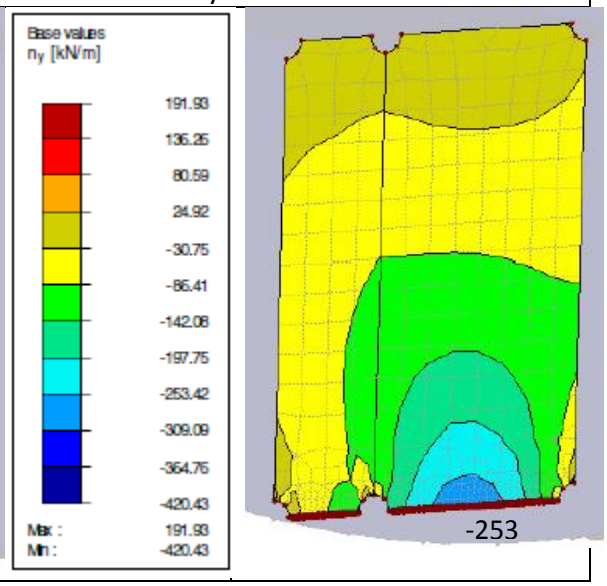

Opening Angle 34°	
Internal force my	Internal force ny
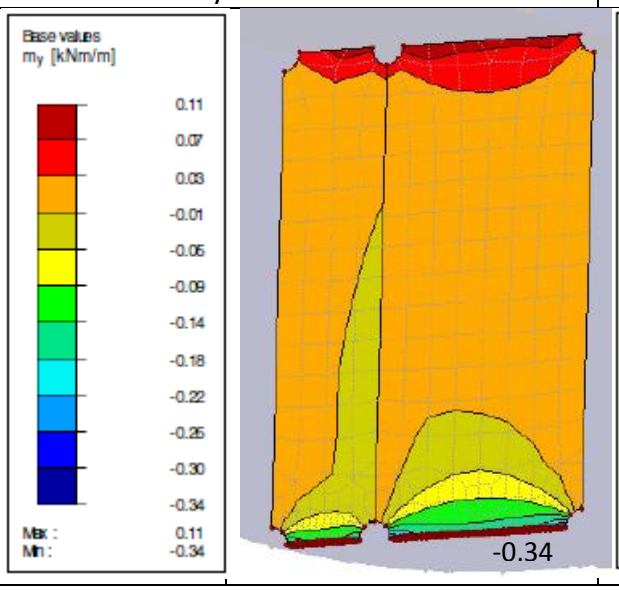	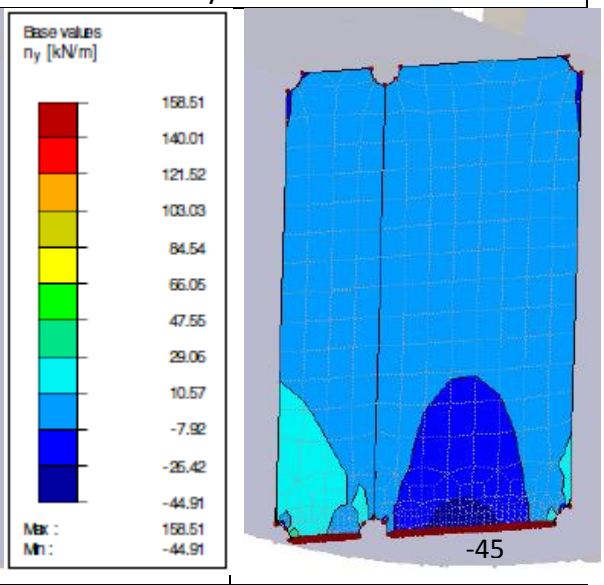
Opening Angle 40°	
Internal force my	Internal force ny
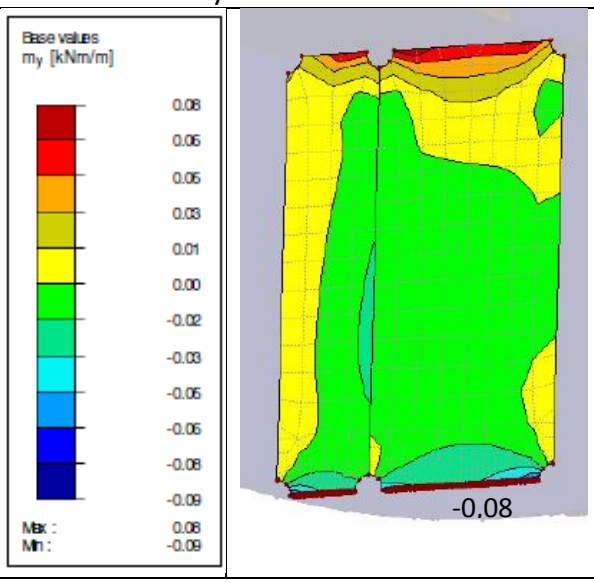	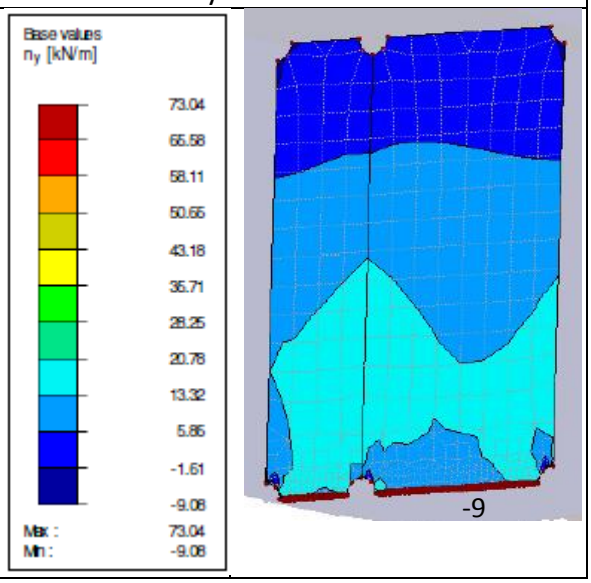

APPENDIX B - RFEM Local Shell Modelling

The results of the finite element modelling using shell elements will be shown in this appendix. The numbering of the models and their configuration is as follows (as shown in Table 4-1).

No. Model	Mesh size (mm)	Distribution of rigid elements (mm)	Mesh refinement	Mesh size (mm)
1	50	115 x 100	No	/
2	20	115 x 100	No	/
3	50	50 x 50	No	/
4	20	50 x 50	No	/
5	50	20 x 20	Yes	20 – plates
6	20	20 x 20	No	/
7	20	20 x 20	Yes	10 – stiffeners
8	20	20 x 20	Yes	10 – longtidunal stiffener 8 – transversal stiffener
9	20	20 x 20	Yes	5 – all stiffeners

Images of the 10 models, where model 10 was modelled with load in between stiffeners.

Model 1	Model 2
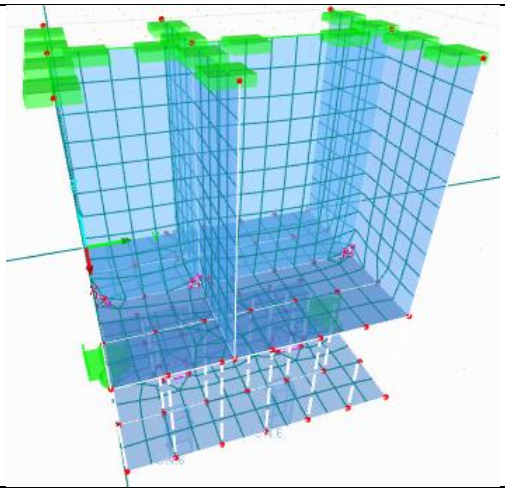	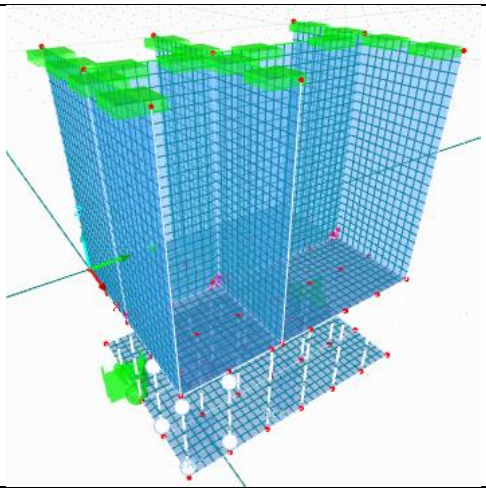
Model 3	**Model 4**
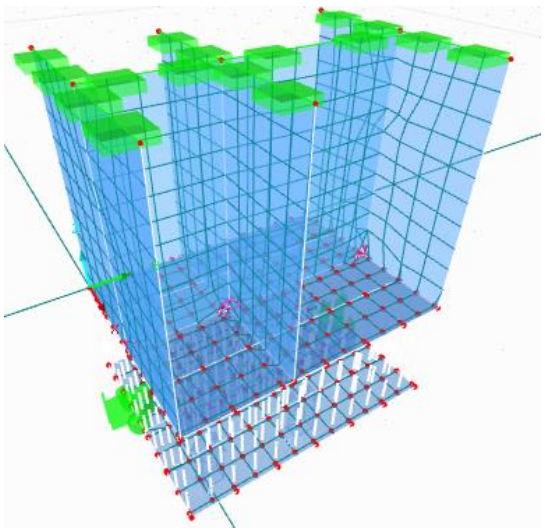	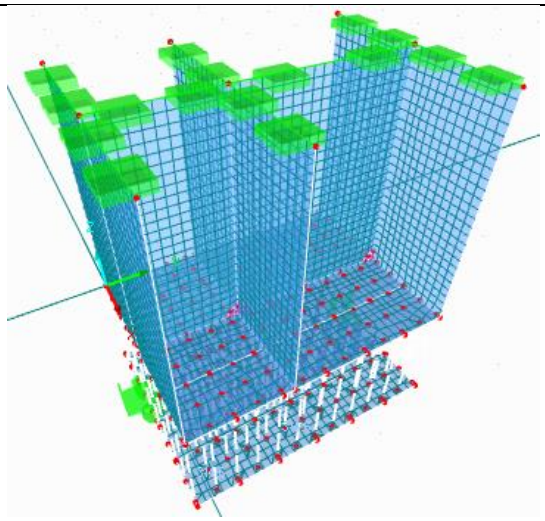

Model 5	Model 6
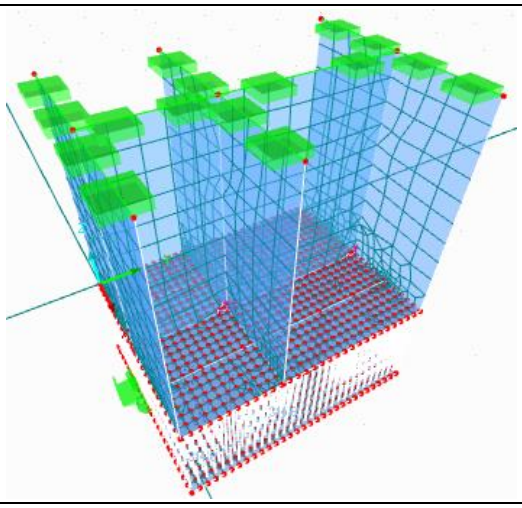	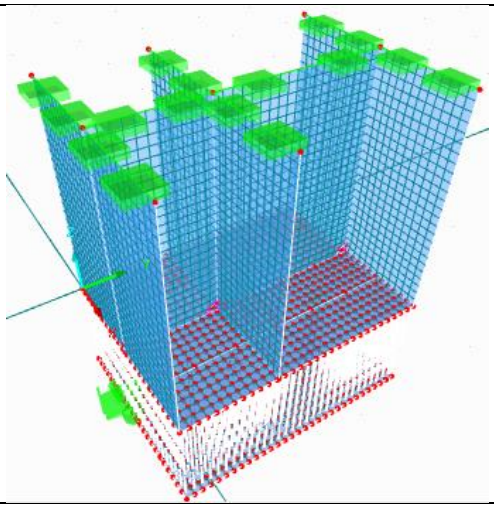
Model 7	Model 8
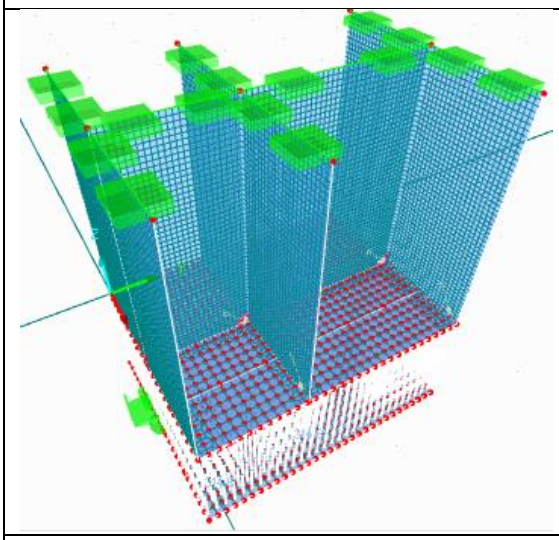	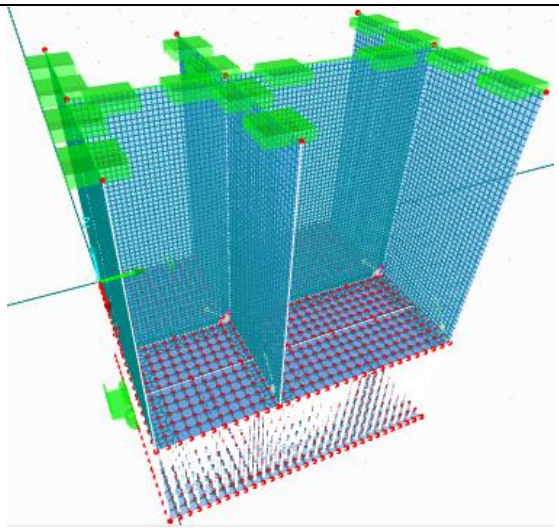
Model 9	Model 10
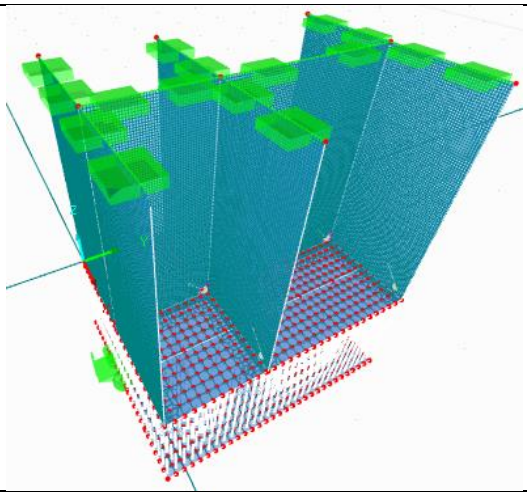	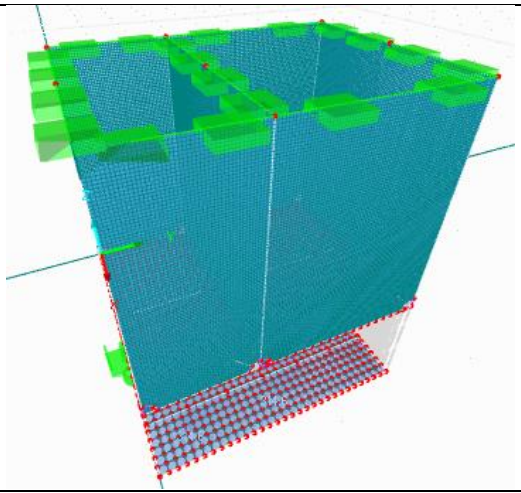

The following images are the results of the internal forces for the modelling, used for the calculation of the respective stresses. The location where the values of forces (or stresses for a different appendix) will be shown in these figures of model 6 and will be the same across all models in both software RFEM and ABAQUS. In the transversal stiffener, the location is above the location of the applied force, as seen with the forces, is where the highest values are located. In the longitudinal stiffener it will be at the right side, not in the middle as this is the location of intersection between the stiffeners, while the analysis performed is between the horizontal plate and the stiffener, therefore values were taken at certain distance from the middle part.

Model 6

Internal force ny (Transversal Stiffener)	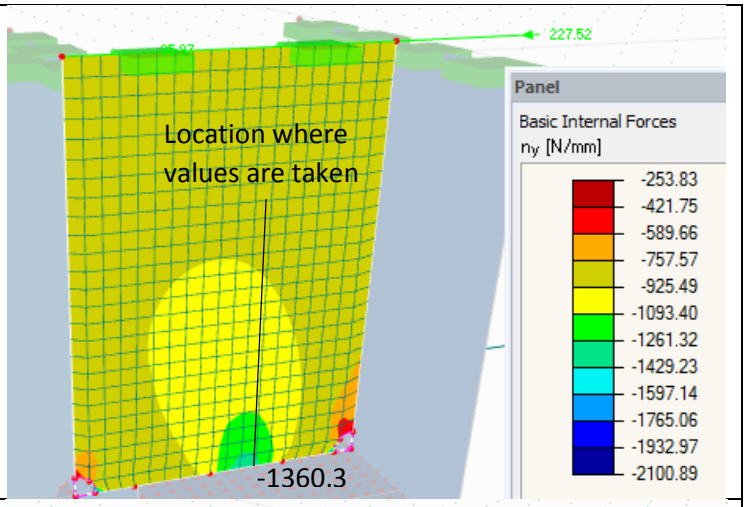
Internal force my (Transversal Stiffener)	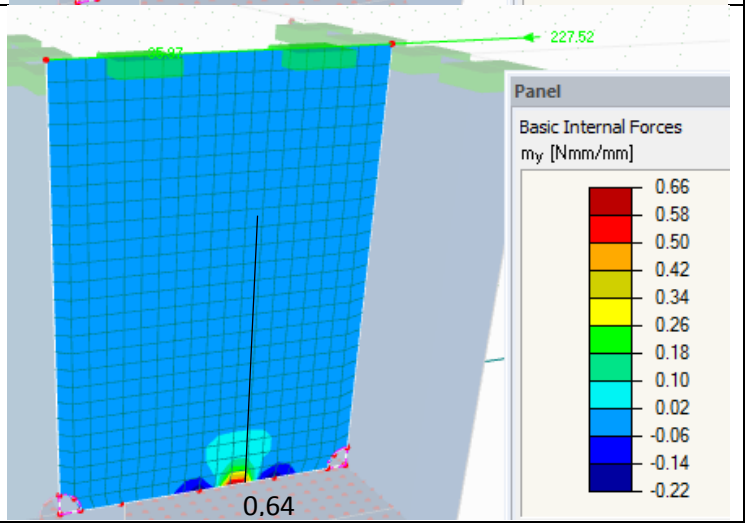

Internal force mxy (Transversal Stiffener)	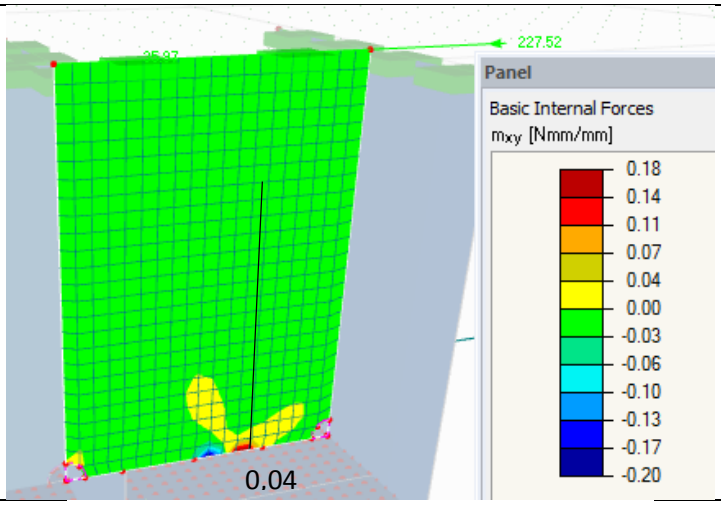
Internal force ny (Longitudinal Stiffener)	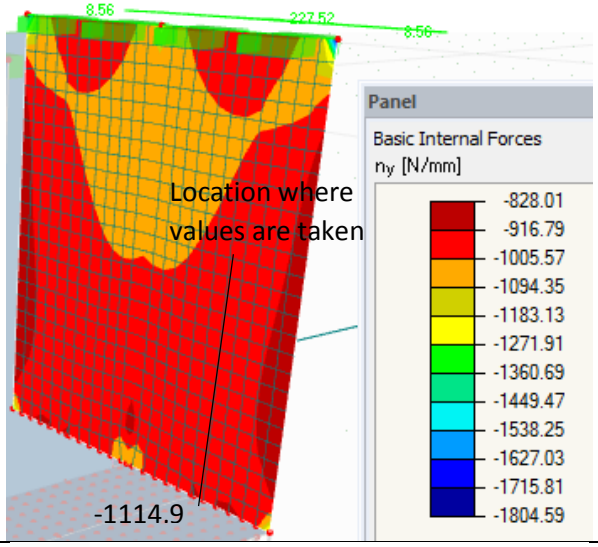
Internal force my (Longitudinal Stiffener)	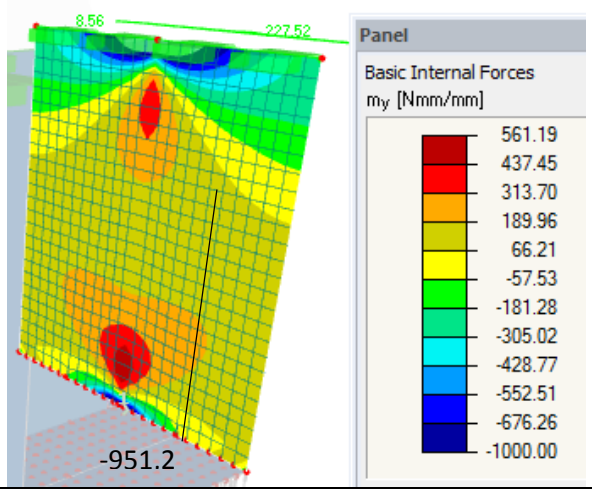

Internal force mxy (Longitudinal Stiffener)	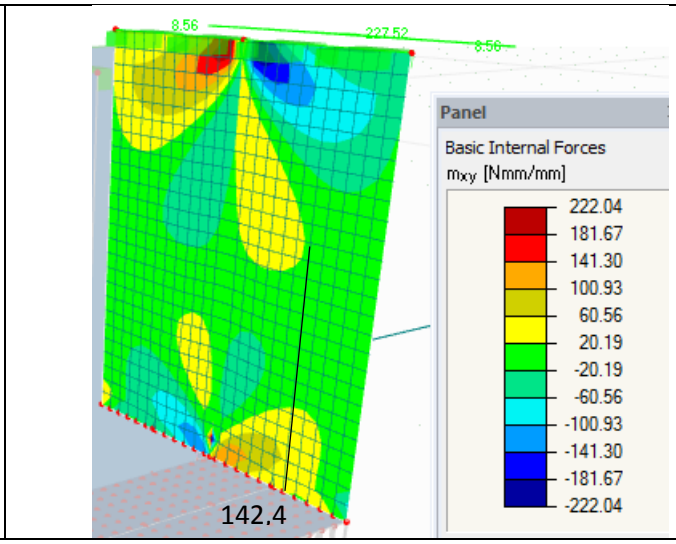

Model 7

Internal force ny (Transversal Stiffener)	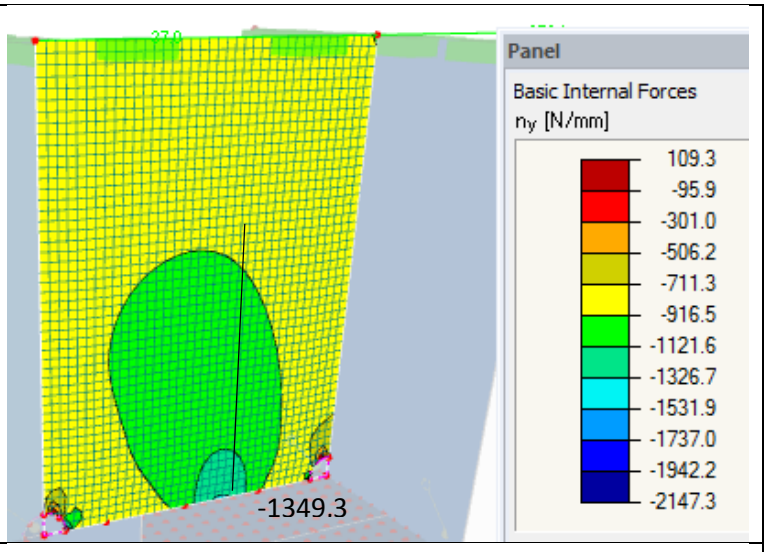
Internal force my (Transversal Stiffener)	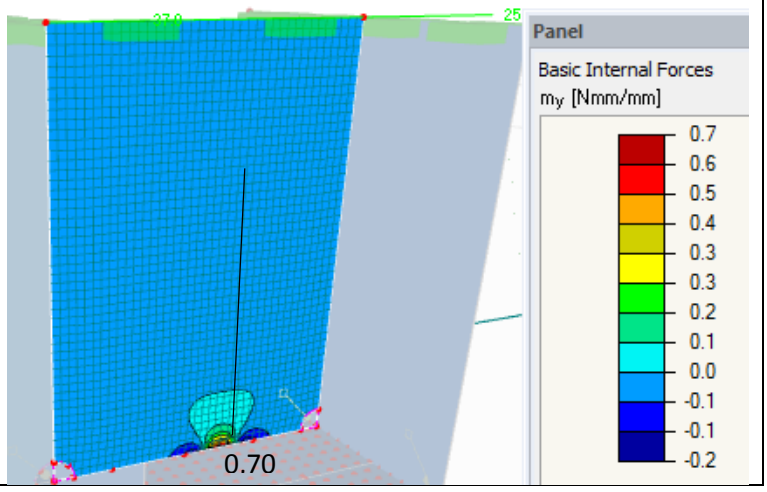

Internal force mxy (Transversal Stiffener)	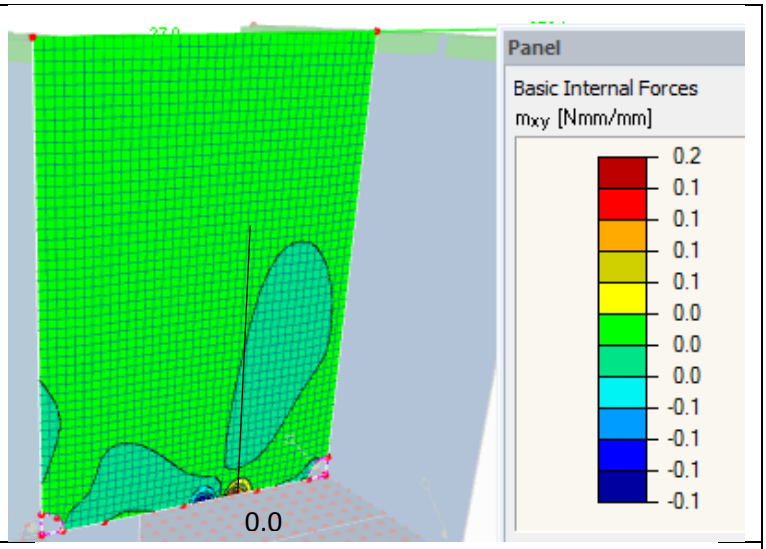
Internal force ny (Longitudinal Stiffener)	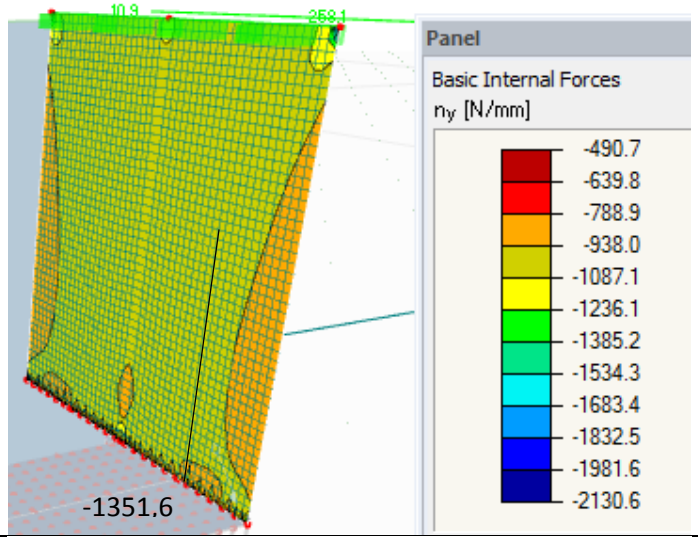
Internal force my (Longitudinal Stiffener)	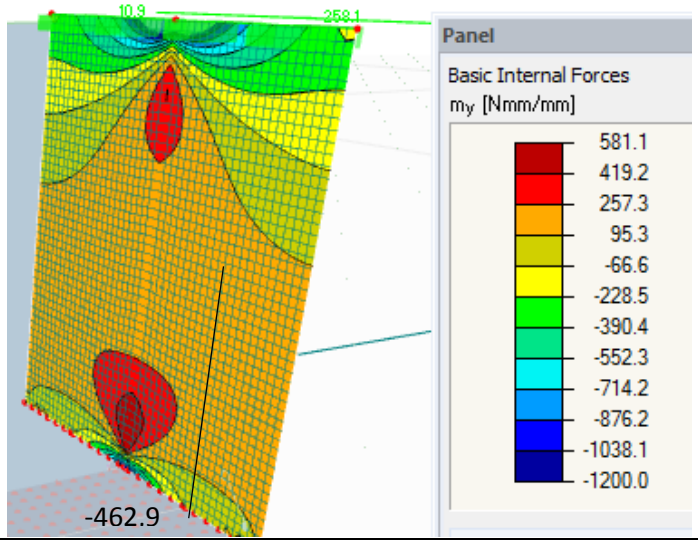

Internal force mxy (Longitudinal Stiffener)	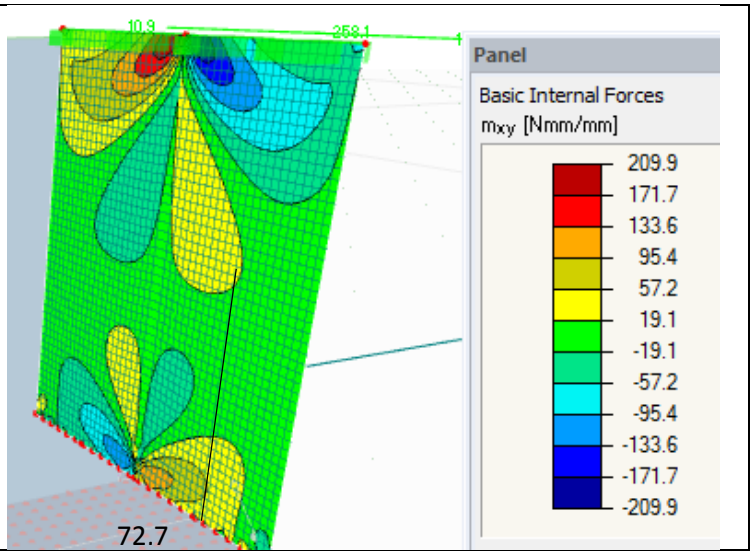

Model 8

Internal force ny (Transversal Stiffener)	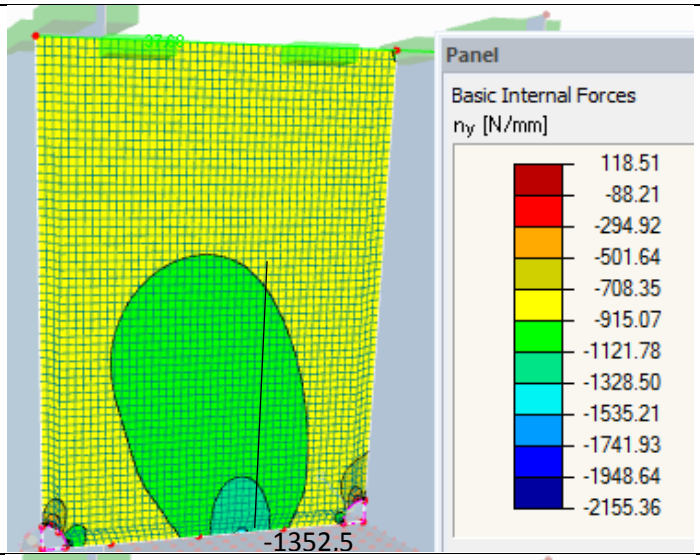
Internal force my (Transversal Stiffener)	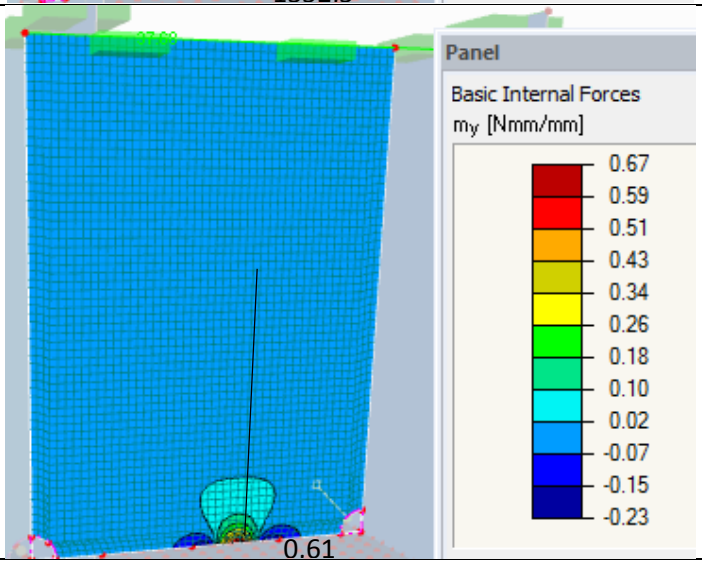

Internal force mxy (Transversal Stiffener)	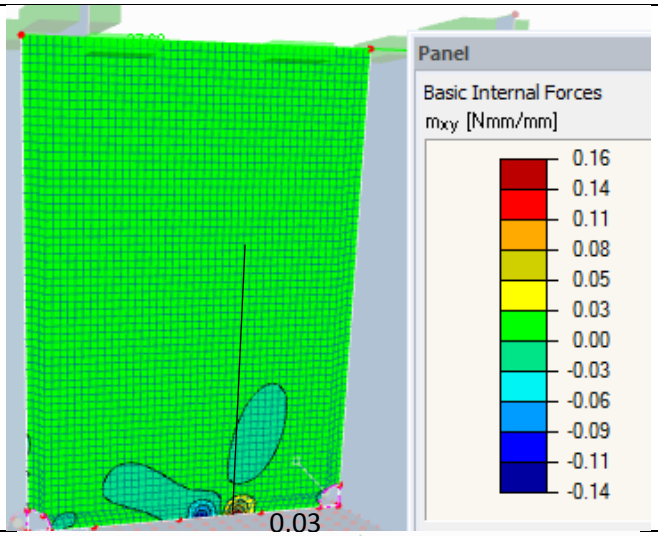
Internal force ny (Longitudinal Stiffener)	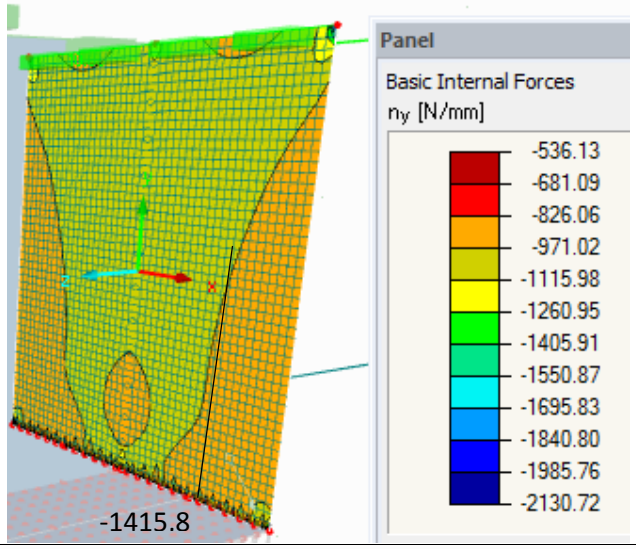
Internal force my (Longitudinal Stiffener)	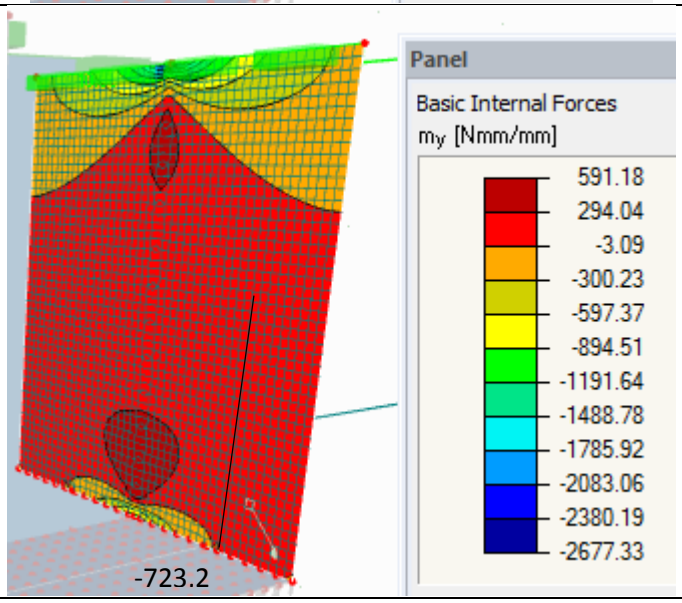

Internal force mxy (Longitudinal Stiffener)	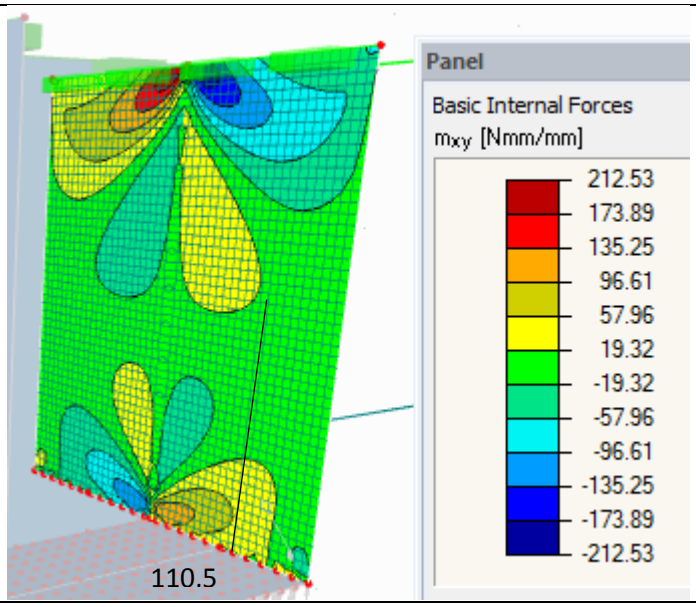

Model 9

Internal force ny (Transversal Stiffener)	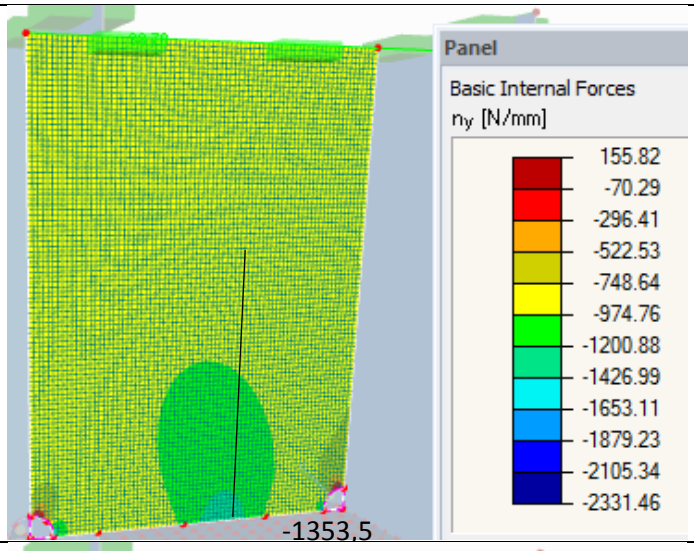
Internal force my (Transversal Stiffener)	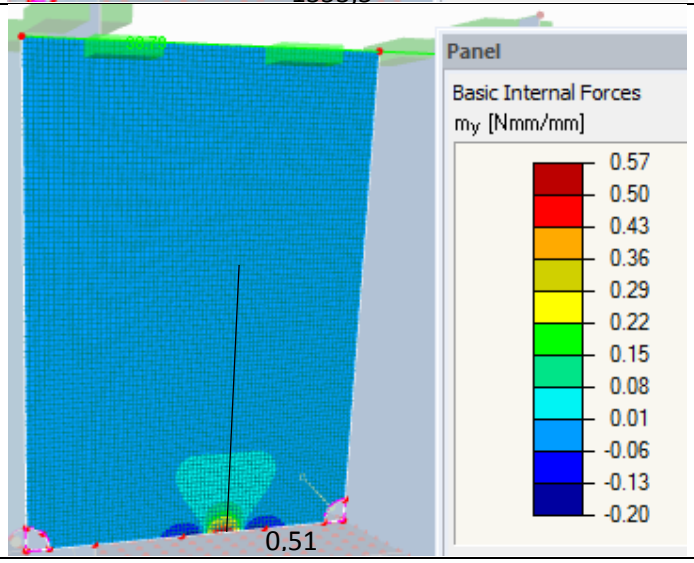

Internal force mxy (Transversal Stiffener)	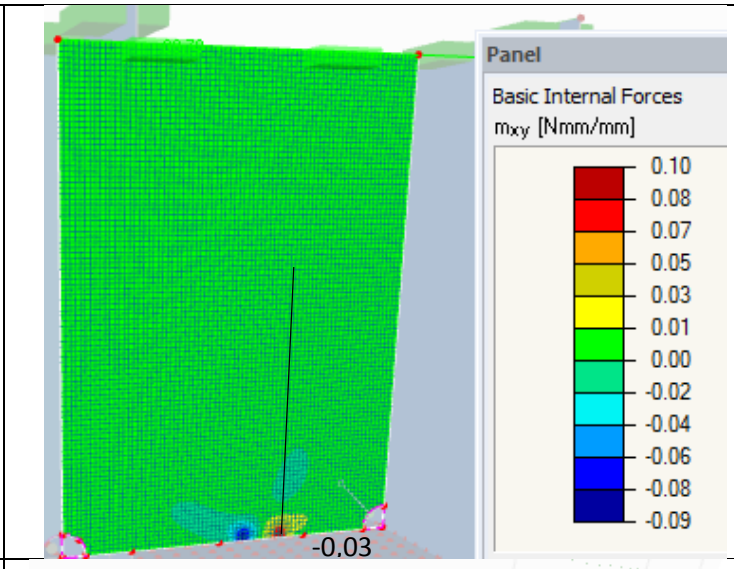
Internal force ny (Longitudinal Stiffener)	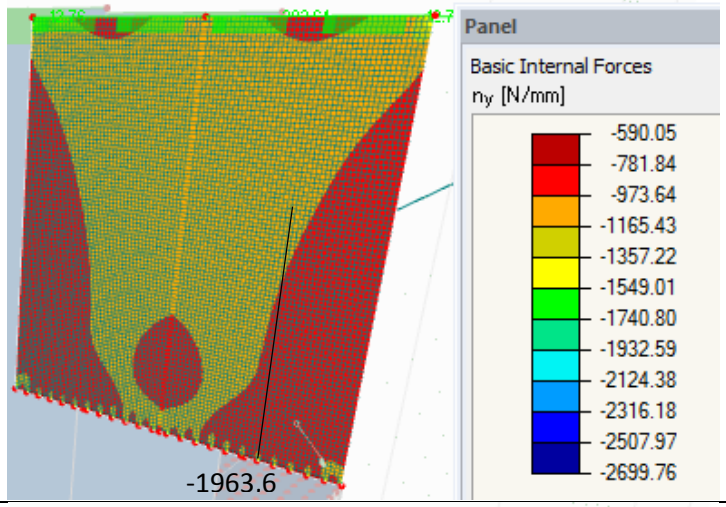
Internal force my (Longitudinal Stiffener)	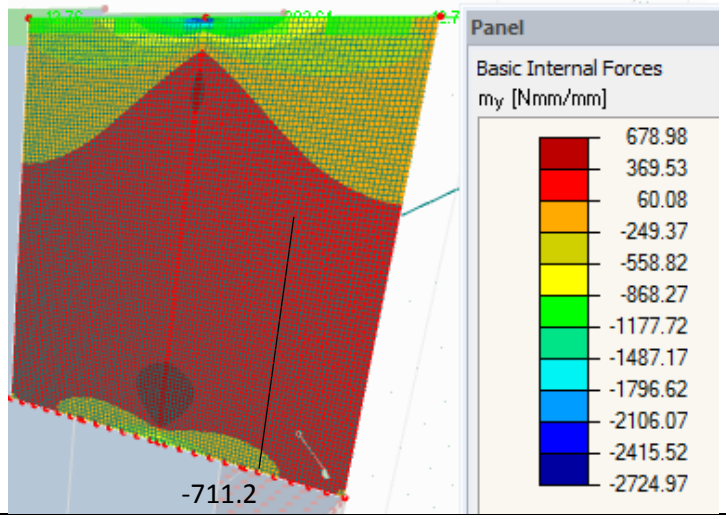

Internal force mxy (Longitudinal Stiffener)	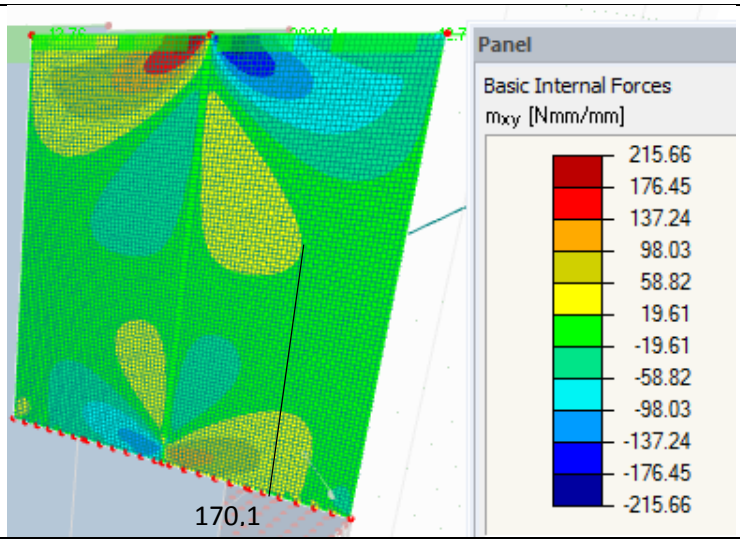

Model 10

Internal force ny (Transversal Stiffener)	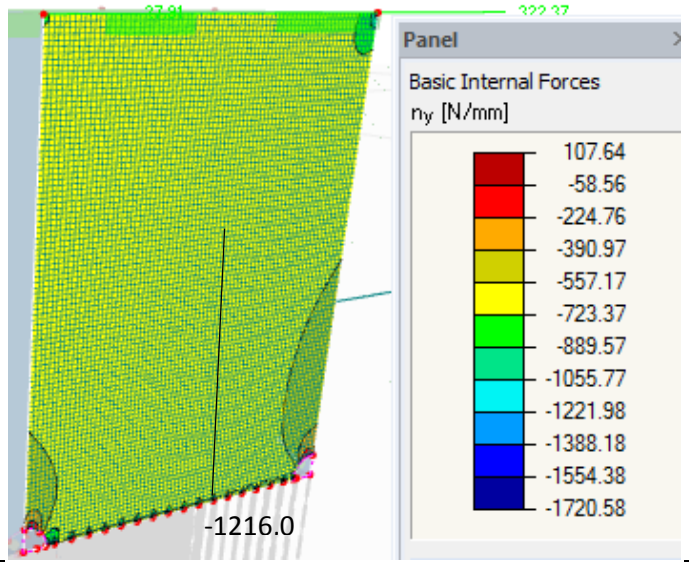
Internal force my (Transversal Stiffener)	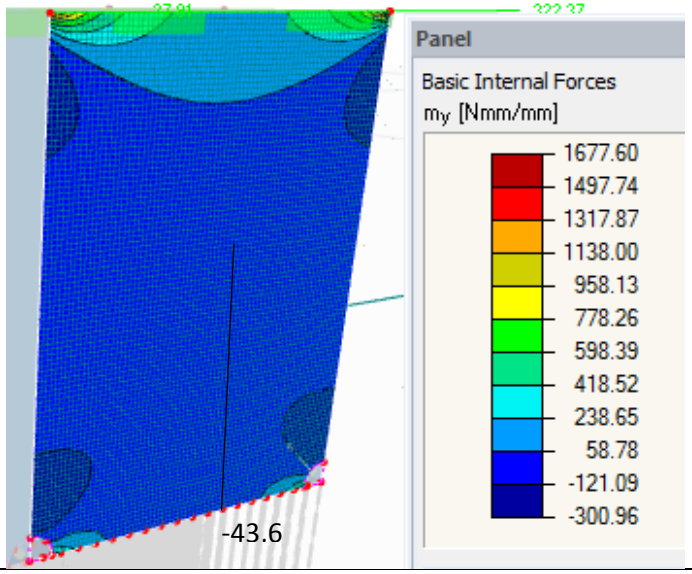

Internal force mxy (Transversal Stiffener)	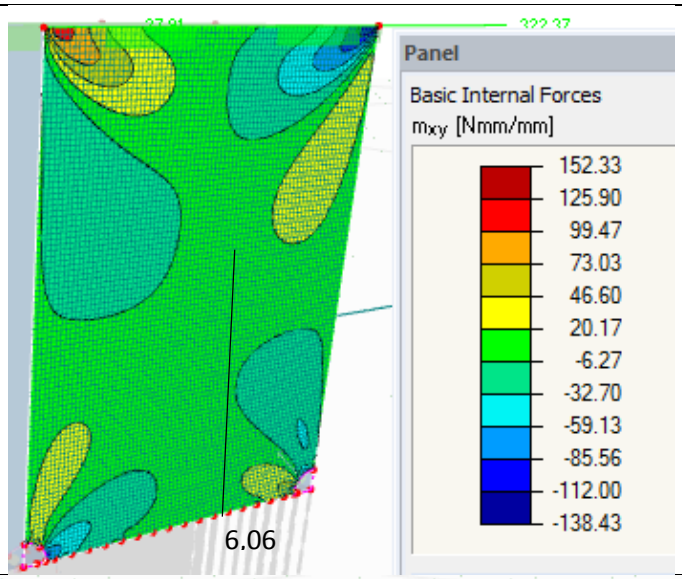
Internal force ny (Longitudinal Stiffener)	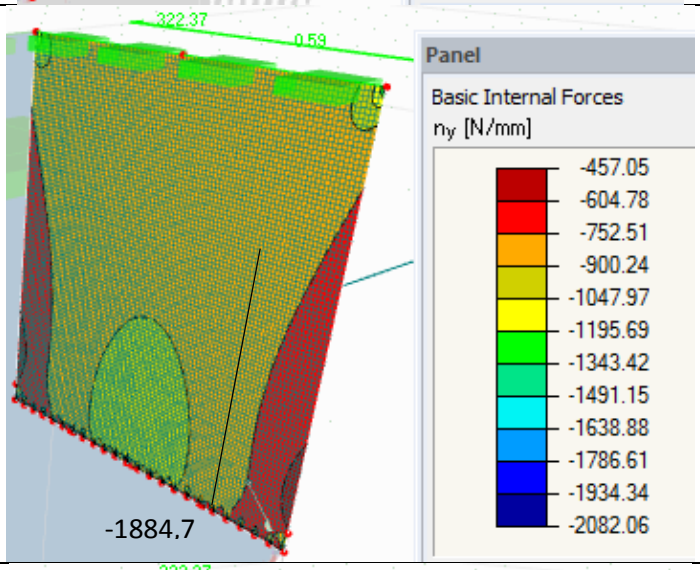
Internal force my (Longitudinal Stiffener)	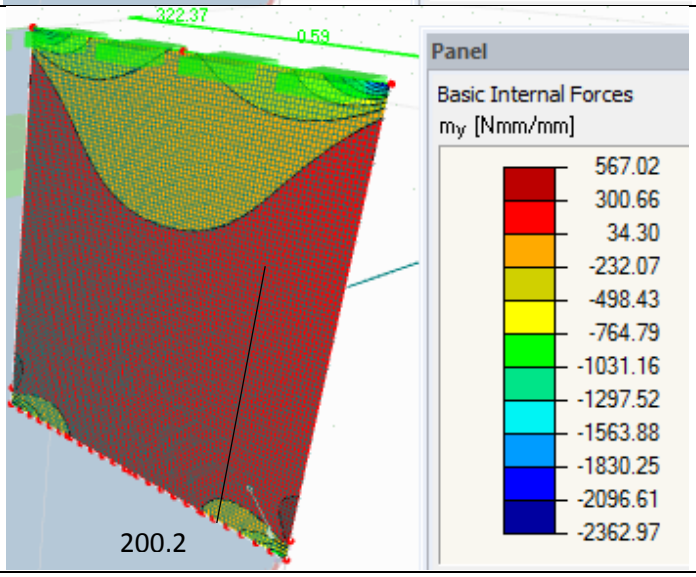

Internal force mxy (Longitudinal Stiffener)	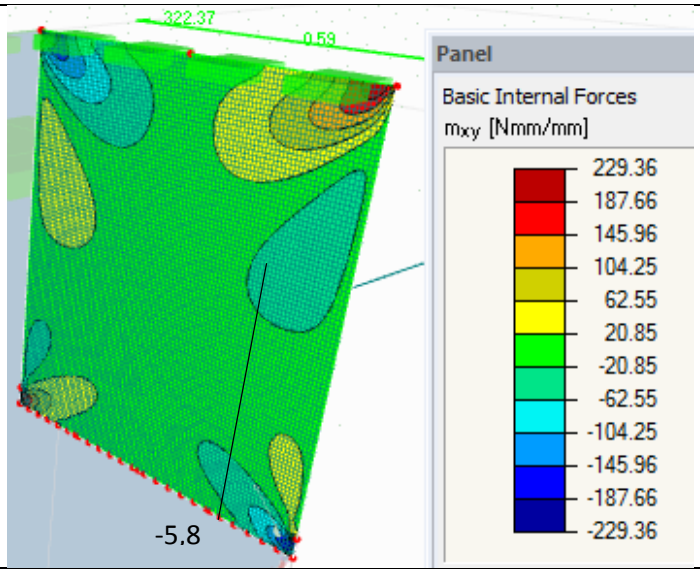

APPENDIX C - ABAQUS Local Shell Modelling

In this appendix, the results of the local modelling in ABAQUS using shell elements will be shown.

The following figures show the model and its fine mesh:

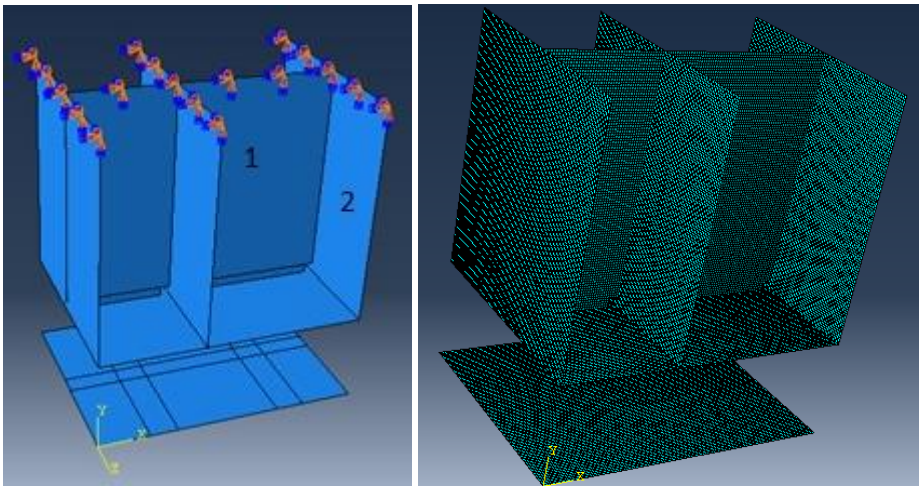

The following figures show the results of the internal forces for the stiffeners, focusing on stiffener 1 (transversal stiffener) and stiffener 2 (longitudinal stiffener) as numbered in the previous picture.

Internal force ny (Transversal Stiffener)	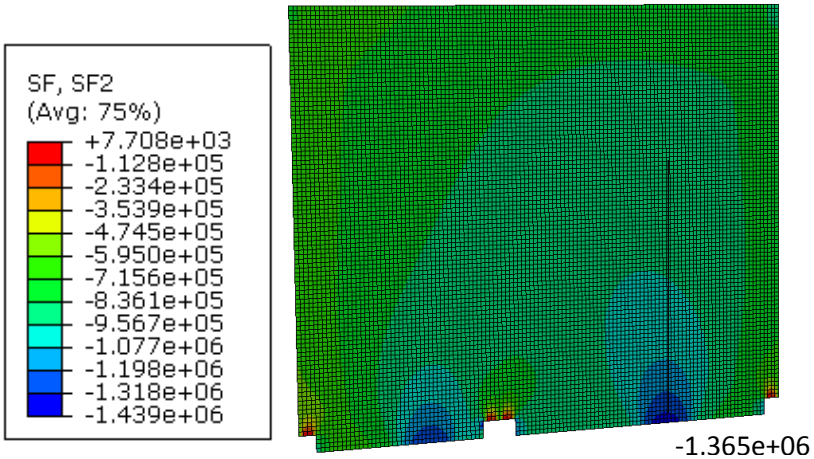
Internal force my (Transversal Stiffener)	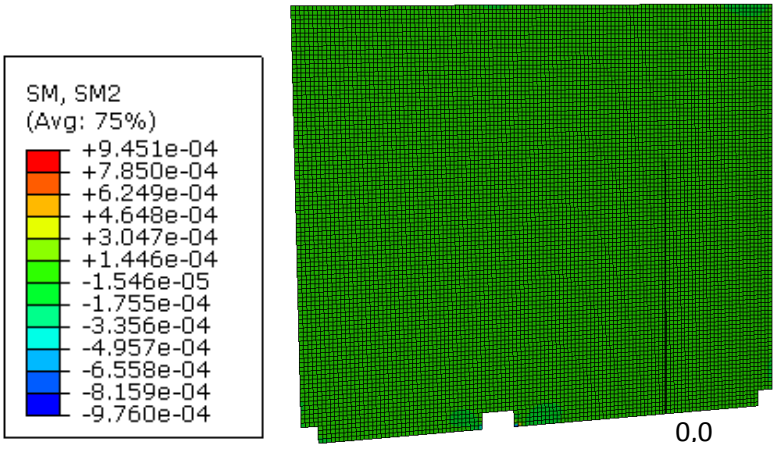

Internal force mxy (Transversal Stiffener)	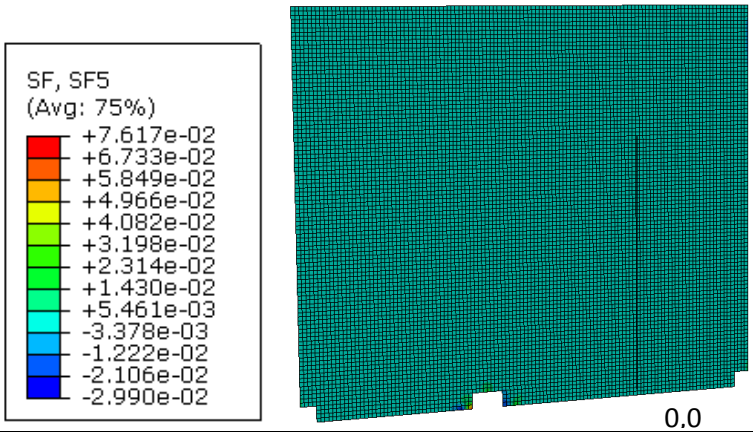
Internal force ny (Longitudinal Stiffener)	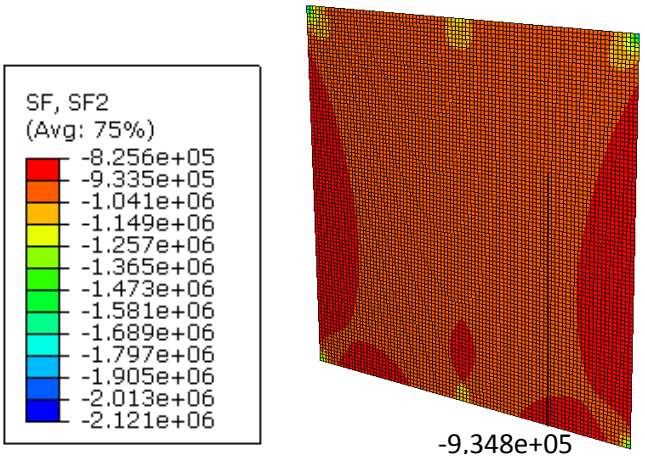
Internal force my (Longitudinal Stiffener)	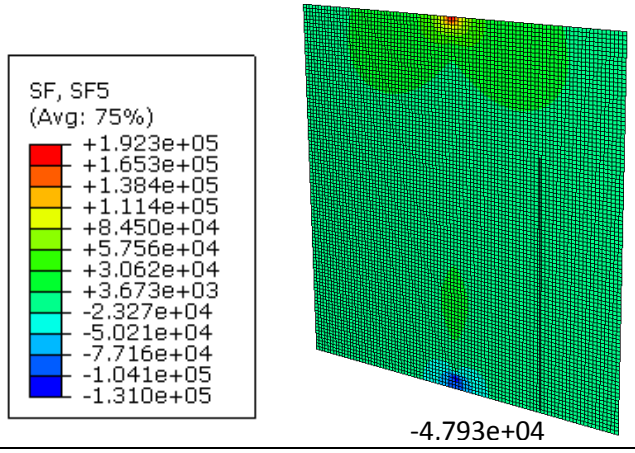
Internal force mxy (Longitudinal Stiffener)	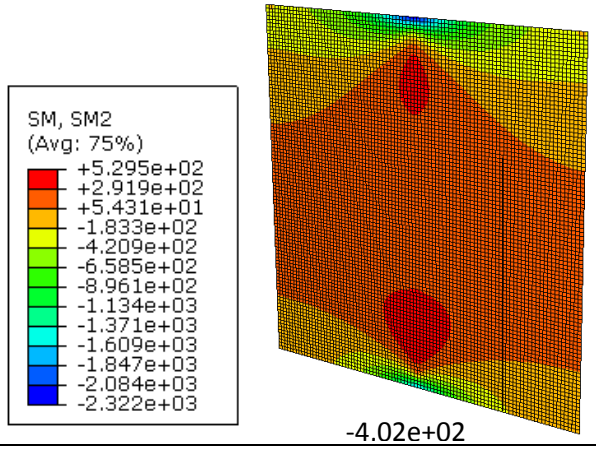

APPENDIX D - ABAQUS Local Solid Modelling

In this appendix, the results of the local modelling in ABAQUS using solid elements will be shown.

The following figures show the results for the fine mesh model without weld modelling.

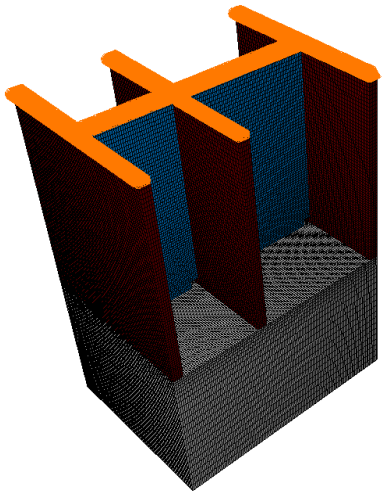

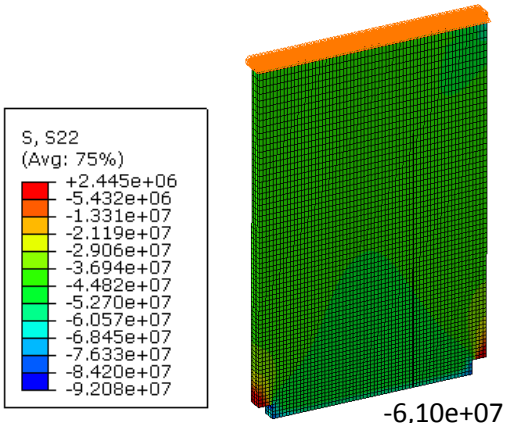

Normal Stresses (N/m^2)
(Transversal Stiffener)

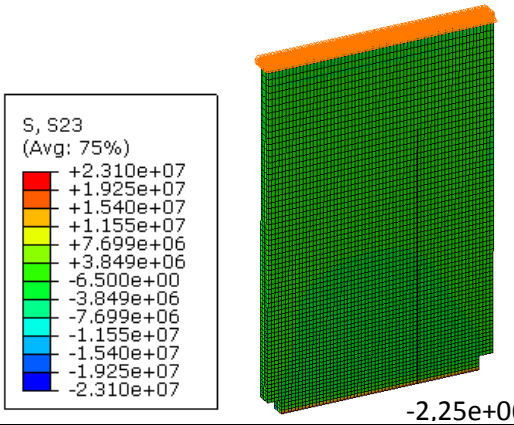

Shear Stresses (N/m^2)
(Transversal Stiffener)

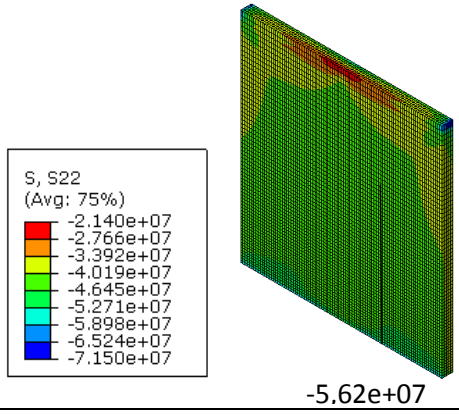

Normal Stresses (N/m^2)
(Longitudinal Stiffener)

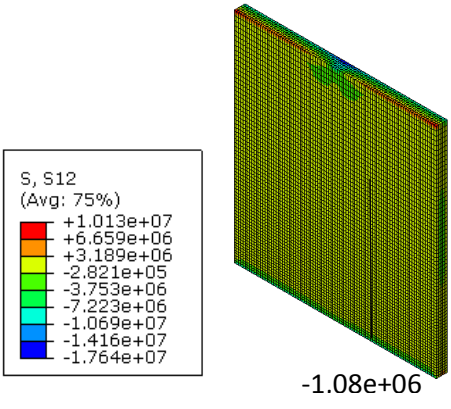

Shear Stresses (N/m^2)
(Longitudinal Stiffener)

The following figures show the results for the fine mesh model with weld modelling.

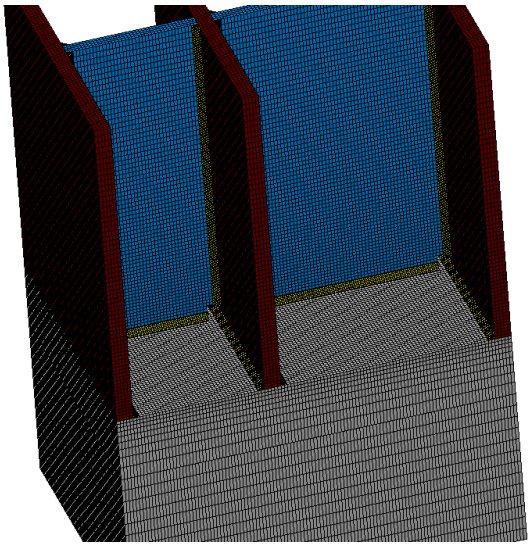

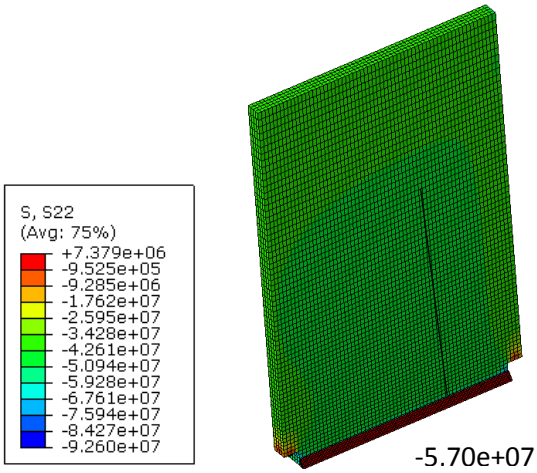

Normal Stresses (N/m^2)
(Transversal Stiffener)

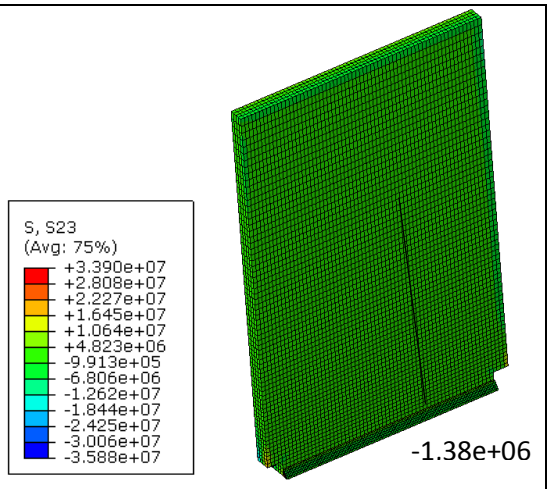

Shear Stresses (N/m^2)
(Transversal Stiffener)

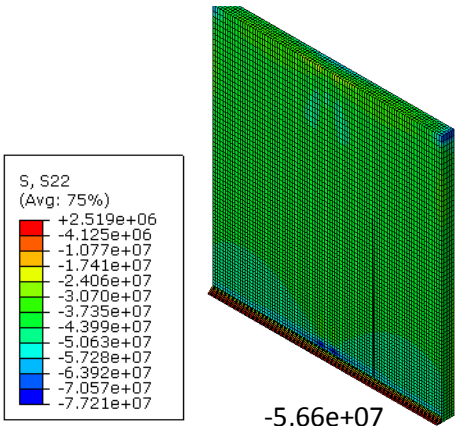

Normal Stresses (N/m^2)
(Longitudinal Stiffener)

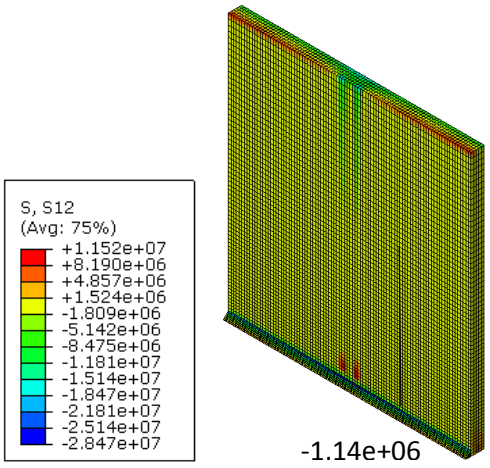

Shear Stresses (N/m^2)
(Longitudinal Stiffener)

The following figures show the stresses on the transversal stiffener under a side surface boundary condition caused by the presence of the rail track itself.

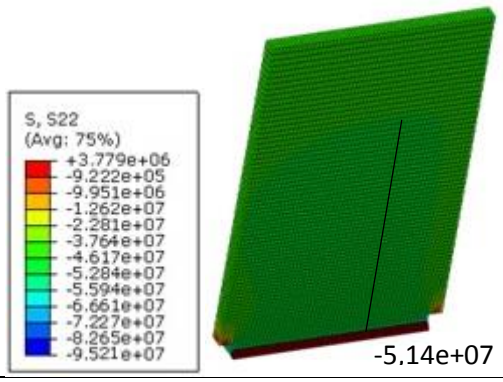	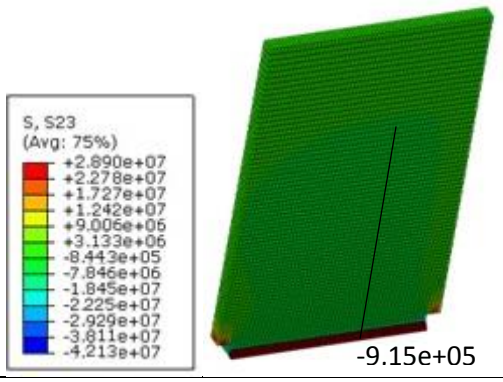
Normal Stresses (N/m^2) (Transversal Stiffener)	Shear Stresses (N/m^2) (Transversal Stiffener)

Bibliography

[1] Al Zamzami I., Susmel L. (2016). On the accuracy of nominal, structural, and local stress based approaches in designing aluminium welded joints against fatigue. The University of Sheffield, Sheffield, UK.

[2] Arola D., Williams C. (2001). Estimating the fatigue stress concentration factor of machined surfaces, International Journal of Fatigue 24, Elsevier Ltd.

[3] Bathe K.J. (2014). Finite Element Procedures, Second Edition, Prentice Hall, Pearson Education, Inc., US.

[4] Chattopadyay A. et al (2011). Stress Analysis and Fatigue of welded structures, Vol.55 Welding in the World, No 07.

[5] Det Norske Veritas (2010). Fatigue Assessment of Ship Structures – Classification Notes No. 30.7, Norway.

[6] Det Norske Veritaas (2010). Fatigue Design of Offshore Steel Structures – Recommended Practice DNV-RP-C203, Norway.

[7] Doerk O. et al (2002). Comparison of different calculation methods for structural stresses at welded joints, International Journal of Fatigue 25, Elsevier Ltd.

[8] Dong P. (2001). A structural stress definition and numerical implementation for fatigue analysis of welded joints, International Journal of Fatigue 23, Elsevier Ltd.

[9] EN 1991-1-4: Eurocode 1: Actions on Structures. Part 1.4: General Actions – Wind Actions (1995), European Committee for Standardization, Brussels, Belgium.

[10] EN 1993-1-9: Eurocode 3: Design of Steel Structures. Part 1.9: Fatigue (2005), European Committee for Standardization, Brussels, Belgium.

[11] Fricke W. (2011). Fatigue strength assessment of local stresses in welded joints, Hamburg University of Technology, Hamburg, Germany.

[12] Fricke W., Kahl, A. (2006). Comparison of different structural stress approaches for fatigue assessment of welded ship structures, Marine Structures 18, Elsevier Ltd.

[13] Fustar B. et al (2018). Review of Fatigue Assessment Methods for Welded Steel Structures, Faculty of Civil Engineering, University of Zagreb, Zagreb, Croatia

[14] Hensel J. et al (2017). Welding residual stresses as needed for the prediction of fatigue crack propagation and fatigue strength, Engineering Fracture Mechanics 198, Elsevier Ltd.

[15] Hobbacher A. (2008). Recommendations for fatigue design of welded joints and components, Doc. IIW-1823-07 ex XIII-2151r4-07/XV-1254r4-07, Welding Research Council, New York, USA.

[16] Hobbacher A. (2008). The new IIW recommendations for fatigue assessment of welded joints and components - A comprehensive code recently updated, International Journal of Fatigue 31, Elsevier Ltd.

[17] Hutton D. (2004). Fundamentals of Finite Element Analysis, First Edition, The McGraw-Hill Companies Inc, US.

[18] Lee J. et al (2010). Comparison of hot spot stress evaluation methods for welded structures, International Journal of Naval Architecture and Ocean Engineering 2.

[19] Liu G., Liu Y., Huang Y. (2014). A novel structural stress approach for multiaxial fatigue strength assessment of welded joints, International Journal of Fatigue 83, Elsevier Ltd.

[20] Maddox S. (2001). Recommended Hot-Spot Stress Design S-N Curves for Fatigue Assessment of FPSOs, TWI Limited, Cambridge, UK.

[21] Osawa N. et al (2011). Study on the preciseness of hot spot stress of web-stiffened cruciform welded joints derived from shell finite element analyses, Marine Structures 24, Elsevier Ltd.

[22] Poutiainen I. et al (2004). Finite element methods for structural hot spot stress determination – a comparison of procedures, International Journal of Fatigue 26, Elsevier Ltd.

[23] Pradhan A. et al (2014). Fatigue Design of Complex Welded Structures Using Finite Element Analysis in Hot Spot Approach and Notch-Stress Intensity Factor Approach, Journal of Basic and Applied Engineering Research, Volume 1-Number 5, Krishi Sanskriti Publications, New Delhi, India.

[24] Program RFEM 5 Spatial Models Calculated According to Finite Element Method – Program Description (2016), Dlubal Software GmbH, Tiefenbach, Germany.

[25] Radaj D. (1990). Design and analysis of fatigue-resistant welded structures. Abington Publisher, Cambridge, UK.

[26] Rong L. et al (2014). Hot spot stress analysis on rib-deck welded joint in orthotropic steel decks, Journal of Constructional Steel Research 97, Elsevier Ltd.

[27] Schijve J. (2009). Fatigue of Structures and Materials, Second Edition, Springer Science+Business Media, B.V.

[28] Shen W. et al (2016). A method of determining structural stress for fatigue strength evaluation of welded joints based on notch stress strength theory, International Journal of Fatigue 90, Elsevier Ltd.

[29] Suominen L. et al (2013). Residual stresses in welded components following post-weld treatment methods, Procedia Engineering 66, 5th Fatigue Design Conference, Elsevier Ltd.

[30] Xiao Z., Yamada K. (2004). A method of determining geometric stress for fatigue strength evaluation of steel welded joints, International Journal of Fatigue 26, Elsevier Ltd.